TECHNISCHEN UNIVERSITÄT MÜNCHEN
Fakultät für Elektrotechnik und Informationstechnik
Lehrstuhl für Nanoelektronik

Inkjet **P**rinting & **S**pray **D**eposition **T**echniques **F**or **F**lexible **E**lectronic **A**pplications

Sara Hassan Ahmed Elmolla

Vollständiger Abdruck der von der Fakultät für Elektrotechnik und Informationstechnik der Technischen Universität München zur Erlangungen des akademischen Grades eines

Doktor-Ingenieurs (Dr.-Ing.)

genehmigten Dissertation.

Vorsitzender: Prof. Dr.-Ing. Wolfgang Kellerer

Prüfende der Dissertation:

1. Prof. Dr. Paolo Lugli, Ph. D

2. Prof. Dr. Gordon Cheng, Ph. D

Die Dissertation wurde am 06.04.2017 bei der Technischen Universität München eingereicht und durch die Fakultät für Elektrotechnik und Informationstechnik am 03.07.2017 angenommen.

To my parents,

To my lovely daughters,
Jana & Larin

To my husband,
Ahmed

To my brother,
Mohammed

To my sisters,
Haidy
Hala
Hadeer

Abstract

Deutsch

Der Tintenstrahldruck hat ein breit gefächertes Anwendungsspektrum, das von Kunst- und Zeitungsdruck bis hin zu gedruckter organischer und flexibler Elektronik reicht. Diese Depositionstechnologie ist ein vielversprechender Ansatz, der die Strukturierung von Materialien mit einem geringen Fertigungsausschuss erlaubt. Die effiziente Herstellung führt zu einer Reduzierung der Materialkosten. Des Weiteren bietet sich der Tintenstrahldruck als hervorragende Möglichkeit zur Skalierung nach oben an. Gedruckte Elektronik mit flexiblen Substraten ist ein interessanter Bereich aufgrund der kosteneffizienten Herstellung und der Möglichkeit multifunktionale Elektronik auf kleinen und großen Flächen herzustellen.

Im Rahmen dieser Dissertation wird ein Überblick über verschiedene Tintenstrahltechnologien gegeben, die Herausforderungen an die funktionellen Materialien untersucht und die Implementierung von flexiblen Geräten für praxisbezogene Anwendungen präsentiert. Der experimentelle Teil der Arbeit wurde mit einem Dimatix Materials Printer DMP-2831 durchgeführt. Der Fokus liegt dabei darauf, die Tinte wie auch das Substrat und deren gegenseitige Wechselwirkung zu untersuchen. In dieser Arbeit wird ein zuverlässiger kapazitiver Kraftsensor basierend auf einem Polydimethylsiloxane-(PDMS)-Film präsentiert. Dieser Film ist in einem flexiblen Printed Circuit Board (PCB) mit Mikrocontroller integriert, der die Signale des Sensors weiterverarbeitet. Die Leiterbahnen des Schaltkreises werden durch gedruckte Silbernanopartikel (AGNPs) definiert. Die Funktion dieser Schaltung wird demonstriert, wodurch die Verwendung für Applikationen mit einer künstlichen Haut ermöglicht wird. Der Hauptzweck dieser Arbeit zielt darauf ab, das Grundverständnis über verschiedene Drucktechnologien herauszuarbeiten und die Herausforderungen an das spannende und aufstrebende Gebiet der gedruckten Elektronik zu untersuchen.

English

The Inkjet printing technique is a field that spans from graphic art and newspaper industry as a manufacturing tool to organic and flexible electronics as a major topic in scientific research. The drop-on-demand inkjet printing is a promising approach, which allows the patterning of materials with a negligible material waste, thus allowing a significant reduction of raw materials. Furthermore, inkjet printing is suitable for large scale production in a roll-to-roll process. Printing electronics (PE) over flexible substrates are an area of significant interest owing to the low-cost fabrication and the possibility of obtaining multifunctional electronics over small and large areas.

In the frame of this Ph.D. thesis, an overview of inkjet printing technologies for flexible electronics is given from the view point of the materials challenges in implementing flexible devices into practical applications. The work is carried out with a Dimatix Materials Printer DMP-2831. The basic research concentrates on defining the ink and substrate materials and their interactions. Throughout this thesis, a reliable capacitive force sensor based on a polydimethylsiloxane (PDMS) film is presented. This film is integrated into a flexible PCB that includes a microcontroller capable of evaluating the sensor. The interconnects of the circuit are defined by silver nanoparticles, which are deposited by inkjet printing. The working principle of the circuit is demonstrated, proving that this simple approach can be used for artificial skin applications. The main purpose of the work is to condense the basic knowledge and highlight the challenges associated with the burgeoning and exciting field of printing techniques for flexible electronics.

Contents

Chapter one

Introduction

During the last few decades, many techniques have been employed to enhance the possibility of fabrication of innovative products from flexible displays to radio-frequency identification tags. The development process of innovative products within shorter intervals becomes increasingly important. There are two important phases in the product realization process: Process planning and design. The most important trends in the electronic equipment technology are decreasing both size and power consumption of complex digital systems and on the other hand increasing in functionality [1]. Also, the flexibility approach is one of the highly demand requirements for improving the electronic devices and for the future of engineering industry in addition to the sustainable approach, which means energy saving materials and methods. Therefore, it is important to match between the needs of the development of electronic devices performance and the development of the process technology. Some scalable materials deposition techniques that show promise are spray deposition technique, inkjet printing technique, screen printing technique, and additive techniques.

Electronic devices as an integral industry for the development and sustenance development of the modern world in virtually all of its aspects been established over the past several decades [2]. Therefore, the development of all types of electronic devices are ubiquitous in today's society. Tremendous part of development of electronic devices technology such as lighting systems,

integrated circuits, displays, and sensors are critical to social, scientific, and industrial endeavors. For example, in the field of display devices, the development from the conventional cathode-ray-tube (CRT) technology towards flat-panel displays (FPDs) such as electroluminescent displays (ELDs), liquid-crystal displays (LCDs), and plasma display panels (PDPs) has been achieved [3]. The development usually implies the reduction of manufacturing costs or materials or manufacturing costs, as well as the invention of novel new fabrication techniques and equipment for innovative applications [4]. Some degree of patterning is required in all cases of electronics manufacturing. Photolithography process for example is one of the manufacturing techniques used for pattering either by selective removal of material after deposition, or by masking areas to prevent material from being deposited on them. But, both methods of photolithography process comprise material wastage which is considered the main disadvantage of that technique. Digital patterning is one of the promising solution rather than masking, therefore the development of deposition techniques is one of the main requirements toward development of electronic devices.

On the other hand, the introduction of flexible substrates instead of using the standard substrates of glass or silicon, upon which much of the electronic devices are built, is well-deserved interested area of research. Such standard substrates are limited in terms of size which is the major technological drawback. For example, approximately 300 mm diameter is the maximum size of silicon wafers which is not suitable for large size of electronic applications [5]. Therefore, flexible substrates will take advantage of the unique opportunities of some scalable materials deposition techniques which in turn provide an increasingly gradual development of complex devices. At the same time, a limited temperature range of flexible substrates, usually < 200°C, is one of certain restrictions to on the fabrication process of such devices. The challenges and the advantages of providing flexible substrates into the electronic industry implies a tremendous fraction of current technology. At variety of processing conditions, providing more and different materials applicable to different flexible substrates for increasingly complex printed devices is also an interested area of research [6]. Thus, the realization of development of electronic devices involves understanding of a wide range of subjects.

1.1 Thesis Summary and Motivation

To help realization of flexible electronics potential, significant advances in techniques used in their fabrication are needed. Therefore, a general framework for the development of innovative processing techniques suitable for scalable manufacturing of solution-processable thin-film electronics is the main aim of this dissertation. The performance and the working principles of different techniques employed in the formation and modification of thin film will be introduced. To pave the way for these technologies to be used in pioneering flexible form factors and electronic skin will be also investigated.

Chapter 2: will provide an overview of flexible electronics technology research in details in addition to a comparison between the characteristics of inorganic semiconductors and organic semiconductors. Also, the challenges of materials used in flexible devices will be also introduced. The last section of the chapter will involve scalable manufacturing of solution-processable thin-film electronics, describing the basic working principles, the main advantages and disadvantages.

Chapter 3: An overview on CNT thin-films on different substrates will be introduced. A high quality CNT thin-films through a reproducible, reliable, and low cost spray deposition technique will be investigated. Also the preparation method for fabrication of SWCNT films using sodium dodecyl sulfate (SDS) as dispersive agents will be explained in details. The performance of CNT thin-films deposition on different rigid substrates such as glass, ITO-coated glass, and spectrosil substrates) will be demonstrated including a comparison of the morphological features of the thinnest CNT films on the different substrates. The work function values for CNT films deposited on different rigid substrates will be also studied. On the Other hand, CNT thin-films deposition on flexible substrates such as ITO-PET and PET substrates will be also analyzed where two films with high and low CNT density were prepared on PET substrate. From the AFM analysis, a comparison between the two CNT densities on ITO-PET, PET and glass in the term of surface coverage will be also investigated. The work function of CNT films on flexible substrate will be also studied. Finally, study of the photogenerated carrier dynamics and

frequency resolved complex photoconductivity in CNT films on PET substrate using time-resolved THz spectroscopy will be also involved.

Chapter 4: An overview of the inkjet printing activity will be present including system identification, working principle and parameters of printer employed in the work; namely the Fujifilm Dimatix Materials Printer DMP-2831. The inkjet printing process step by step will be explained including the ideal printing parameters to achieve high quality printing patterns. The physical and chemical properties of the suitable ink for the dimatix printer will be mentioned. As viscosity and surface tension are the most important physical parameters of printing fluids which strongly influence the final printing performance, the effect of these two parameters will be presented. In order to allow for structural versatility, device miniaturization, and purely selective system deposition, the Ag ink DGP-40LT-15C was employed as the main conductive ink during this thesis for Fujifilm Dimatix Materials Printer DMP-2831. The effect of plasma treatment of different substrates will be introduced. As a consequence, it is proved that plasma treatment is an essential step for surface modification of the substrates prior to printing process for successful printing patterns. The relationship between the drop spacing, continuous printed lines, line width and electrical resistance will be studied. It is found that the continuous printed lines and printed line width highly depend on drop spacing. Finally, the effect of photonic sintering of the printed patterns have been investigated thoroughly by using the optical microscopy and the result is confirmed by Scanning Electron Microscope (SEM).

Chapter 5: In this chapter, an overview on the tactile sensing for robotic application will be presented. In addition to a short review of the tactile sensing technologies for robotic application, especially the capacitive tactile sensors, will be presented. A capacitive sensor based on a polydimethylsiloxane (PDMS) film integrated into a printed circuit board (PCB) on a flexible substrate whose layout is defined by inkjet printing will be introduced; as a main application of this thesis. A full description of the fabrication and characterization of capacitive tactile sensor will be involved. The influence of the dielectric thickness of the PDMS on the sensor behavior has been studied in the terms of sensitivity and dynamic response. The evaluation of the fabricated sensor will be also investigated by integration of the film into a flexible PCBs including a microcontroller.

Chapter 6: The main conclusions of the thesis will be introduced in this chapter.

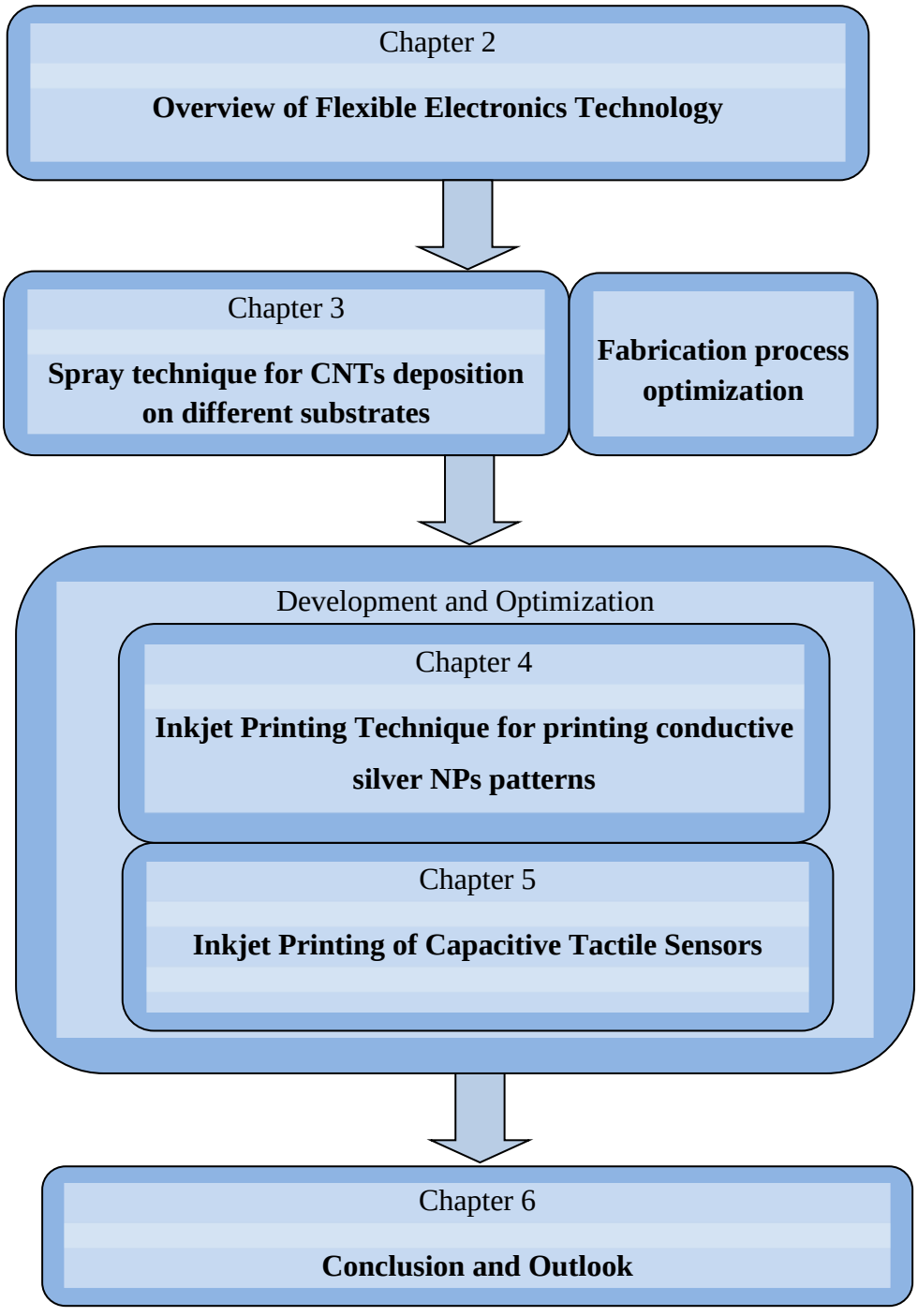

Figure 1.1: Chart shows the outline of the presented work.

Chapter 2

Flexible Electronics

Flexible electronics represent a wide-open and rapidly developing technology, for building electronics circuits onto flexible substrates. Flexible electronics for industrial community means flexible displays and X-ray sensor arrays whereas this technology for researchers means sensors, electronic textiles, and electronic skin. This chapter will provide a general overview of the flexible electronics and the evolution of the technology. Also, a survey of the materials used to fabricate these flexible devices will be discussed.

The most widely utilized methods for practical fabrication technology for flexible electronics will be introduced, including spin coating, spray deposition technique, and inkjet-printing. The advantages and disadvantages of each deposition techniques will be highlighted.

2.1 Overview of Flexible Electronics Technology

Flexible electronics, also known as printable/organic electronics, has a long story. The flexible electronics field has open boundaries that move with its development and application, it is a highly interdisciplinary field. The flexibility, a critical issue in flexible electronics, which associate with many qualities: bendable, lightweight, nonbreakable, elastic, and large-area manufacturable. Many researchers are trying to build flexible electronic devices in various fields of applications such as flexible displays, flexible sensors, flexible lighting devices, medical devices, packaging, electrophoretic displays, textiles. From the development of flexible thin film single crystal solar cell to flexible organic light-emitting diode displays on plastic substrates has been spanned the

development of flexible electronics devices over the past forty years. In 1960s, the first assembling of flexible thin film solar cell on a plastic substrate has been introduced [7, 8]. In 1973, the development of thin-film solar cells has been continued as a path to reducing the cost of photovoltaic electricity. A Pt/a-Si:H Schottky barrier solar cell deposited on a stainless steel substrate was reported by Wronski, Carlson, and Daniel at RCA Laboratories in 1976 [9]. In the early 1980s, Plattner et al. reported n^+–i a-Si: H/Pt Schottky barrier [10]. At the same time Okaniwa et al. presented p^+–i–n^+ a-Si:H/ITO solar cells on organic polymer film substrates and studied the flexibility of their solar cell [11, 12]. By continuous deposition, CdS/Cu_2S solar cells on a moving flexible substrate were reported around the same time [13]. A Si:H solar cells on flexible steel substrates and organic polymer substrates were introduced by roll-to-roll fabrication method in the early beginning of 1980s [14, 15]. In 1968, Brody and some colleagues fabricated the first flexible TFT of tellurium on a strip of paper and then they expanded their research to fabricate TFTs on anodized aluminum wrapping foil, Mylar, polyethylene as flexible substrates. They reported that by bending TFTs to a 1/16" radius or even cut in half along the channel direction, TFTs remained operational to function [16, 17].

In Japan, in the mid-1980s, to develop the fabrication of a-Si:H solar cell, the industry of the active-matrix liquid-crystal display (AMLCD) started. A-Si:H TFT circuits on flexible polyimide substrates had been demonstrated at Iowa State University by Constant et al. in 1994 with two approaches to achieve overlay registration in photolithography. The first approach based on using vacuum compatible epoxy resin to affix the edge of the polyimide substrate to a rigid silicon wafer. To form a polyimide film on a silicon wafer, Constant et al. applied, as a second approach, conformal coating of polyimide on the wafer and then the TFT circuitry was detached from the wafer after its fabrication on top of the polyimide film [18]. A flexible stainless steel foil a-Si:H TFTs had been fabricated in 1996 [19]. By using laser-annealing, flexible plastic substrates polycrystalline silicon (poly-Si) TFTs had been reported in 1997 [20, 21]. Since then, many companies and research groups and companies expanded their research on flexible electronic and flexible displays on either steel or plastic foil substrates have been demonstrated. A prototype rollable electrophoretic display has been demonstrated by Philips in 2005 [22]. On the other hand, a 7" flexible liquid crystal panel was announced by Samsung at the same time [23]. A prototype flexible organic light-emitting diode (OLED) display on steel foil with a poly-Si TFT backplane with full-motion and full-color was presented by Universal Display Corporation and the Palo Alto

Research Center in 2006 [24]. Berggren and Richter-Dahlfors has introduced the term of organic Bioelectronics since 2007 [25]. A particularly attractive challenge of the integration of organic electronic devices and OLEDs with living system has been considered in 2010 [26]. Furthermore, the dye-sensitized solar cells has been developed by Michael Grätzel and Finnish Academy awarded him the Millennium Technology Prize was in 2010 [27]. Some examples of flexible printed electronics can be shown in Figure 2.1. To build functional devices on mechanically flexible substrates, two main processes are involved using solution processable organic, inorganic and hybrid materials.

Figure 2.1: Some examples of printed flexible electronics.

2.2 Organic versus Inorganic Electronics

For more than forty years, inorganic semiconductors such as silicon, germanium and gallium arsenide have been widely used in the microelectronics industry [28-30]. As a result of combinational studies in chemistry, physics and materials science, organic electronics technology was introduced and developed enormously in recent years. Due to the numerous advantages of solution processable semiconductors, which are generally organic based materials such as such as

polymers, oligomers, and hybrid composites, a fast replacing of conventional inorganic materials inorganic materials has occurred.

The most important advantages of solution processable materials are large area of applications, possibility of handling under ambient conditions, low cost electronic circuits, ease control of electrical, optical and magnetic properties, compatibility with light weight and mechanically flexible base materials, ease of device fabrication and electronic tunability. For example, long and expensive fabrication steps of photolithography and high temperature and high vacuum evaporation are required to build a silicon chip. On the other hand, the direct patterning of active material can be provided by using solution processability of organic materials. Also, by using "roll-to-roll" fabrication processes is also possible to manufacture very large area products. A comparison between the most important characteristics of organic electronics can be summarized in Table 2.1

	Inorganic Technology	**Organic Technology**
Economic Differentiation	The cost is high per unit area	The cost is low per unit area
	High capital in dedicated place	Low capital flexible place
Technological Differentiation	small area products	Large area products
	Rigid substrates Fragile	Flexible substrate Robust

Table 2.1: Characteristics of inorganic electronics versus organic electronics [31].

Organic materials are promising candidates which could be used to fabricate almost all levels of electronics [32], such as full color displays, light emitting diodes, wearable electronics namely called "sensitive skin", smart sensors, radio frequency identification tags, pressure-sensitive materials and also individual electronic components such as transistors, capacitors and resistors [33, 34].

Therefore, Organic electronics area recently are the actively working area. Most of the materials used in organic electronics technology are polymeric materials. Major part of the polymers are used as passive insulators because of its electrical resistivity and good mechanical properties. Beside of organic dielectrics material, organic semiconductors and organic metals are also employed in the fabrication of organic devices. Organic semiconductors involve conjugated polymers and organic-inorganic hybrid materials whereas metal nanoparticles, metal nanoclusters, colloidal nanocrystals of metals are the main members of organic metals.

The conduction in organic polymers comes from the delocalized π-electron bonding along the polymer chain. To understand the conduction phenomena, some basics of Organic Chemistry should be introduced. As carbon atoms are the main constituent of organic molecules, thus the electronic configuration will be discussed briefly. The stable configuration of carbon atom is $1s^2 2s^2 2p^2$ with four electrons located in the valence shell. These valence shell electrons give the carbon atom the possibility to bind with other atoms such as with Carbon, Hydrogen, Oxygen, Nitrogen and Phosphor to form molecules. Carbon atom can have up to four bonds. This gives rise to formation of four hybridized orbitals which can be combined in three possible different orbital geometries Sp^3, SP^2 and SP. The Hybridized orbitals for a Carbon atom can be illustrated in Figure 2.2.

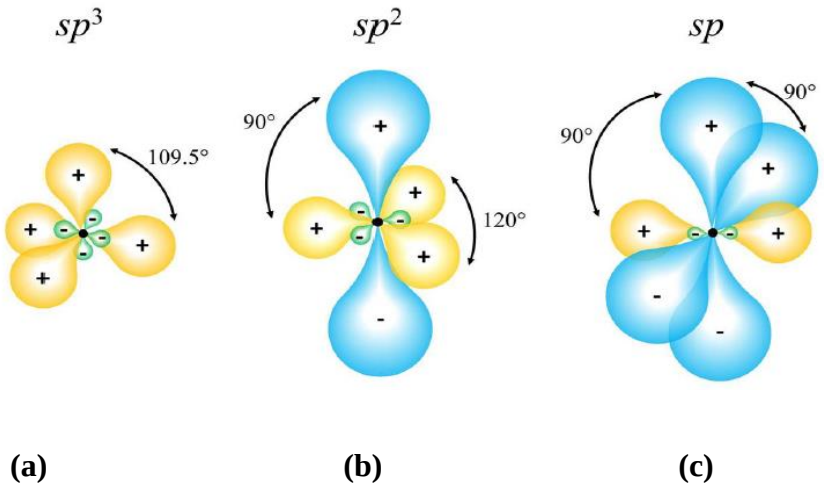

Figure 2.2: The Hybridized orbitals for a Carbon atom (a) sp^3 (b) sp^2 (c) sp.

- ***Sp³-geometry:*** As shown in Figure 2.2a, the 2s orbital combines with all the 2p orbitals. It gives a tetrahedral geometry with four degenerate half-filled orbitals.
- ***Sp²-geometry:*** As shown in Figure 2.2 b, the 2s orbital combines with two 2p orbitals. It gives a trigonal planar geometry with three degenerate orbitals. The unhybridized 2p orbital arranges perpendicularly with respect to the other orbitals. One π-bond is formed when these two unhybridized 2p orbitals overlap.
- ***Sp-geometry:*** As shown in Figure 2.2 c, the 2s orbital combines only with one 2p orbital. It gives a linear geometry with two degenerate orbitals. The two unhybridized 2p orbital arranges perpendicularly to each other and to the direction of the hybridized sp orbitals. Two π-bond are formed when the remaining unhybridized 2p orbitals overlap.

Therefore for the Carbon-Carbon single bond, it is composed of an σ bond which has a binding energy higher than twice the Carbon-Carbon double bond which composed of σ bond and a π-bond. According to the Molecular Orbital (MO)- Linear Combination of Atomic Orbitals (LCAO) theory, 2p orbitals can sum up giving π-bonding orbital or can subtract giving π^*-anti-bonding orbital as shown in Figure 2.3.

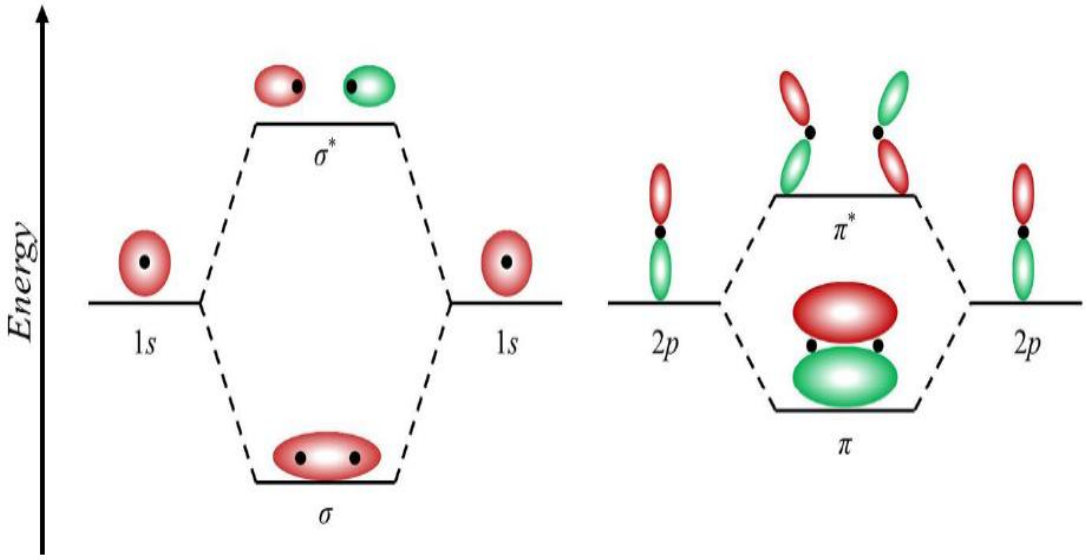

Figure 2.3: Bonding and anti-bonding molecular orbitals.

So the energetic structure of Organic molecules along the polymer chain is obtained from the bonding and anti-bonding orbitals of the single atoms. The energy levels of the polymer chain are discrete levels which are divided into bonding levels and anti-bonding levels. The highest bonding level can be considered as valance band and it is known as the Highest Occupied Molecular Orbital (HOMO). Whereas the lowest anti-bonding level can be considered as conduction band and it is known as the Lowest Unoccupied Molecular Orbital (LUMO). The valence band and the conduction band are separated by an energetic gap (E_g).The energetic gap is the basic principle to determine the electronic and the electric properties of the organic molecules as shown in Figure 2.4. It is important to note that the energy separation for π- π^* orbitals is lower than that for σ-σ^* orbitals.

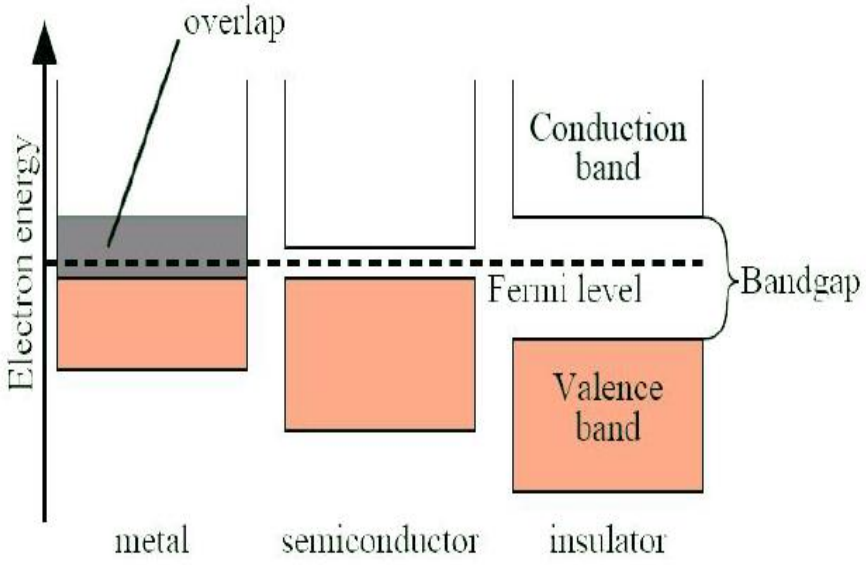

Figure 2.4: A schematic diagram to illustrate the dependence of the electronic and the electric properties of the organic molecules on energy bands.

2.3 Materials used in Flexible Electronics

In this section, a full description of the organic materials used in the organic electronics will be discussed in details. Starting with an introduction to the polymer as it is the main constituent of most of organic electronics. The introduction of organic semiconductors, as a promising candidates of semiconducting materials for the manufacture of active components in flexible electronics will be discussed. Finally, the solution processable metals "Organic metals" will be discussed in details.

2.3.1 Polymers for Flexible Electronics

In 1832, Jacob Berzelius was the first person used the term polymer. Polymer refers to many repeating chemical units or molecules the monomers as shown in Figure 2.5.

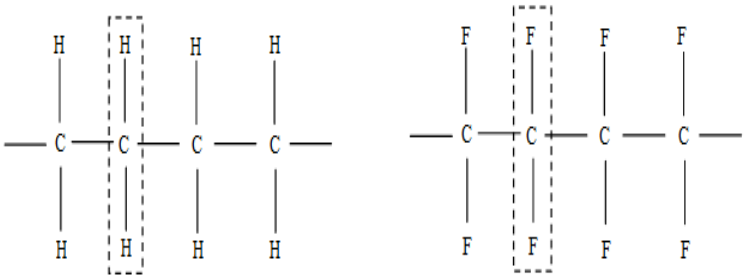

Figure 2.5: Example of some polymers whereas the dashed square show the repeated units.

There are two main bonding forces exist in any polymer, a strong covalent bonds within the back bone of the molecular chain and because of the secondary interchain interactions a second week bonding forces exist between these chains [35]. As the conductivity of polymers decreases for semiconductors at low temperatures and increases for metallic materials leading to superconductivity, polymers are considered as having insulating behavior. The dependence of conductivity of polymers on temperature is summarized in Figure 2.6.

The synthesis conditions and chemical properties of the backbone play an important role on the variation of the mechanical, optical and electrical properties of the polymers. For example, the electrical conductivity of the doped trans-polyacetylene is 10^{7} S/m and for insulating polymers is about 10^{-18} S/m [36]. The rubber has differnt valuse of Young's modulus, it is usually between 10 kPa and 100 MPa. The chemical properties of some polymers, such as poly(cis-1,4-isoprene) and poly(chloromethylstyrene) can be changed if theses polymer is exposed to ultraviolet light [37]. Moreover, the electronic properties of the polymer is determined by the number of repeat chemical units as every repeating unit can be considered as a separate molecule having molecular orbitals in a certain electronic state.

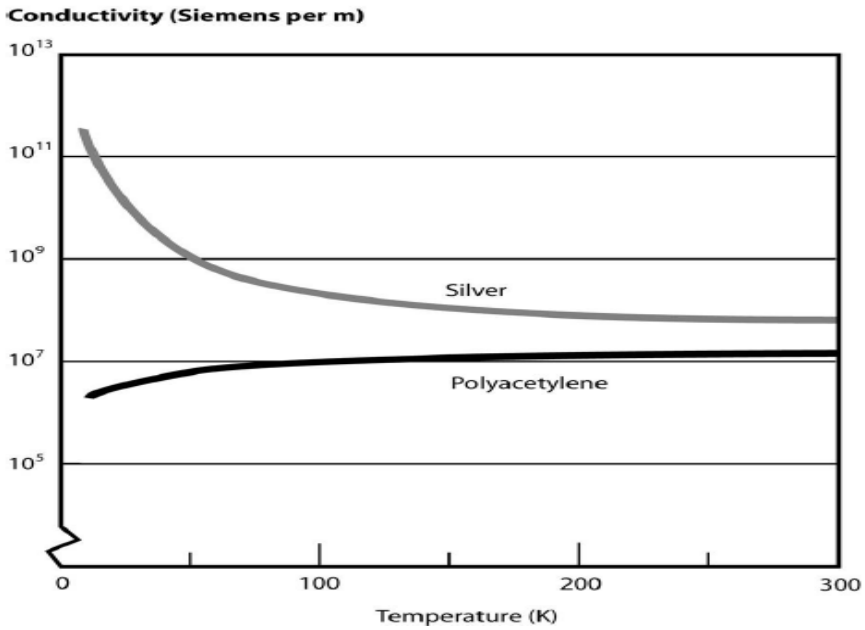

Figure 2.6: The dependence of conductivity of polymers on temperatures. In metals, the conductivity increases at low temperature and decreases in semiconductors, it decreases.

The polymers are generally do not take any active role in the functioning device and are used as a passive material, this attributes to the high electrical resistivity and good mechanical properties of polymers. So, this section will concern with giving an overview of insulating polymers for flexible electronics applications as passive elements. The insulting polymers for electronic devices are classified into four main categories; encapsulants, radiation sensitive polymers, interconnect dielectrics, and substrate materials.

2.3.1.1 Encapsulants

In order to enhance the life time of the electronic device, it is important to protect it from some environmental conditions such as humidity, radiation and mechanical shock. The process of protection is known as "Encapsulation" which is considered one of the most important application area of polymers in electronics. Some fundamental properties should be available in encapsulation polymers such as high resistance to humidity and mechanical and thermal impact, good adhesion, high electrical resistance. The organic encapsulants for flexible electronics have been studied extensively [38- 40], thermosetting polymers, thermoplastics and elastomers are the main types of the organic encapsulants [41].

Silicone compounds, polyimides, polyesters and alkyl resins are classified as encapsulant thermosets [42, 43]. Silicon compounds are the backbone of conformal coatings for integrated circuits. High thermal stability silicon compounds attribute to the high average bond energy of the Si-O bond also the intermolecular forces do not change significantly with temperature. Therefore silicone compounds are the most widely used as encapsulants in electronics [44]. The possibility of changing the organic substitute attached to silicon atoms [$(R_2SiO)_n$] gives rise to control physical properties of silicone such as refractive index, dielectric constant and processability [42].

The most important characteristics of thermoplastic organic encapsulants such as Polystyrene, polyethylene and fluorocarbon polymers are their capability of hardening when cooled and the capability of softening when heated repeatedly [45].

	Solid Silicon	**RTV silicon**	**Polyurethane**	**Polymer resin**
Commerical name	Bisco®	Translastic®	Conathane EN-2	Crastin® PBT
Electrical properties	Dielectric Strength:400 V/mil	Dielectric Strength: 500 V/mil	Dielectric Strength: 645 V/mil	Dielectric Strength: 380-660 V/mil
	Dielectric Constant: 3.0-3.2	Dielectric Constant: 3.1-4.0	Dielectric Constant: 3.42	Dielectric Constant: 3.2
Thermal conductivity (W/mK)	0.21-0.29	0.29-0.31	0.15	0.25
Mechanical Properties	Tensile Strength: 5.3- 7.6 MPa	Tensile Strength: 2.6- 5.9 MPa	Tensile Strength: 5.5 MPa	Yield Stress: 58 MPa
	Elongation: 250-450 %	Elongation: 130-175 %		TensileModulus: 1600 MPa

Table 2.2: Some physical properties of selected organic encapsulants [46].

2.3.1.2 Radiation Sensitive Polymers

Polymethylmethacrylate (PMMA), Poly(hexafluorobutylmethacrylate), Riston® (DuPont), SU-8 (Microchem Corp., Shell Chemicals etc.) and Polysiloxanes are the most commercially available radiation-sensitive polymers [47-49]. This category of the insulting polymers plays an important role in semiconducting application. The idea of the radiation sensitive polymers relies on their sensitive to high-energy radiation such as ultraviolet light. After exposure, molecular rearrangement occurs following by changing the chemical properties of the exposed area. This idea is the basic principle of the photolithography process in electronics which in turn easing the fabrication of advanced logic and memory chips [37, 44].

2.3.1.3 Interconnect Dielectrics

Low dielectric constant, low dissipation factor, high mechanical strength, ability to withstand high temperature, high electrical and chemical resistance to form multilayer films without producing mechanical defects are the main characteristics of the polymeric interconnect dielectrics. Extensive studies have been performed to search for polymeic interconnect dielectics [50, 51]. It is found that polyimides group and parylenes group are the most common examples of polymeric interconnect dielectrics [52]. Parylenes group are limited to some applications because of their poor temperature stability in air so they need special vacuum deposition processing to form thin films. The physical and chemical properties of commonly used polymeric interconnect dielectrics can be summarized in Table 2.3.

Properties	**Polyimide**	**Parylene**	**Polyphenyl Sulfide**
Process Temperature (°C)	300-350	80	>315
Decomposition Temperature (°C)	450	125	1000
Dielectric Constant	3.2-3.8	2.65-3.15	3.0-4.4
Dissipation factor	0.01-0.02	0.0002-0.02	0.01-0.068
Thermal Conductivity(W/cm.C)	0.0017	0.36	0.8
Density (g/cm^3)	1.42	1.11-1.42	1.35-1.40

Table 2.3: Some physical properties of selected interconnect dielectrics [42, 53].

2.3.1.4 Substrates

Low cost, ease of manufacture, frequency or mechanical strength and reparability are the basic parameters affecting the choice of polymeric materials that are used as substrate materials in flexible electronics depending on the physical characteristics required by the application.

Polyimide film (Kapton®), Poly(ethylene therephthalate) (PET), Poly(ethylene naphthalate) (PEN), Poly(dimethylsiloxane) (PDMS), poly(4,4'-oxydiphenilene pyromellitimide), and Poly(1,1-difluoroethylene-1,1,2-trifluoroethylene) (PVDF- TrFE) can be used as base material in flexible electronics. The most employed substrate in flexiable applications are PET, PEN and Kapton®. Because of the mechanical properties of PDMS, it can be used as substrate and as encapsulation layer. A full detailed description of each type of substrate can be introduced as follows:

Polyimide film (Kapton®)

It is one of the most commonly used substrates in flexible electronics applications. Polymerizing an aromatic dianhydride and an aromatic diamine [47] is result in synthesis of Kapton. It can be used to produce laminates with metal such as copper [54]. Despite of having excellent solvent resistance, thermal stability and adhesion, it has difficult fabrication steps and its cost is too high [53].

Poly(ethylene therephthalate) (PET)

It is derived from the polyester family. The working temperature of that polmer is from -40 to 115 °C. This thermoplastic polymer has very interesting properties such as good resistance to most of solvents except alkalis and excellent tensile strength averages between 190 and 260 MPa. PET undergoes irreversible deformation under high temperature which is an undesired effect for the fabrication of OFET-based strain sensors. The structure of PET can be shown in Figure 2.7.

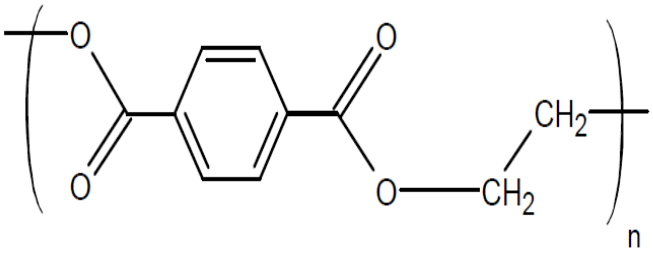

Figure 2.7: The structure of Poly(ethylene therephthalate) (PET).

Poly(ethylene naphthalate) (PEN)

It is also thermoplastic polymer, it can be heated nominally up to 150 °C. It has good resistance to most solvents, even to alkalis. The high surface roughness is the main drawback of this polymer which is an undesired property especially for the deposition of thin layers. The structure of PET can be shown in Figure 2.8.

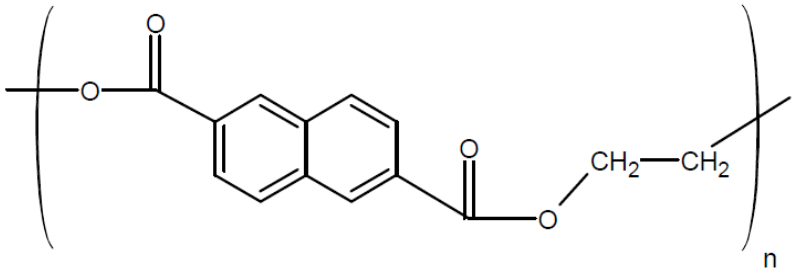

Figure 2.8: The structure of Poly(ethylene naphthalate) (PEN).

Poly(4,4'-oxydiphenilene pyromellitimide)

It is also named as the name Kapton HN®. This polyimide film is developed byDuPont® [47]. It is widely used in different applications fields such as spacecraft, coverage for aircraft and x-ray instrumentation because of its radiation resistance and the wide range of the working temperature from -270 to 300 °C. It is the best candidate substrate for post-processing annealing of organic printed layers owing to its thermal resistance for temperatures as high as 200 °C. The structure of Poly(4,4'-oxydiphenilene pyromellitimide) can be shown in Figure 2.9.

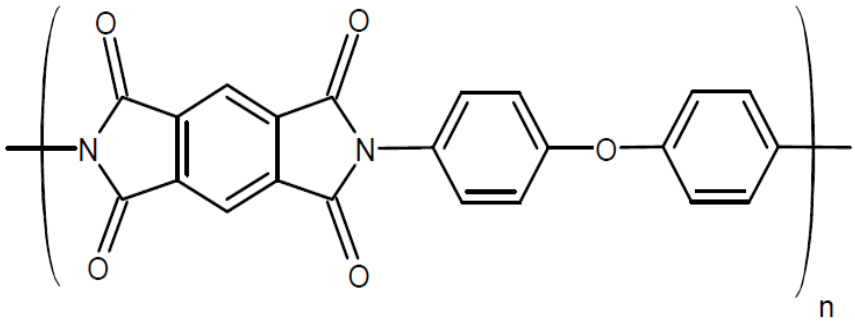

Figure 2.9: The structure of Poly(4,4'-oxydiphenilene pyromellitimide).

Poly(1,1-difluoroethylene-1,1,2-trifluoroethylene)

It is special type of plastic copolymer, it is derived from the fluoropolymer family. it is composed of two monomers of alternated repetition, 1,1-difluoroethylene and 1,1,2-trifluoroethylene respectively. This copolymer is also known as poly(vinylidene difluoride trifluoroethylene) (PVDF-TrFE). Piezoelectricity and pyroelectricity are the interesting properties of PVDF-TrFE. The Piezoelectricity comes from 1, 1-difluoroethylene whereas the pyroelectricity comes from 1, 1, 2-trifluoroethylene. PVDF-TrFE is usually employed in applications which require pressure sensing such as optical devices, medical instrumentation, acoustic components, transport, and more. PVDF-TrFE has low thermal resistance and undergoes irreversible deformation at temperature higher than 50 °C which is an undesired effect for the post processing. The structure of Poly PVDF-TrFE can be shown in Figure 2.10.

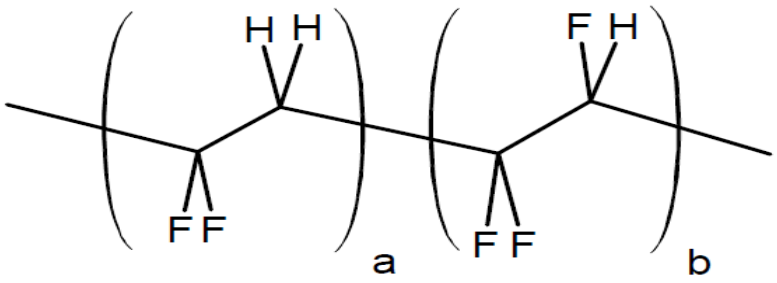

Figure 2.10: The structure of Poly(1,1-difluoroethylene-1,1,2-trifluoroethylene) (PVDF-TrFE).

Poly(dimethylsiloxane) (PDMS)

It is an amorphous polymer with viscoelastic properties in its solid form i.e. it is elastomer. PDMS has high failure strain and low Young's modulus compared with other materials. PDMS can be used as substrate and as encapsulation layer owing to its mechanical properties. The chemical structure of PDMS can be shown in Figure 2.11.

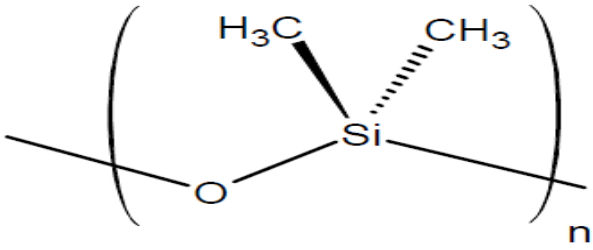

Figure 2.11: The structure of Poly(dimethylsiloxane) (PDMS).

2.3.2 Organic Semiconductors

List and description of organic molecules employed for specific applications of organic electronics have provided by several articles [55]. Feast et al. [56] suggested a general classification of organic polymers on the basis of their structure into three major groups: Hydrocarbons, Heterocyclic Polymers or organic-inorganic polymers, and short polymer chains or oligomers.

2.3.2.1 Hydrocarbons or Conjugated Polymers

The conjugated polymers acts as semiconductors that emit light and conduct current owing to the possibility of transport charge (holes and electrons) due to the π-orbital overlap of neighboring molecules. By doping the conjugated polymers with an oxidizing or a reducing agent, their electrical conductivity of can be controlled. Alan J. Heeger, Alan G. MacDiarmid and Hideki Shirakawa discovered the highly conductive polyacetylene as a type of conjugated polymers and thus received Nobel Prize in Chemistry in 2000. The low mobility of the main disadvantages of conjugated polymers. Polyacetylene, as the simplest polyconjugated organic polymer, consists of a linear chain of Carbon atoms with alternating single bonds and double bonds between them. The structure of polyacetylene can be shown in Figure 2.12.

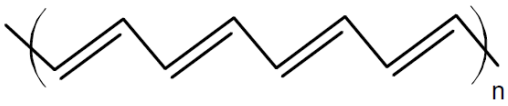

Figure 2.12: The structure of polyacetylene [57].

Also, polydiacetylenes, as another type of hydrocarbons, consists of Carbon atoms with alternating single and triple bonds between them, and two different functional groups. This polymer is employed for the development of several organic films and for the immobilization thanks to the variety of the possible functional groups. The structure of polydiacetylene can be shown in Figure 2.13.

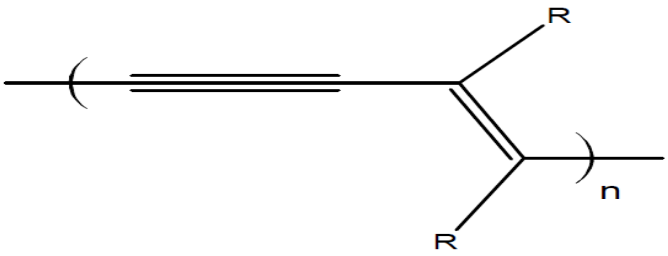

Figure 2.13: The structure of polydiacetylene.

Another class of conjugated polymers is Polyphenylenes group. This class is based on the benzenic ring. Poly(p-phenylene) is the most commonly used type of this group as precursor of other organic composites due to good electrical properties together with good thermoplastic properties. The structure of Poly(p-phenylene) can be shown in Figure 2.14.

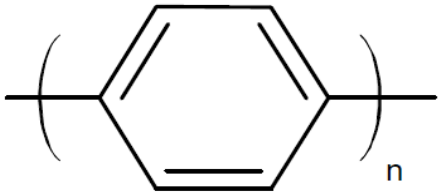

Figure 2.14: The structure of Poly(p-phenylene).

Another class of conjugated polymer which is between polyacetylene and polyphenylene is Poly(phenylene vinylene) (PPV). Poly(phenylene vinylene) is one of the most important candidates for polymer-based optoelectronic applications, such as Organic Light Emitting Diodes (OLED) for photovoltaic devices and mobile telephone displays. The structure of the Poly(phenylene vinylene) can be shown in Figure 2.15.

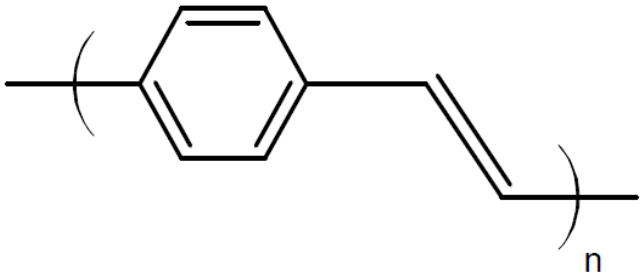

Figure 2.15: The structure of Poly(phenylene vinylene) [57].

The low mobility is the major drawback of conjugated polymers compared to that of inorganic semiconductors. Organic-inorganic hybrids will be discussed in details in the next section as another promising family of semiconductor materials for flexible electronics applications.

2.3.2.2 Heterocyclic Polymers (Organic-inorganic hybrids)

The desirable characteristics of both inorganic and organic are integrated into one molecular composite [58]. Heterocyclic polymers are composed of a cyclic compound with two different member of the ring, carbon as a base element and another substituting element. Several classes of heterocyclic polymers with the different chemical and physical properties are formed depending on that substituting element.

Polythiophenes are example of the heterocyclic polymer, Polythiophene consists of five-membered rings, where one of carbon atoms has been replaced with Sulfur atom. Polythiophenes can provide a range of optical and electronic responses as they are the best candidates for the realization of organic sensor devices and organic Field-Effect Transistors (OFET) because of their excellent reactivity to environmental condition and their good optical properties in addition to the

most interesting electrical conductivity. The structure of Polythiophenes can be shown in Figure 2.16.

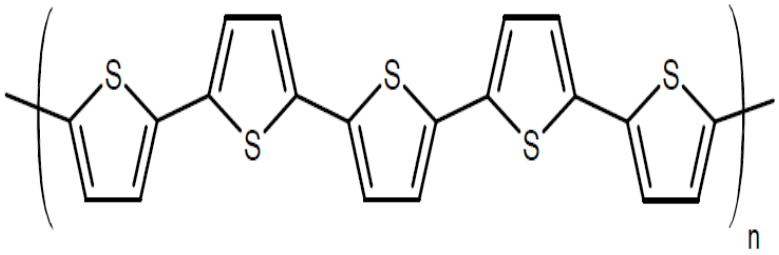

Figure 2.16: The structure of Polythiophenes.

Polypyrroles are quite similar to that of polythiophenes, polypyrrole as a monomer is composed of five-membered rings where one of the Carbon atoms has been replaced with Nitrogen atom. Polypyrrols have the same characteristics of Polythiophenes regarding to their excellent reactivity to environmental condition. So, they are good cndidates for chemical sensors and organic Field-Effect Transistors (OFET) as polythiophenes. The structure of polypyrroles can be shown in Figure 2.17.

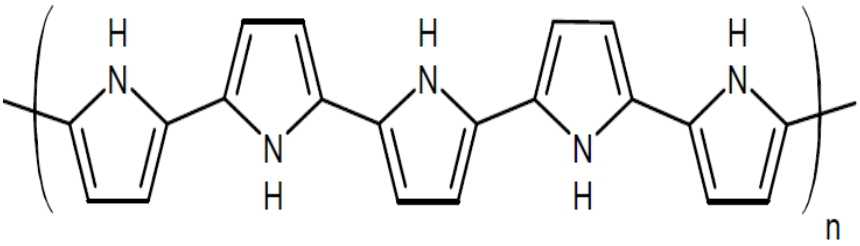

Figure 2.17: The structure of polypyrroles.

Another polymer of the heterocyclic polymers group is polyaniline. It is composed of a series of a benzene ring and a Nitrogen atom, which is linked to a Hydrogen atom. The ease of production processes, the low-cost and the stability of its conducting forms are the main advantages of Polyaniline. Manufacturing as electrically conducting systems, as a corrosion inhibitor, as electromagnetic shielding of electronic circuits, biosensors and realizing acid/base chemical

vapour sensors are the main applications for Polyaniline. The structure of Polyaniline can be shown in Figure 2.18.

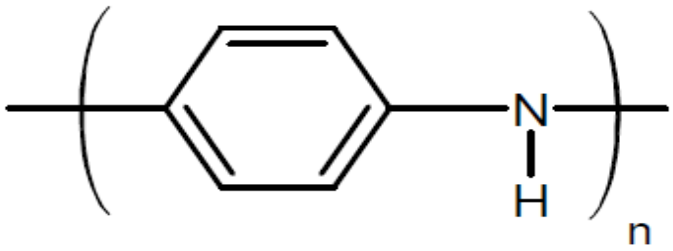

Figure 2.18: The structure of Polyaniline [57].

2.3.2.3 Oligomers (short polymer chains)

Oligomers are composed of a small repetitions number of monomers. The higher mobility than conjugated polymers is the main advantage of oligomers [59]. As the benzene ring of Pentacene is repeated only five times, it is considered as an example of oligmers which uses in the synthesis of organic thin film owing to its high performance and potential [60].

Another examples of oligomers is the oligothiophenes group, which is composed of few thiophene monomers. Hyperpolarizability, good electrical conductivity, and thermochromism are the interesting properties of oligothiophenes group. One of the most familiar member of oligothiophenes group is α-sexithiophene. This compound is a promising candidate used for the realization of organic transistors.

Oligopyrroles and oligoanilines are two more examples of oligomers. Because of the complexity of their structure, they have not been widely investigated. The electroluminescent properties are the considerable attracted interest of them. Solution processable metals, the last group of organic materials will be briefly summarized in the next section.

2.3.3 Solution processable metals "Oragnic metals"

The possibility of introducing new applications and developing new products can be achieved by making use of the unique properties of metallic nanoparticles such as surface effects and small size effects. Organometallic compounds and encapsulated or chemically modified metal nanoparticles are the two main groups of solution processable metals. Gold nanoparticles, silver nanoparticles,

copper nanoparticles and others nanoparticle have been studied as promising ink particles. Metal nanoparticle inks offer the best performance when high conductivity is required. The most stable metal nanoparticles are gold nanoparticles. Owing to its very high conductivity, they are widely employed in the electronic industry as well. Gold nanoparticles can be patterend on different substrates including plastics by inkjet printing, micro contact printing, photolithography, and self-assembly. Due to the ability to reduce carbon dioxide, platinum and palladium nanoparticles have particular importance as catalysts. Platinum and palladium nanoparticles are also excellent catalysts for hydrogenation [61]. An ether soluble titanium nanoparticles $[Ti(0)\cdot 0.5\ THF]_x$ can be used as an activator for heterogeneous hydrogenation catalysts has been reported by Bönnemann and Brijoux as organic metals [62].

Silver nanoparticles are employed in the electronic industry and used in many different areas such as catalysis, optics, and surface-enhanced Raman scattering due to low reactivity in air and the its highest conductivity of all metals [63- 65]. Silver nanoparticles can be stored for long time at room temperature in solid form without any oxidation or degeneration so many stable dispersions are commercially available. A fairly homogenous and highly stable dispersion of silver NPs is suitable for a wide range of fabrication of flexible electronic devices. It is recommended to a void high humidity conditions because it results in short circuit failure due to the electrochemical migration of silver [66]. Also, for cost-sensitive applications, the relatively high cost of silver remains a limitation. On the other hand, Copper NPs are highly interesting because its price are 1% and its electrical conductivity is 95% of that of silver NPs. Therefore, copper NPs are considered suitable substitutes for silver NPs [67]. In ambient conditions, the reactivity of copper NPs is challenging compared with silver NPs. For highly conductive and low cost printed electronics applications, copper is still the promising metal. The following section will concentrate on the possible manufacturing methods which can be used to integrate organic materials into functional devices.

2.4 Fabrication Technology for Flexible Electronics

The variety of device fabrication methods is one of the most important advantages of conducting polymers. To fabricate organic electronic devices, some researchers use traditional vacuum and lithography methods [68- 70]. But traditional methods are considered expensive methods because of requiring high temperature and high vacuum toward some production steps such as plasma etching and chemical or physical vapor deposition. Solution-based preparation methods are inexpensive and potentially environmentally friendly and at the same time are characterized by atmospheric pressure and room temperature. On the basis of the advantages of solution-based preparation methods, new fabrication techniques, have been introduced recently. In this section, different techniques which involve in the fabrication of organic electronic devices such as spin coating, spray technique, screen printing and inkjet printing technique, will be explained.

2.4.1 Spin Coating Technique

The spin coating technique is considered the quickest and most reproducible method so it was employed for decades to deposit anti-reflective coatings on optical components [71] deposit Photoresists [72], and protective coatings [73]. Many advantages of this technique can be mentioned such as the ability to o produce monolayer and the ability to control the film thickness by adjusting spin time and spin speed.

Figure 2.19 shows the operation principle of spin coating which involves principally dispensed a suspension or a liquid by a pipette onto the desired surface which place on the center of a rotating cylinder via vacuum pumping. Two main parameters should be adjusted to get the desirable thickness; spin time and spin speed. In addition to these two parameters, it is necessary to take some additional factors into consideration such as the amount of solid content in the suspension [74], surface tension of the liquid [75], the viscosity and volatility of a solvent [76]. The net viscosity of the suspension increase as the substrate rotates owing to evaporation of the solvent until the liquid no longer spreads. Various forces are involved during the spin coating process, such as viscous force, evaporation rate of the solvent, centrifugal force. For non- volatile suspension or for a suspension in a low-viscosity solvent, a high spin coating speed is require to get a thinner film.

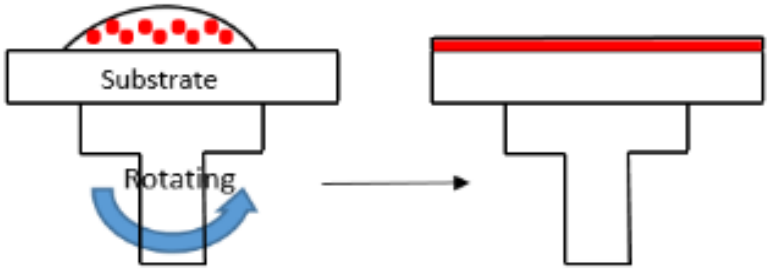

Figure 2.19: Schematic of the spin coating technique.

2.4.2 Screen Printing Technique

Screen printing method is environmentally friendly and a very simple printing process. It is used generally for depositing ceramic and polymer "inks" to manufacture for example conductive interconnections between electronic components on circuit boards. Figure 2.20 represents the principle operation of the screen printing process which involves pattering the ink by means of a stencil. The ink is placed upon a screen mesh and it is pushed by moving a squeegee blade across the screen mesh. The result of this process is obtaining a material pattern on the substrate which placed below the screen mesh [77]. High viscosity materials including various adhesives materials, conductive inks, UV curable materials, and dielectric pastes can be used by screen printing technique. This method is compatible with high viscosity materials including conductive inks, dielectric pastes, UV curable materials and various adhesives.

By using a screen mask made of a stainless steel fabric with 400 mesh count/in, organic FETs were fabricated by Bao et al. through depositing an insulating polymer layer (polyimide) and a source-drain electrode (conductive ink 479SS from Acheson Co.) [78]. Also by screen printing semiconductor active layer of poly(3-alkythiophene), organic FETs were manufactured by Knobloch et al. [79]. Some researchers reported manufacturing a wide range of applications by using Screen printing technique such as Screen printed inductors [80], strain sensors [81], biosensors [82, 83], gas sensors [84, 85], and solar cells [86, 87].

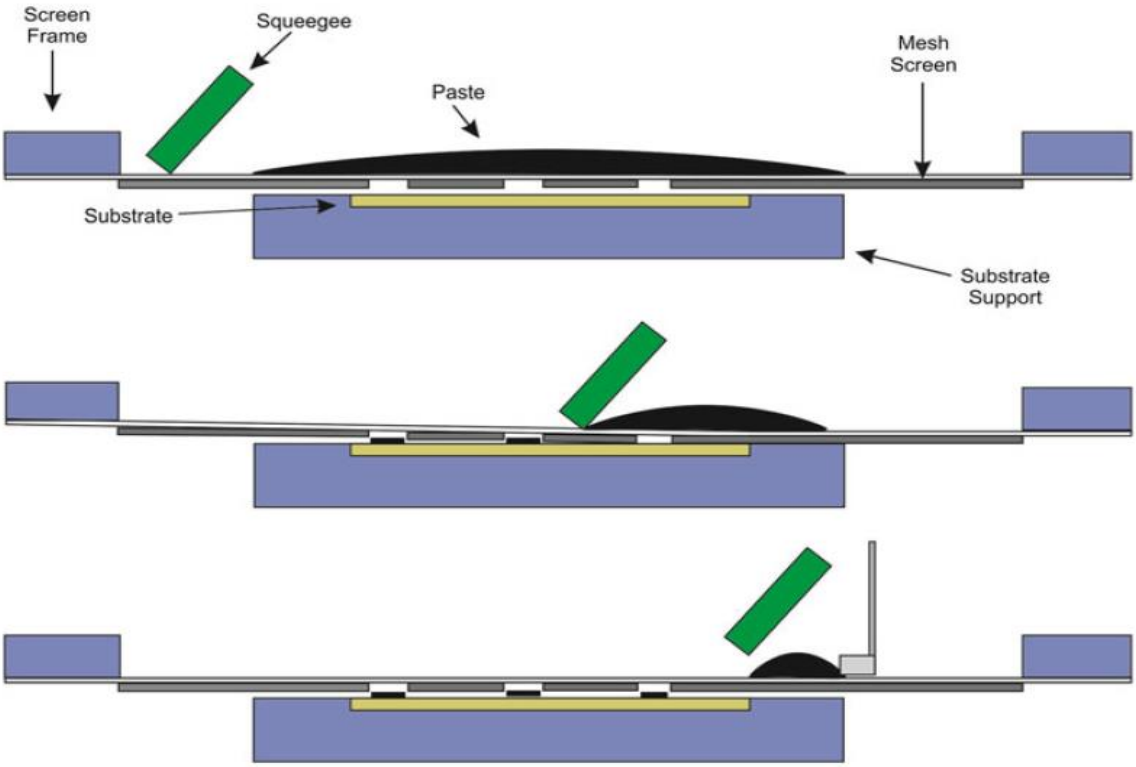

Figure 2.20: Schematic of the screen printing process.

2.4.3 Spray Deposition Technique

One of the most widely used coating techniques is spray technique. It is non-contact printing technique used for electronic printing. The types of spray technique such as electrostatic spray technique, air pressure spraying technique, and Hybrid spraying technique will be discussed in details.

2.4.3.1 Electrostatic spray technique

By applying a high voltage, micro droplets can be generated from the solution injected into the capillary tube of the nozzle as shown in Figure 2.21. An extremely strong electric field at the tip of the capillary is generated by applying a high electric potential to the capillary which result in elongation of a jet and obtaining extremely small and highly charged droplets. The magnitude of the charge is up to a fraction of the Rayleigh limit at which the surface tension force is overcome leading to drop fission [88, 89]. The electric field strength is high if the outer diameter of the capillary tip is small or the applied voltage is high resulting in generating small droplets from the injection solution. One of the requirements of organic electronics device application is forming a

dense thin film with a good surface roughness and this can be achieved by using electrostatic spray technique. The main drawback of that technique is the probability of nozzle clogging owing to the long time process to coat by obtaining smaller particles from a small nozzle.

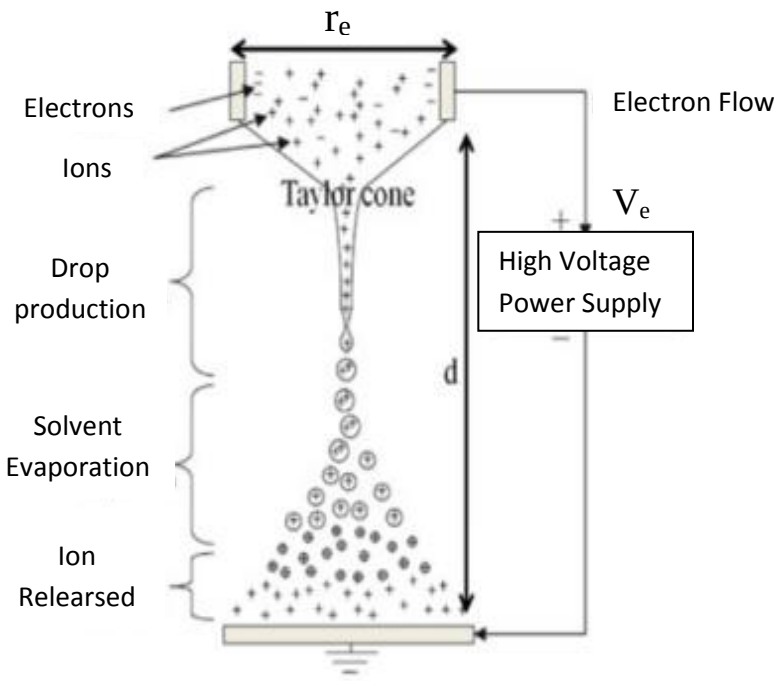

Figure 2.21: An electrostatic spraying system with a single spray nozzle [90].

2.4.3.2 Air pressure spray technique

For organic light-emitting diode (OLED) manufacturing or organic photovoltaic (OPV) device, a large-area coating is required and this cannot be achieved by electrostatic spray technique. The air-pressure spray technique is introduced as a continuous process at which its nozzle consists of two parts a large external nozzle and a small internal nozzle with a diameter in the range of 100 µm, as shown in Figure 2.22, which overcome the nozzle clogging problem. The air pressure spray technique involve an unavoidable phenomena which result from the collision of the generating droplets with air. The collision results in an unstable velocity of flow. To avoid the air turbulence, a high air pressure can be used to obtain smaller droplets for forming a thin film with good surface roughness. On the other hand using high air pressure causes much damage to the surface of thin film made of organic materials.

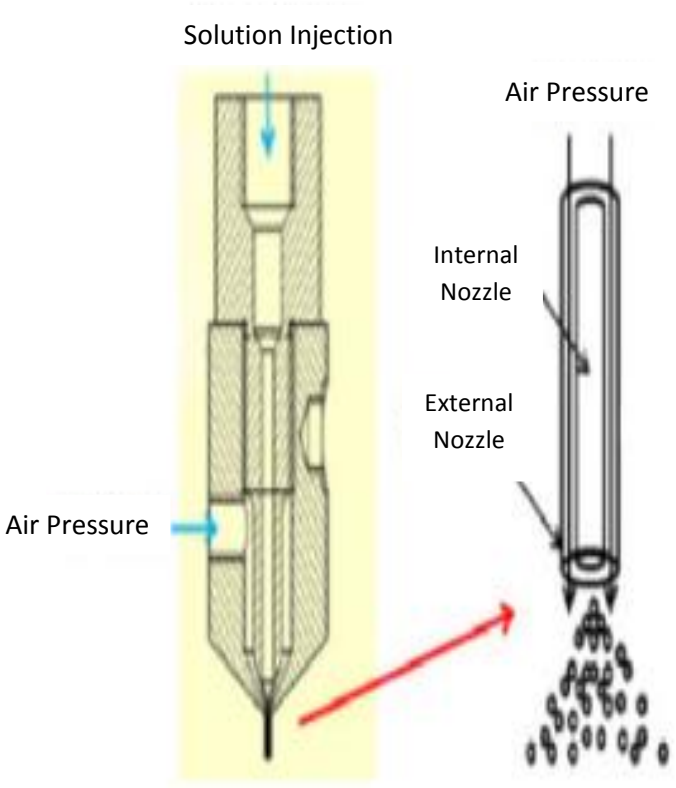

Figure 2.22: The nozzle of air pressure spray technique [90]

2.4.3.3 Hybrid spraying technique

In this hybrid technique, generating smaller droplets and at the same time improving the stability of the spray is achieved by combining air spray technique with electrostatic spray technique. The working principle of the hybrid spraying technique depends on both the air pressure and electrostatic spray force. The spray force of air pressure spray technique is used firstly by supplying the air pressure in the gap between the external nozzle and the internal nozzle. By applying a high voltage, the external nozzle is charged. Finally, the generated charged droplets are directed on the substrate without any shifts. The hybrid spray technique and the materials used in this thesis will be discussed in details in chapter 3.

2.4.4 Inkjet Printing Techniques

Inkjet Printing techniques are one of material deposition techniques which recently have been acquired a great attention. Much effort has been done in order to deposit minute quantities of materials accurately by turning ink jet printing into a versatile tool for various industrial manufacturing applications [91]. In the field of defined polymer deposition such as the manufacturing of polymer electronics, and manufacturing of multicolor polymer light-emitting diode (PLED) displays, inkjet printing is one of polymer deposition key technologies. No-mask patterning, low cost, simplicity of fabrication, feasibility of non-contact, compatibility with different substrates, and low temperature processing are the main features of inkjet printing techniques [92, 93]. A schematic classification of the different inkjet-based printing technologies can be shown in Figure 2.23. Continuous inkjet printing (CIJ) and drop-on-demand (DOD) inkjet printing are the two main operation modes of inkjet printing [91]. The working principle of each operation mode of inkjet printing can be shown in Figure 2.24.

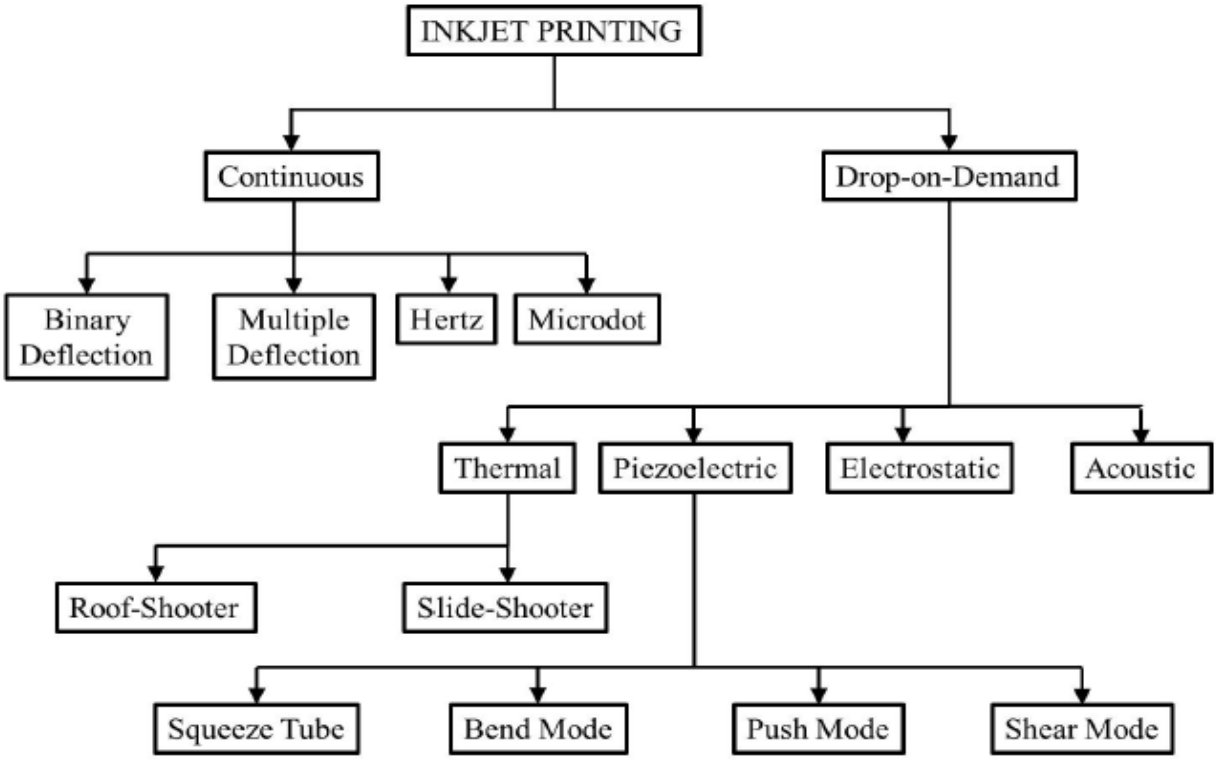

Figure 2.23: Schematic classification of the different inkjet-based printing technologies.

Uniformly sized droplets can be pumped through a nozzle in continuous inkjet printing operation mode by applying sufficient pressure to a common ink reservoir. To break-up into uniformly spaced stream droplets, a periodic signal at the nozzle is applied. The main application of that mode is for high-speed graphical applications such as labeling and textile printing. On the other hand drop-on-demand (DOD) operation mode is the most familiar used method in all applications because it produces smaller drops as needed and at the same time higher placement accuracy in comparison to continuous inkjet printing mode. The drops formation can be generated either by piezoelectrically pulses or thermally pulses.

Continuous-mode inkjet printing (CIJ) **Drop on demand-mode (DOD)**

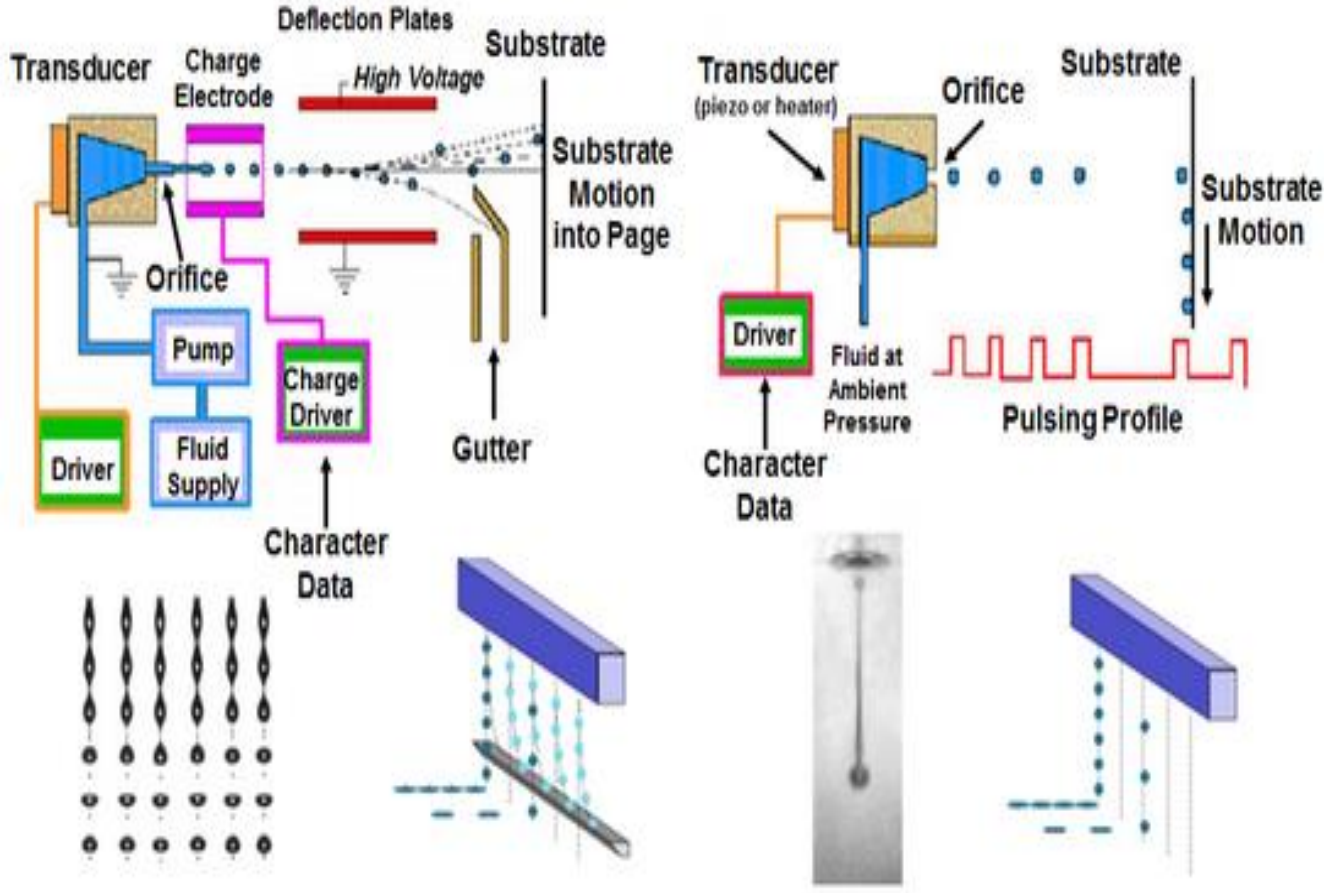

(a) **(b)**

Figure 2.24: The working principle of (a) Continuous inkjet printing (b) Drop on Demand Inkjet printing [98].

To eject droplets in a thermal drop-on-demand inkjet printer, the working principle relies on locally heating the ink in order to eject droplets by forming a rapidly expanding vapor bubble. Using water as a solvent is the main drawback of thermal DOD as it can be used only for limited numbers of polymers. On the other hand, the working principle of piezoelectric DOD inkjet printers depends on causing a sudden volume change of some piezoelectric materials and therefore generating an acoustic pulse. The main advantage of Piezoelectric DOD is its capability to use a variety of solvents but the viscosity and surface tension are the most crucial part of the piezoelectric DOD inkjet printer "The Fujifilm Dimatix Materials Printer DMP-2831" is the main technique used in this thesis as will be discussed in details in chapter 4.

2.4.5 Three-dimensional Printing Technique

Three-dimensional printing technique is a cost effective method for rapid prototype production. It is related to a number of other mold-free manufacturing techniques where the components are created layer by layer at the micron level from fine powder materials. The technique aims to create a complex stable and light shape directly from a computer file by slicing CAD data with professional software [95]. By Sintering, polymerization or fusing of materials, the models are fabricated with no needs of tools. Thickness of the layers range from 10Âµm up to 200Âµm depending on the used machine and parameters. The advantage of that technique is the quality of the final products can be controlled as the layers are clearly visible on the part surface in the operation of additive manufacturing. There is a relation between surface orientation and the thickness of layer which is known as staircase effect where a high resolution and a long processing time are required for a thin layer.

The additive printing method is a high-throughput process because of its interesting advantages such as uses device materials efficiently, doesn't require vacuum through manufacturing, and may provide a solution to overlay registration problem through digital compensation. This method is compatible with printing Noble-metal conductors, organic conductors, semiconductors, insulators, as well as certain inorganic materials [96, 97]. A wide range of applications can be involved by using this method such as printing organic TFTs [98, 99] and masks for etching or lift-off patterns [100, 101].

2.5 Summary

An overview of flexible electronics technology research is introduced in details in addition to a comparison between the characteristics of inorganic semiconductors and organic semiconductors. Also, the challenges of materials used in flexible devices is discussed. The scalable manufacturing of solution-processable thin-film electronics, describing the basic working principles, the main advantages and disadvantages is involved.

Chapter 3

Spray technique for CNTs deposition on different substrates

As stretchable and flexible conductors are significant components of optoelectronic and electronic devices that facilitate human interaction and compatibility such as interactive electronics, robotic devices with human-like sensing capabilities and implantable medical devices, carbon nanotubes (CNTs) are the suitable materials for these applications. In this chapter, an overview on CNT thin-films on different substrates will be introduced. A high quality CNT thin-films through a reproducible, reliable, and low cost spray deposition technique will be investigated. Also the preparation method for fabrication of SWCNT films using sodium dodecyl sulfate (SDS) as dispersive agents will be explained in details. The performance of CNT thin-films deposition on different rigid substrates such as glass, ITO-coated glass, and spectrosil substrates) will be demonstrated including a comparison of the morphological features of the thinnest CNT films on the different substrates. A high transparency with a mean transmittance of 97% at 550nm is achieved. Also, SWCNT thin-films with a sheet resistance of 165 Ω/ with a mean transmittance of 83% without any further doping are presented. The work function values for CNT films deposited on different rigid substrates will be also studied at which surface treatment and layer thickness have no effect on the work function.

On the Other hand, CNT thin-films deposition on flexible substrates such as ITO-PET and PET substrates will be also analyzed where two films with high and low CNT density were prepared on PET substrate. From the AFM analysis, a comparison between the two CNT densities on ITO-

PET, PET and glass in the term of surface coverage will be also investigated. The work function of CNT films on flexible substrate will be also studied. Finally, study of the photogenerated carrier dynamics and frequency resolved complex photoconductivity in CNT films on PET substrate using time-resolved THz spectroscopy will be also involved.

3.1 Overview on CNT Thin-Films on Flexible Electronics

For flexible electronics, carbon nanotubes (CNTs) are ideal candidates as transparent electrodes and as the channel material in field-effect transistors (FETs) due to their remarkable properties such as high conductivity, the potential for production at low cost, high intrinsic carrier mobility, and high mechanical flexibility [102- 104]. Carbon nanotubes are considered as sheet of graphene at which they can exist either as a multiwalled nanotube (MWCNT) or as single-walled nanotube (SWCNT) according to the created state along the graphene sheet, either metallic electronic states or semiconducting states [105]. The schematic diagram of SWCNTs and MWCNTs n be shown in Figure 3.1. SWCNTs possess high conductivity (up to 400000 S cm^{-1}), high mobility (on the order of 100000 $cm^2V^{-1}s^{-1}$), low mass density, and tube diameter-dependent band gap (Egap $\approx 1/R_{tube}$) for semiconducting nanotubes as shown theoretically and experimentally [106, 107].

Many researches and studies focused on nanotube thin films and device applications such as mechanical and chemical sensors [108, 109], transistors and circuits [110, 111], and transparent electrodes [112- 117]. CNT thin films can be used as the active layer in thin film sensors and transistors due to their semiconductor behavior [118- 124]. Films with thickness in the range of 10-100 nm can be used as a replacement for indium-tin-oxide (ITO) electrodes as they possess high optical transparency and electrical conductivity [118]. For fuel cells, supercapacitors, and battery applications, Micrometer-thick nanoporous CNT films can be used as electrodes [125-136]. Forming stable dispersions and modification of nanocarbon materials to improve the dispersability are two main considerations should be take into account.

A full description of the main conducting mechanisms of CNT networks has been introduced by Bekyarova et al. through characterization of conductivity and transmittance of spray deposited thin films with differently functionalized CNTs [137]. On the other hand, the same is done by Kim et al. by making a comparison of the performances of organic solar cells with CNT electrodes

obtained via spray and spin deposition techniques using different dispersants [138]. Recently, for the deposition of CNT thin-films on flexible substrates, several techniques have been reported such as spray deposition and spin coating techniques. The limitation of film thickness obtained by spin coating is the main disadvantage of that technique and thus the spray coating is the promising technique [138].

Some approaches for fabrication of carbon nanotubes on flexible substrates have been introduced. An approach to prepare printable elastic conductors comprised of uniformly dispersed in a fluorinated rubber single-walled carbon nanotubes (SWCNTs) has been developed by Sekitani et al. [139]. A stretchable supercapacitor based on buckled single-wall carbon nanotubes (SWCNTs) macrofilms obtained by spray coating technique have been reported by Yu et al. [140]. A class of wearable and stretchable devices fabricated from thin films of aligned SWCNTs has been developed by Yamada et al [141]. Flexible and stretchable SWCNTs conductive film on the PDMS as a substrate has been reported by Liu et al. [142]. Transparent and stretchable supercapacitor based on highly aligned multi-wall carbon nanotubes (MWCNTs) sheet with excellent stretchability and transmittance has been reported by Chen et al. [143].

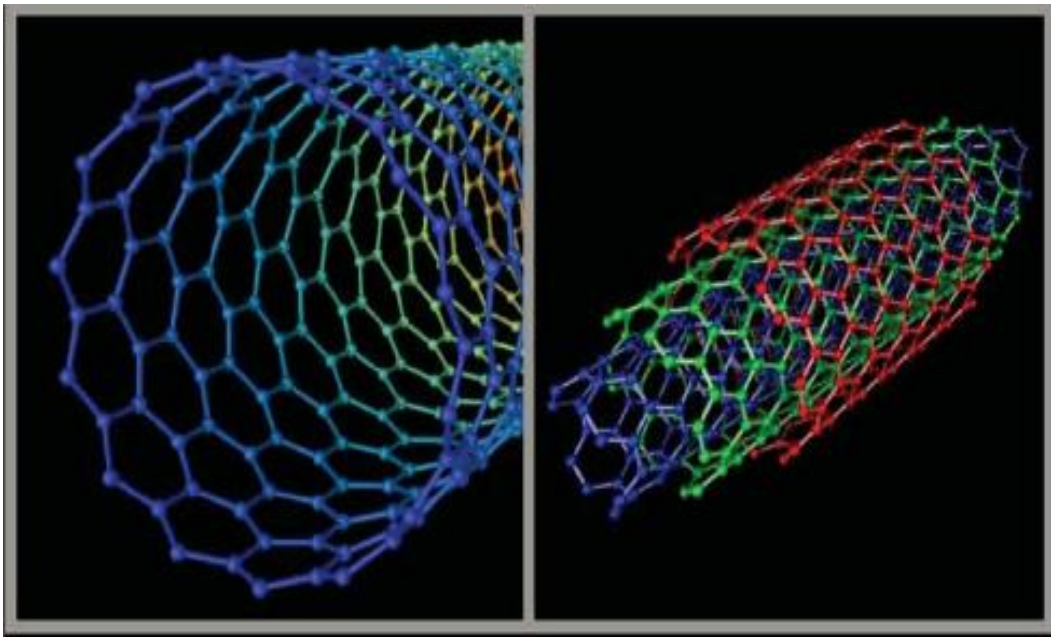

Figure 3.1: Schematic diagram of (a) single-wall carbon nanotubes (SWCNTs) (b) multi-wall carbon nanotubes (MWCNTs) [144].

3.2 Materials and Methods

3.2.1 Preparation of Carbon Nanotubes Dispersion

As mentioned in the previous section, forming stable dispersions and modification of nanocarbon materials to improve the dispersability are two main considerations should be take into account to get a homogenous and high quality patterns. In addition to these two main factors, choice of surface treatment and removal of dispersing aids after deposition are also important parameters for high quality CNTs deposition. The first step toward preparation the desired dispersion is overcoming strong van der Waals forces exist between the CNTs bundles. This challenge can be achieved via high power sonication of purified powder of CNTS dispersed into a suitable solvent. CNTs can be dissolved in organic solvents with limited solubility so to yield high quality dispersion, it is preferable to used surfactant based aqueous dispersion. So all experiments in this thesis are based on CNT aqueous solutions. The most widely used surfactants sodium dodecyl sulfate (SDS), sodium dodecyl benzene sulphonate (SDBS), carboxymethyl cellulose (CMC), and Triton X-100 and are water soluble and hence can be removed by subsequent washing of the sprayed film.

Single-walled carbon nano-tubes (SWCNTs) are employed in this work because of its remarkable properties compared with indium-tin-oxide (ITO) such as their high conductivity, high transparency, and work function. To prepare spray-coatable aqueous dispersions of SWCNTs, sodium dodecyl sulphate (SDS) is used. Firstly, make 1 wt% aqueous solution by dissolving SDS in distilled water. In order to uniformly dissolve the surfactant in water, only one hour of stirring is required. A 0.03 wt% of SWNTs is used and the complete dispersion is prepared by sonication the whole solution for 25 min using a horn sonicator (Branson Sonifier S-450D) at 50% power (48 Watt). Finally, the dispersion is centrifuged at 15000 rpm for 90 minutes, the desired dispersion is that taken from the top after centrifugation.

3.2.2 Substrate Preparation

To achieve a homogeneous, uniform and stable SWCNTs film, the substrate surface treatment is an essential step. To avoid any contamination, the substrate should be cleaned first by acetone and isopropanoal respectively. For each cleaning solvent, the substrate should be subjected in an ultrasonic bath for 10 minutes and dried the substrates by using N_2 flow. For plastic substrates,

the cleaning by acetone is skipped due to the degradation that caused by acetone. To convert the substrate surface from hydrophobic to hydrophilic to enhance the surface adhesion and allow the deposition of uniform surface coating, Plasma cleaning step is an essential one after cleaning by solvents. In our experimental work, the substrates used are plain glass, ITO-coated glass, spectrosil, in addition to Indium Tin Oxide coated PET substrates.

3.2.3 Spray Deposition Technique

An air atomizing spray gun is used for depositing the CNT films. The spray technique employed in the preparation of films is automated spray system at which an industrial air atomizing spray valve is used in combination with an overhead motion platform. The spray gun's parts are resistant to any organic solvents. A schematic drawing of the spray deposition technique involved in this thesis is illustrated in Figure 3.2. The physical properties of the liquid injected in the spray gun, the geometry and the size of the spray nozzle play an important role on its performance. It is also advisable to study the viscosity and the surface tension of the used fluid as discussed in Chapter 4. Also, the drying behavior of sprayed droplets and thus the layer formation depend on vapor pressure and boiling point of solvents. For obtaining desired spray characteristics, some spray parameters should be taken into account such as the distance between the spray nozzle and the substrate, atomizing gas (N2), substrate temperature, material flow rate, and the motion speed. It should be noted that the spray deposition can be occurred in three different regimes which are dry regime, intermediate regime and wet regime. The dry regime is obtained through either increasing the hot plate temperature or increasing the nozzle-to-sample distance. According to the arrangement required in that regime, non-overlapping and non-homogeneous layers of CNT thin film is the result due to evaporating of the solvent to evaporate before reaching the substrate. While the intermediate regime, homogenous and uniform layers as a result of good overlapping between the droplets is achieved as well as the thickness of the film can be precisely controlled. By either decreasing the nozzle-to-sample distance or decreasing the hot plate temperature, the wet regime can be obtained. Such arrangement allows the formation of a layer with wet droplets on the top of the substrate and non-uniform thickness distribution of the produced layers is the final result. Thus, the intermediate regime is considered the most suitable one for depositing CNT thin-films.

In our experimental work, a 0.3 mm orifice diameter nozzle was used. To achieve a reasonable spray pattern, the atomizing gas pressure is adjusted below 0.5 bars during our experiment. Also, the distance between the sample and nozzle is kept at 27 cm and the hot plate temperature is set to 60^{o} C in order to speed up the drying of wet droplets arriving at the substrate as we operate within the wet spraying regime. Finally transparent conductive film is obtained.

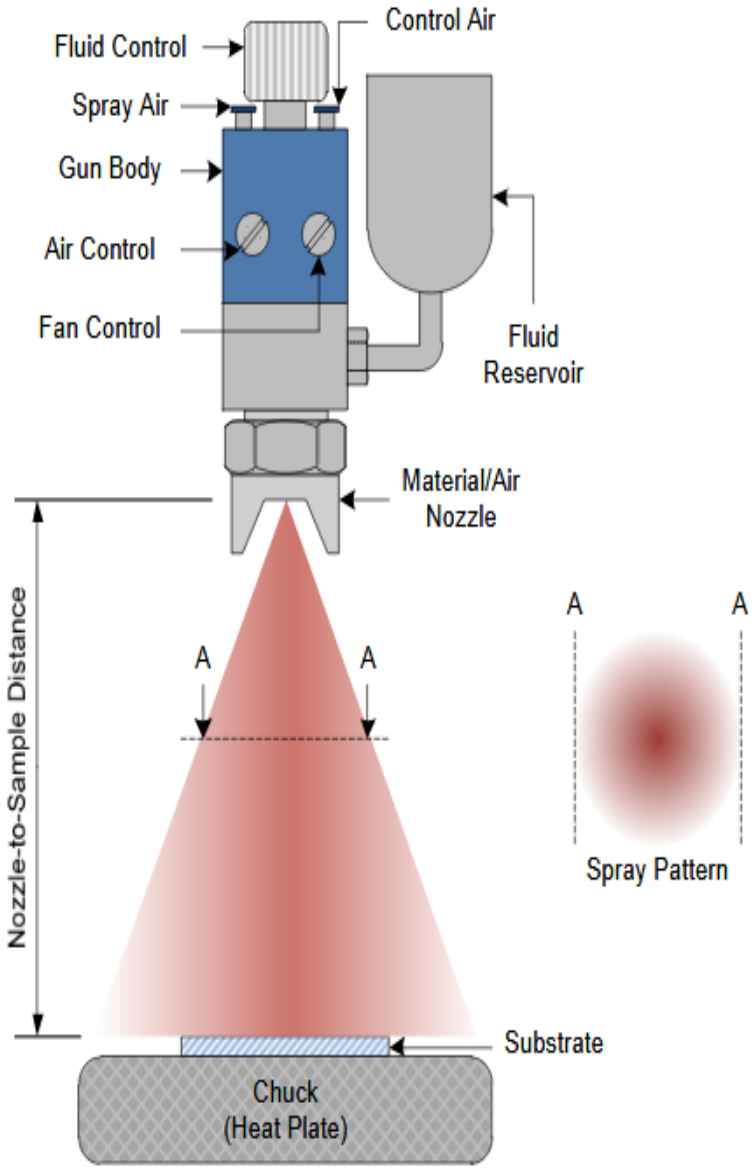

Figure. 3.2: A schematic drawing of the experimental setup of the spray deposition technique [145].

3.2.4 Post-deposition Treatment

To enhance the film conductivity and to remove the majority of dispersant, a post deposition treatment is a required step after spraying. At room temperature, SDS based solution samples require only immersing the sprayed films in distilled water for 10 minutes at which SDS based films can be easily removed from the substrate. The films then left in air for drying.

3.3 The performance of CNT thin-Films Deposition on Different Rigid Substrates

It is necessary to optimize and evaluate the elementary films performance and their dependence on different process parameters before employing CNT films in any specific application. The sheet resistance or conductivity, optical transmittance, work function, and morphology are the most important parameters to determine the films performance.

3.3.1 Optical Transmission Characteristics

Figure 3.3 obtained from AFM image analysis of thin CNT films on top of different types of substrates, it compares the morphological features of the thinnest CNT films on the different substrates (i.e. glass, ITO-coated glass, and spectrosil substrates).

According to Figure 3.3, the choice of substrate material has a high effect on the deposition process rather than the surface treatment. The CNT films deposited on glass substrates shows the best morphological features at which the highest coverage and the lowest roughness is achieved. On the other hand, the CNT films on spectrosil do not show an optimal deposition as confirmed by the AFM images in Figure 3.4. So, the best results are achieved for films onto glass substrates in the terms of in terms of roughness and coverage. Since the CNT density was kept low in every samples, the complete coverage does not achieve for the thinnest film deposited as shown in Figure 3.4. A high transparency with a mean transmittance of 97% at 550 nm is achieved.

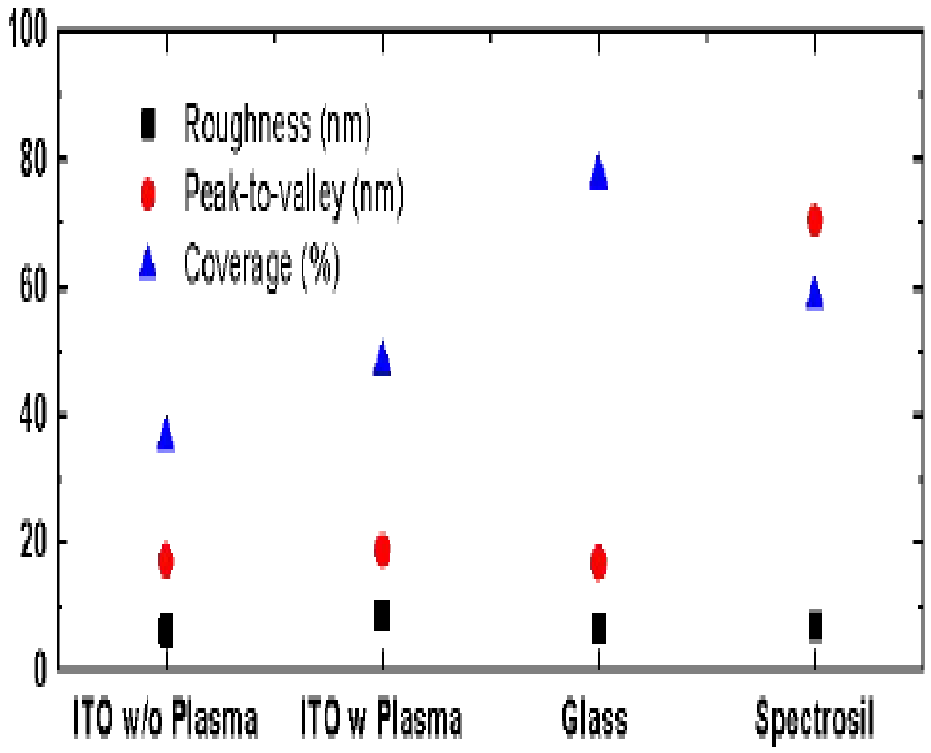

Figure 3.3: A comparison between the morphological features of the thinnest CNT films on the different substrates [146].

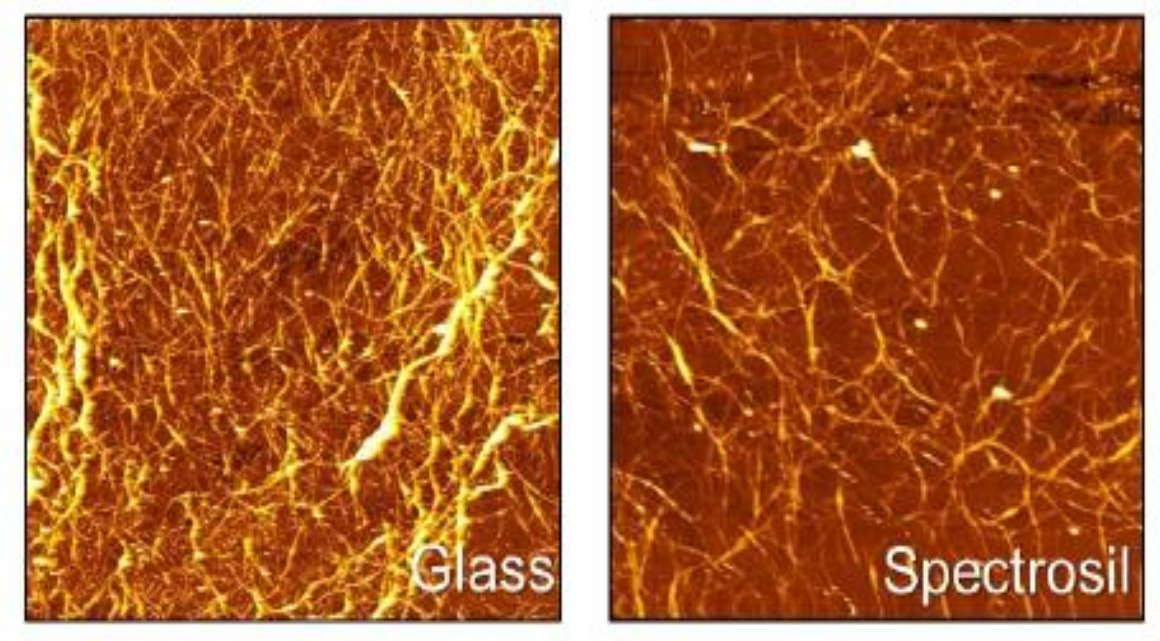

Figure 3.4: AFM images (10x10 μm^2) of the CNT film onto glass and spectrosil [146].

Figure 3.5 shows the experimental values of sheet resistance and transmittance (measured at 550 nm) for CNT films of different thickness. A reasonable trade-off can be achieved with films exhibiting 165 Ω/sq at 83 % without any further doping, matching state-of-the-art performance of films fabricated using more common and less scalable deposition techniques.

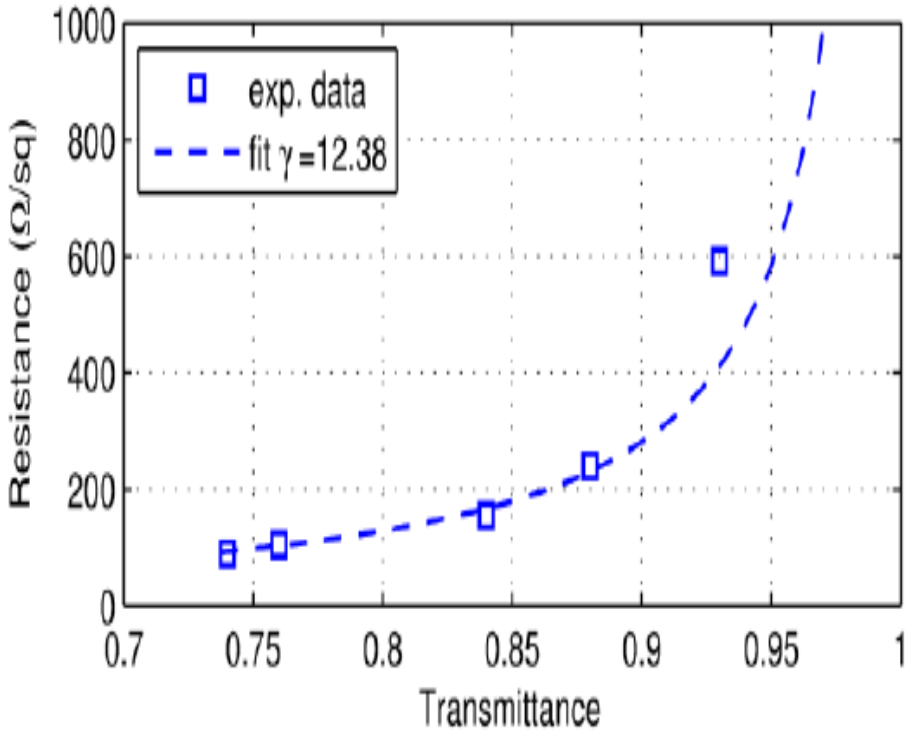

Figure 3.5: The experimental values of sheet resistance and transmittance (measured at 550 nm) for CNT films of different thickness [146].

3.3.2 Work Function Measurement

The work function values for CNT films deposited on different rigid substrates can be shown in Figure 3.6. We observed that the Fermi levels of the films deposited on ITO substrates are not strongly affected by the treatment by using oxygen plasma or even by the thickness of the sprayed film. It should be noted that all the values obtained are within the statistical deviation of the collected data. Note that the intrinsic error of the measurement is 0.02 eV (full black and black lined square in Figure 3.6). This suggests that the work function does not depend on both surface treatment and layer thickness of the films. The presence of exposed regions of ITO is the reason of the small variation observed owing to its effect can affect the measurement. Additionally, a Schottky model can be used to describe the electronic level matching at the interface with ITO.

Assuming that, as for conjugated polymers, the depletion length is in the order of few micrometers for carbon nanotubes and much bigger than the thickness of our films. Thus, we are measuring the work function of ITO itself. In fact, the Fermi level of ITO is approximately 4.70 eV. After oxygen plasma treatment, the value of ITO Fermi level increases [147].

We observed that the Fermi level is generally lower than the one for the ITO substrates for the glass and spectrosil substrates. According to the literature review, the data reported in the range between 4.5 to 4.95 eV. There is no clear trend of dependence of the Fermi level on the CNT film thickness for these substrates (full red and red lined circles in Figure 3.6). Thus, no influence on the work function from the substrate surface is reported.

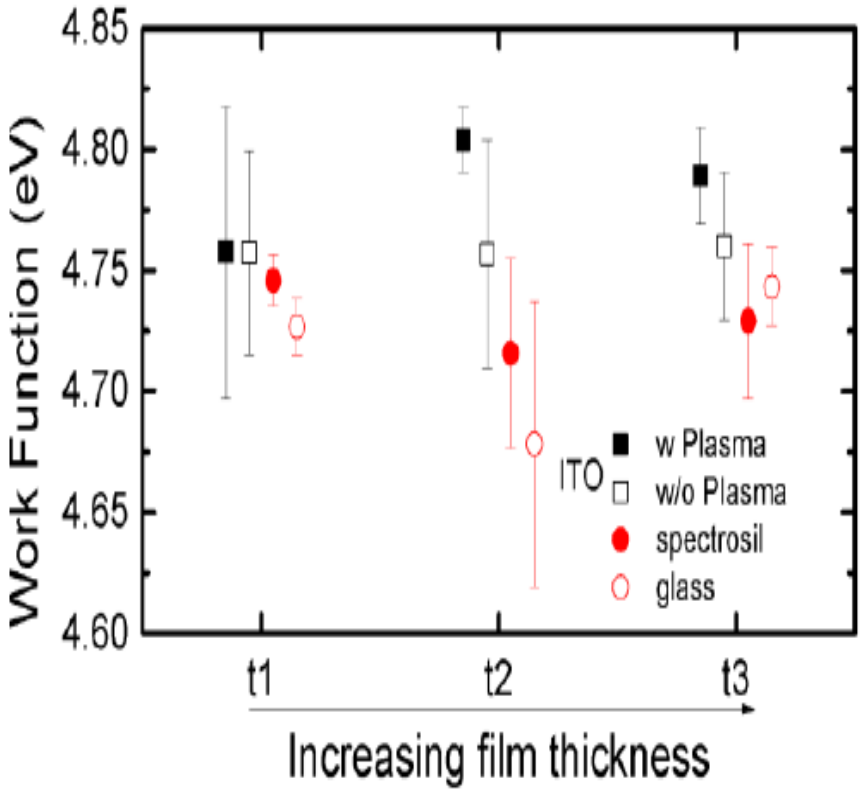

Figure 3.6: Plot of the work function of the sprayed CNT films [146].

3.4 CNT Thin-Film Deposition on Flexible Substrates

Films prepared on flexible substrates were also analyzed. We used Indium Tin Oxide coated PET purchased from Sigma-Aldrich. The bare PET substrates were obtained by chemical removal of ITO. We spray deposited two films of low and high CNT density, referred to as thin and thick films, respectively. Oxygen plasma treatment was performed on each substrate.

3.4.1 Optical Transmission Characteristics

AFM images of the CNT films prepared onto bare PET are shown in Figure 3.7. The surface coverage on PET is compared to glass for the two considered CNT densities and shown in Figure 3.8. A significantly higher roughness, especially for thicker films, is observed on CNT films deposited onto the flexible substrates in accordance with the mean value for bare flexible ITO film and bare flexible PET which are 3 nm and 9 nm, respectively. The thick CNT film on ITO coated PET has a mean value of roughness equals to 54 nm, on the other hand the thin film's mean value of roughness is 16 nm. The roughness mean values observed for CNT films on bare PET are 29 nm for thick films and 15 nm for thin films.

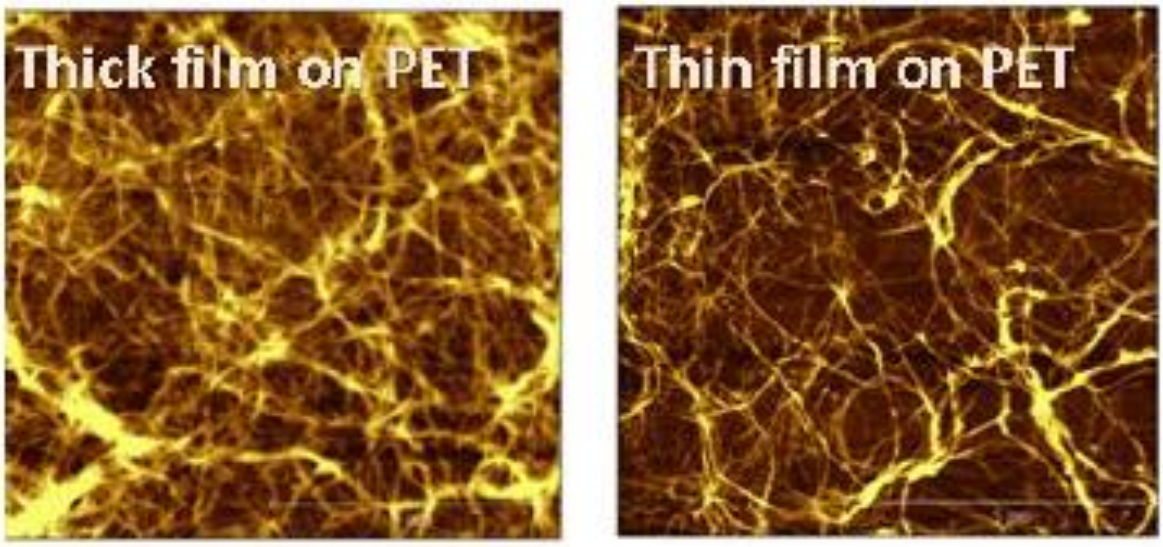

Figure 3.7: AFM images (10x10 μm2) of (a) the thick and (b) thin CNT film onto PET Substrate [146].

Figure 3.9 shows the values obtained for the work function of CNT films on flexible substrates. The obtained result is similar to the observed results for the rigid substrates, work function remains

nearly constant with some fluctuation independent on the substrates and thickness. On the other, we do not observe any influence of the ITO on the work function of the CNTs. The bare flexible substrates are promising candidate for replacing ITO, this result is concluded by making a comparison between the work function of CNT films on rigid as well as flexible substrates with the one of untreated ITO.

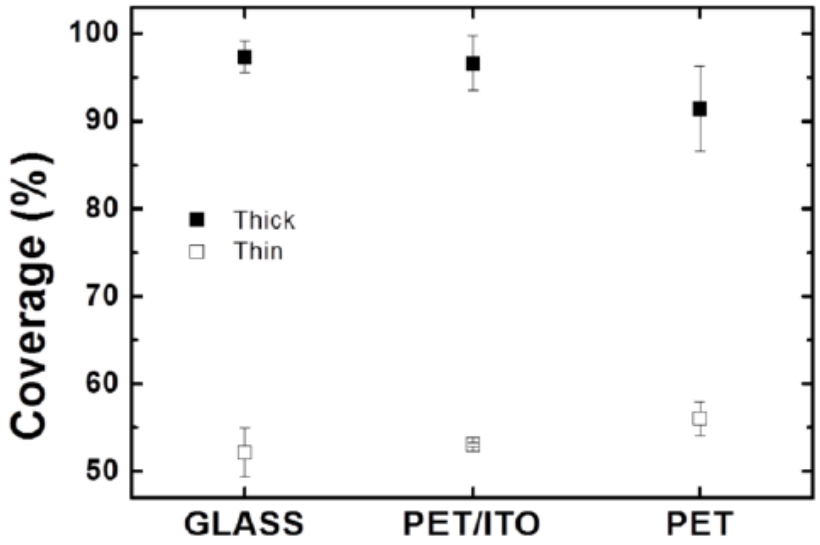

Figure 3.8: CNT surface coverage onto PET and PET/ITO compared to the surface coverage onto glass [146].

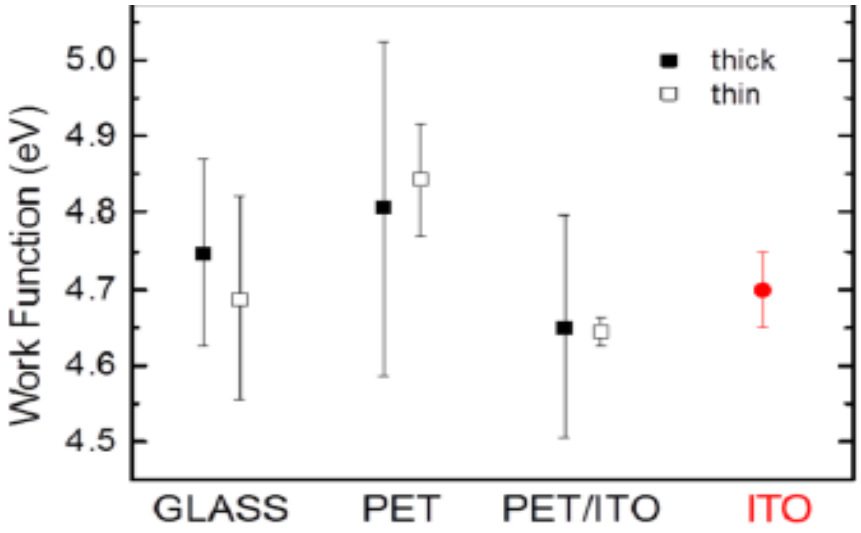

Figure 3.9: plot summarizing the work function of the sprayed CNT films on different substrates. The work function of the ITO is reported as a reference [146].

3.4.3 Time-resolved THz spectroscopy Measurement

The photogenerated carrier dynamics and frequency resolved complex photoconductivity in CNT films were studied using time-resolved THz spectroscopy, as shown in Figure 3.10 for a CNT film on a PET substrate. Measuring changes in transmission of the main peak of the THz pulse (Figure 3.10 (a)) allows monitoring dynamics of the photoinduced conductivity and relaxation of photogenerated carriers [148, 151]. We find that the photoconductivity of the CNT films is short-lived, with photoexcited carrier relaxation occurring on picosecond time scales, similar to previously reported data for other CNT systems [150, 151]. The complex photoinduced conductivity of the CNT film at a specific time after optical excitation was determined by analyzing the changes in the transmitted THz pulse waveform, as shown in Figure 3.10 (b) for the pump-probe delay time of 3 ps (indicated by a red arrow in Figure 3.10 (a). Non-Drude complex conductivity. As a result a significant suppression of the real conductivity component at low frequencies (σ_1) and of the negative imaginary conductivity component at frequencies below ~ 1.5 THz (σ_2) is exhibited. Similar spectral shapes have been reported previously for as well as for CNTs dispersed in gels and for agglomerated CNT films [150, 152]. The interpretation of the observed complex conductivity spectra in CNT ensembles is still under investigation, with proposed models involving either a combination of confined collective plasma modes on the tube-length scale as in Drude-Lorentz model [152], or involving backscattering free carriers due to nanoscale dimensions of the CNTs as in Drude-Smith model [150, 151] and Drude-like intertube transport. Both of these models are fitting well to the observed photoinduced conductivity in CNT films on PET substrate, as illustrated in Figure 3.10(b). A carrier scattering time ($\tau = 70.5 \pm 0.5$ fs), and a carrier localization parameter ($c=-0.823 \pm 0.026$) are obtained from the Drude-Smith fit at which a significant degree of carrier localization is indicated as the fully localized carriers are characterized by c=-1, and the free carriers are characterized by c=0 [148, 151]. The red line represents Drude-Lorentz model which provide equally adequate quantitative description of the experimental data with a Drude scattering time $\tau = 15 \pm 2$ fs, and an overdamped ($\tau_{Lorentz} = 13 \pm 2$ fs) Plasmon oscillator centered at 3.1 ± 0.5 THz. to clarify the nature of photoinduced conductivity in CNT films, it is essential to employ bandwidth extending to 4 THz and higher measurements using THz pulses.

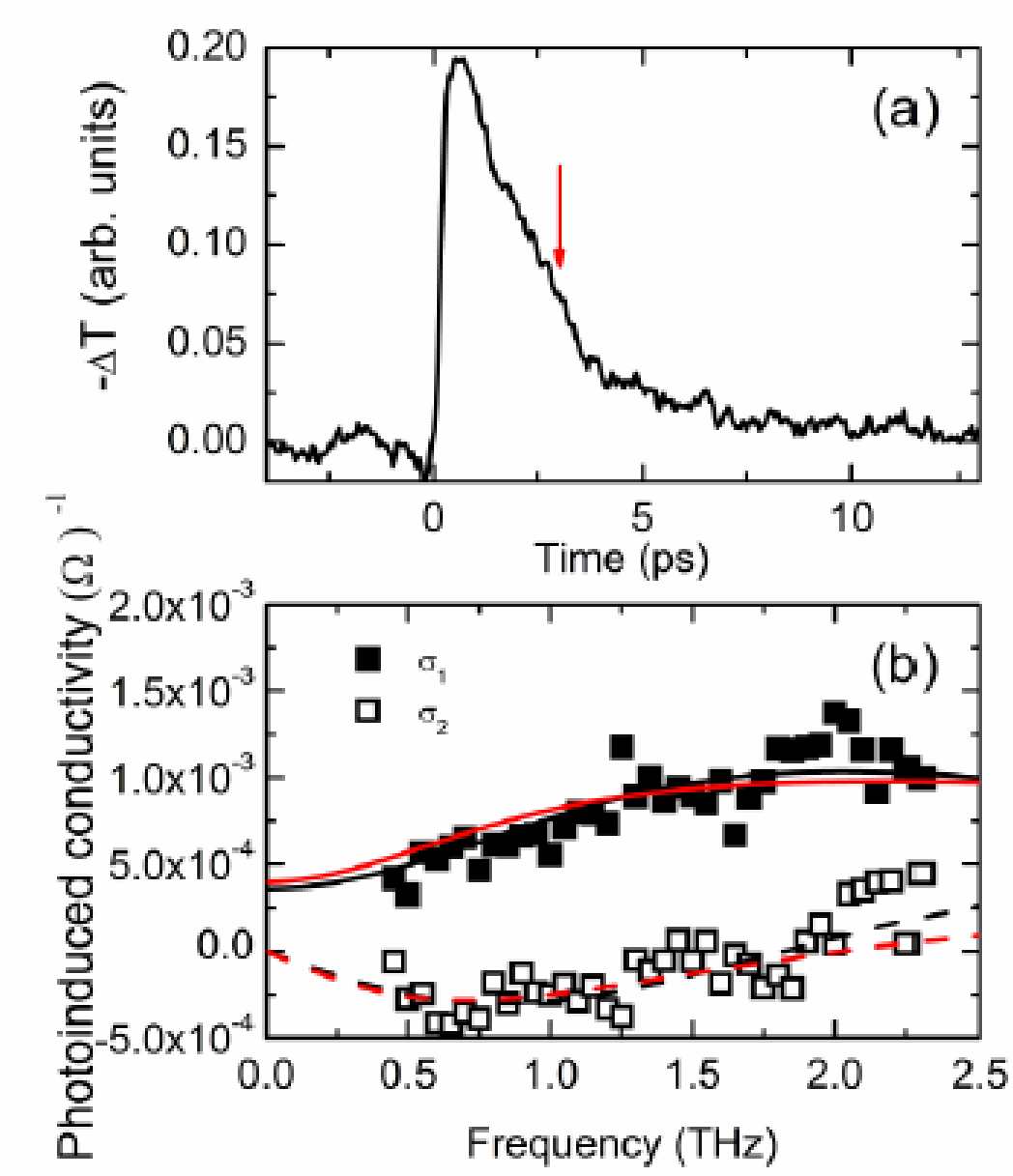

Figure 3.10: (a) shows a change in the main peak transmission of the THz probe pulse as a function of time delay with respect to 100 fs excitation pulse and an 800-nm, the pump influence is 150 μJ/cm2. **(b)** Real (solid squares) and imaginary (open squares) components of the complex conductivity of a CNT film on PET measured 3 ps after photoexcitation, as indicated by the red arrow in (a). Solid lines are global fits of real conductivities whereas the dashed lines are global fits of imaginary conductivities in accordance to Drude-Smith (black lines) and Drude-Lorentz (red lines) models [146].

3.5 Summary

The morphology of sprayed CNT films is influenced by the substrates, and in particular films onto glass give best results in terms of roughness and coverage. On the other hand, there are no significant changes in the work function of such films by changing both substrates and thickness. The best CNT films deposited onto flexible substrates have lower transmittance and slightly higher sheet resistance than ITO. At the same time, they demonstrate comparable work function, rendering them suitable for application in flexible optoelectronic devices. AFM analysis point out how coverage and roughness values increase with increasing thickness of deposited films. Finally, in sprayed CNT films on flexible PET substrates, time-resolved THz spectroscopy measurement has showed picosecond transient photoconductivity dynamics.

Chapter 4

Inkjet Printing Technique

Inkjet printing technique recently has emerged as a very promising technical trend to produce flexible and stretchable electronics/devices. This technique is a cost-effective, especially for the materials, and very versatile technique for fabricating flexible and stretchable electronics. Despite of the unlimited advantages of inkjet printing technique, some challenges still need to be overcome such as low conductivity of printed circuits, weak adhesion between the printed materials and the substrates, limited choices of substrate materials, and nozzle clog which results in instable printing.

In this chapter, an overview of the inkjet printing activity will be present including system identification, working principle and parameters of printer employed in the work; namely the Fujifilm Dimatix Materials Printer DMP-2831. The inkjet printing process step by step will be explained including the ideal printing parameters to achieve high quality printing patterns. The physical and chemical properties of the suitable ink for the dimatix printer will be mentioned. As viscosity and surface tension are the most important physical parameters of printing fluids which strongly influence the final printing performance, the effect of these two parameters will be presented. In order to allow for structural versatility, device miniaturization, and purely selective system deposition, the Ag ink DGP-40LT-15C was employed as the main conductive ink during this thesis for Fujifilm Dimatix Materials Printer DMP-2831. The effect of plasma treatment of different substrates will be introduced. As a consequence, it is proved that plasma treatment is an essential step for surface modification of the substrates prior to printing process for successful printing patterns. The relationship between the drop spacing, continuous printed lines, line width and electrical resistance will be studied. It is found that the continuous printed

lines and printed line width highly depend on drop spacing. Finally, the effect of photonic sintering of the printed patterns have been investigated thoroughly by using the optical microscopy and the result is confirmed by Scanning Electron Microscope (SEM).

4.1 System Identification

The inkjet printing technology is the main core of this thesis for the fabrication of flexible printed electronics. The inkjet printer employed in this thesis is the Dimatix Materials Printer 2831 (DMP2831), a piezoelectric Drop-on-Demand printer purchased from FUJIFILM Dimatix [153], shown in Figure 4.1. This printer makes use of user-filled cartridges, each containing sixteen independently controllable print nozzles/apertures [154]. The most important requirements for the operation of DMP is the surrounding environments. It is recommended that DMP to be used in a reasonably controlled temperature and humidity environment to aid in uniform test results.

Figure 4.1: The Fujifilm Dimatix Materials Printer DMP-2831 [153].

The major components of the Fujifilm Dimatix Materials Printer DMP-2831 are illustrated obviously in Figure 4.2, which are mainly platen, maintenance station blotting pad, drop watcher and print cartiage.

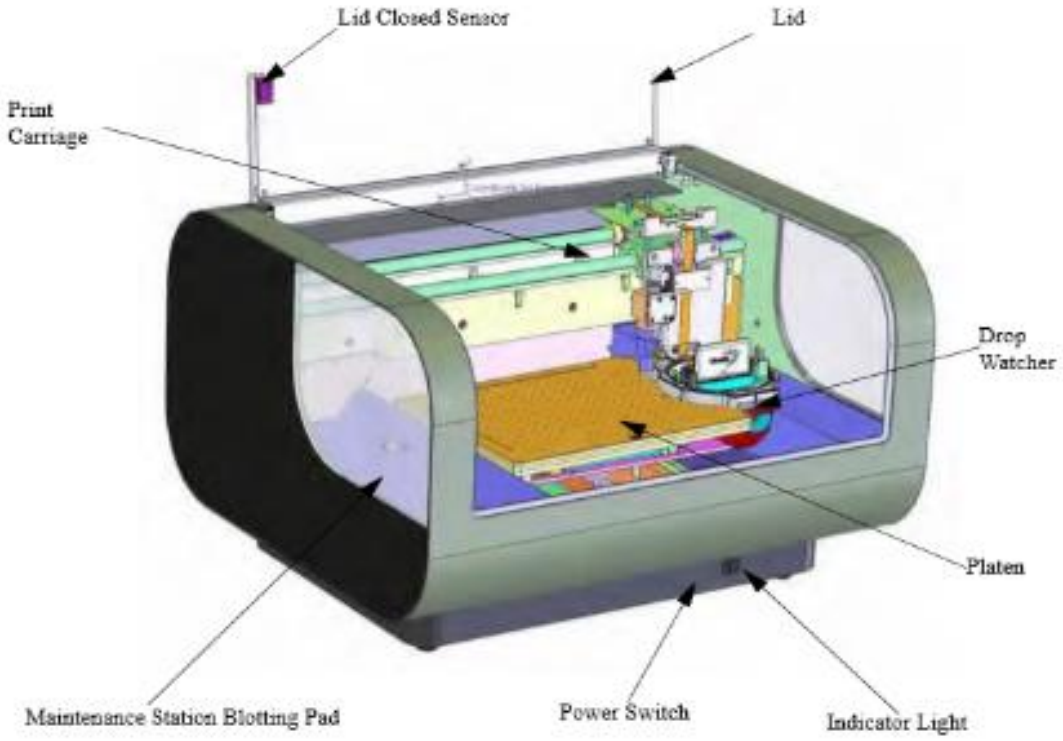

Figure 4.2: Schematic of the Fujifilm Dimatix Materials Printer DMP-2831 [153].

4.1.1 Platen

It is a large vertically movable metallic plane with many very small holes, as shown in Figure 4.3, where the desirable substrate is firmly placed during the printing process. To obtain good final printed patterns, the platen is connected to a vacuum pump system, vacuum platen, and temperature adjustable; ambient to 60^{o} C. By switching on the vacuum system, the vacuum goes through the holes on the surface of the platen and help in holding the substrate during the printing process. On the other hand, the importance of the heating system comes from its contribution in the drying process of the printed patterns.

Figure 4.3: The platen of the Fujifilm Dimatix Materials Printer DMP-2831.

4.1.2 Maintenance Station Blotting Pad

It is the cleaning station of the nozzles surface of the cartridge before, during and after printing. It consists of a changeable single cleaning pad as shown in Figure 4.4. To keep the nozzles clear and functioning properly, it is necessary to replace the cleaning pad with a new one if the cleaning pad gets filled or clogged by fluid residue and does not effectively blot the nozzle surface of the cartridge. Also, if the cartridge fluid is changed to a void cross contamination resulting from contacting the pervious material on the cleaning pad.

Figure 4.4: The Maintenance station Blotting Pad of the Fujifilm Dimatix Materials Printer DMP-2831 [153].

The mechanism of the cleaning operation relays on using air pressure to pressurize the outside of the fluid bag, which forces fluid out through the nozzles. The Fujifilm Dimatix Materials Printer DMP-2831 includes a pump for this function. The cleaning operation can be very simple or can consist of several combinations of actions since Dimatix Printer DMP-2831 contains three different cleaning operations **S**pit, **P**urge and **B**lot:

1- ***Spit:*** is jetting drops out of all the nozzles at a selected frequency and at a selected designated time. This action clears the nozzles, brings fresh fluid to the pumping chamber and also the nozzles. Also it keeps fluid path surface wet.
2- ***Purge:*** refers to pushing fluid out through the jetting device with pressure to remove trapped air. This process usually clears severely clogged nozzles.
3- ***Blot:*** this process implies coming down the cartridge, keeping contact with the cleaning pad for the designated time. The cleaning gets close enough to absorb excess fluid residue on the nozzle plate which can partially attach to ejected drops causing misdirected or even fall onto the substrate or printer components.

A sequence of cleaning operations, known as cleaning cycle, can be selected at a designated time. The cleaning cycle usually involves a delay time, which is the time after each cleaning process before going to the next cleaning process in the cleaning cycle.

4.1.3 Drop Watcher

This system consists of video camera which allows direct viewing of the jetting nozzles, the faceplate surrounding the nozzles and the actual jetting of the fluid, as shown in Figure 4.5. Also, it consists of drop watcher pad which is located in the center of the drop watcher mechanism and acts as receptacle fluids during jetting. It need to be changed periodically as it absorbs fluid. Typically this occurs when stray drops being deposited on the nozzle surface during the drop watching or fluid is covering the side or the pad holder. The drop watching step is a fundamental step prior to any printing process.

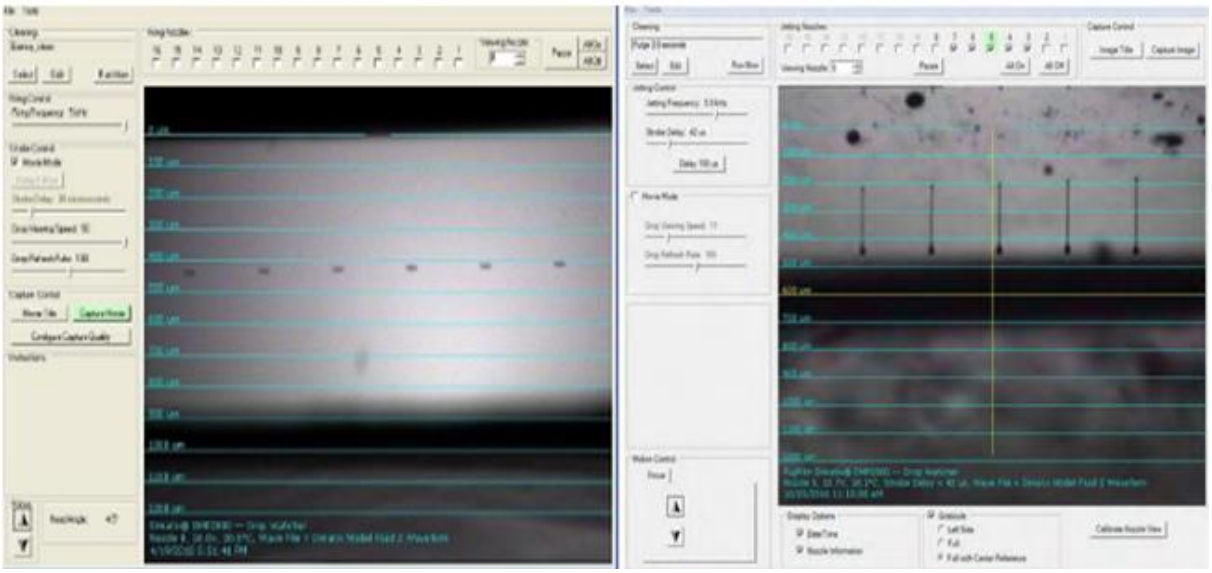

Figure 4.5: (a) drop watcher Screen (b) Video capture a view of jetting nozzles.

4.1.4 Print Carriage

It is the main nerve of the Fujifilm Dimatix Materials Printer DMP-2831 since it consists of the most important parts of the printer, which are the cartridge and Fluidal camera. The schematic of the print carriage can be shown in Figure 4.6. The print carriage can be considered as an arm which moves horizontally during the printing process above the platen where the substrate is placed.

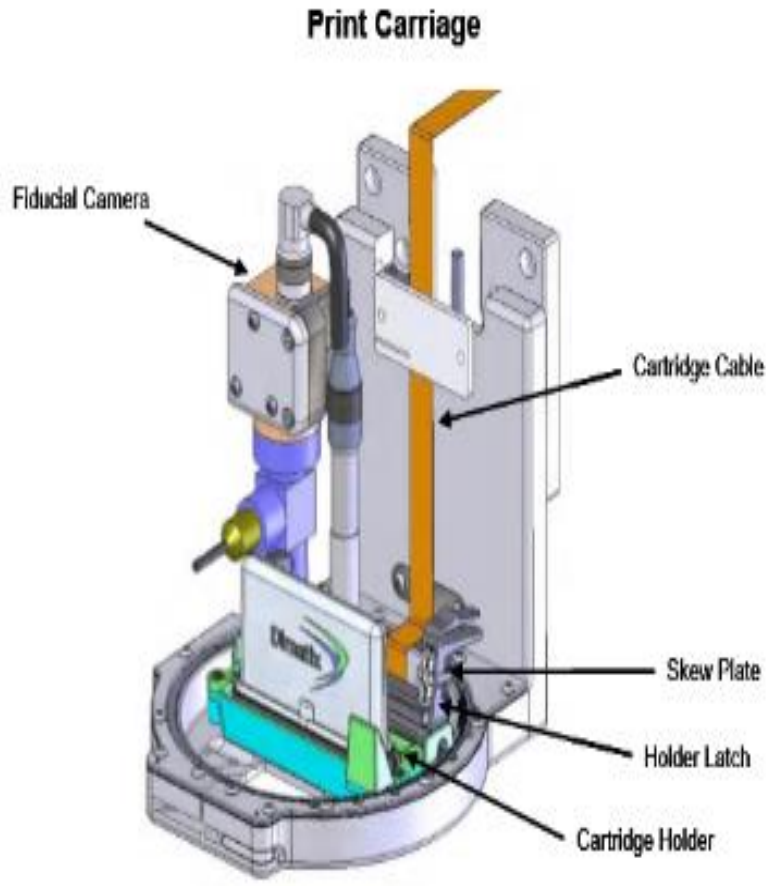

Figure 4.6: Shows the major components of the Fujifilm Dimatix Materials Printer DMP-2831 print Carriage [153].

The cartridge is a Piezo-driven jetting device with integrated reservoir and heater. The major parts of the cartridge can be illustrated in Figure 4.7, it consist of a fluid bag, which acts as the ink reservoir, and a single row of 16 nozzles, 254 μm spacing, from which the ink is ejecting. The drop volume depends on the type of the cartridge installed, the cartridges print heads are available with nozzles designed for either 1 (DMC-11601) and 10 (DMC-11610) picoliter nominal (pL). The usable ink capacity of the dimatix model fluid cartridge is up to 1.5 ml. The cartridge is compatible with many water-based, solvent, acidic or basic fluids materials. An important feature before filling the cartridge is filtering the fluid to avoid nozzle clogging.

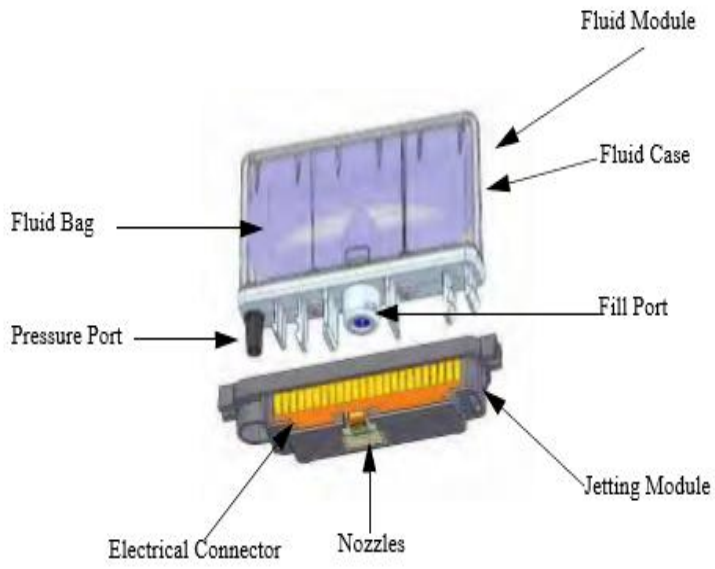

Figure 4.7: The major parts of the cartridge [153]**.**

On the other hand, the second important part of the print carriage is the Fluidal camera. The Fluidal camera is a video camera with field of view of 1.62 mm and a height of 1.22 mm with a resolution of 2.54 μm per pixel. A Fluidal camera screen can be shown in Figure 4.8. According to the selection of the light source, the camera field of view can be operated in a dark field mode or a bright field mode or in both modes if both light sources are switched on. For viewing clear patterns on highly reflective surface, a low light intensity is required and the mode will be a dark field mode; position 3 as shown in Figure 4.9. In this mode, the light source illuminates the sample in a way that the objective only collects scattered light from the substrate. This results in dark backgrounds with a bright objects on the top of them. For a Bright Field Mode, a high light intensity is required; position 1 as shown in Figure 4.9. In this mode, the light shines on the object and gets directly reflected back in to the objective.

The Fluidal camera is important for alignments procedures. A series of alignments have to be performed in several cases such as deposition on a pre-patterned substrate using reference marks or positioning a print origin/reference point to match substrate alignments or jetting a layer with a different cartridge fluid or providing the printed features and locations…… etc.

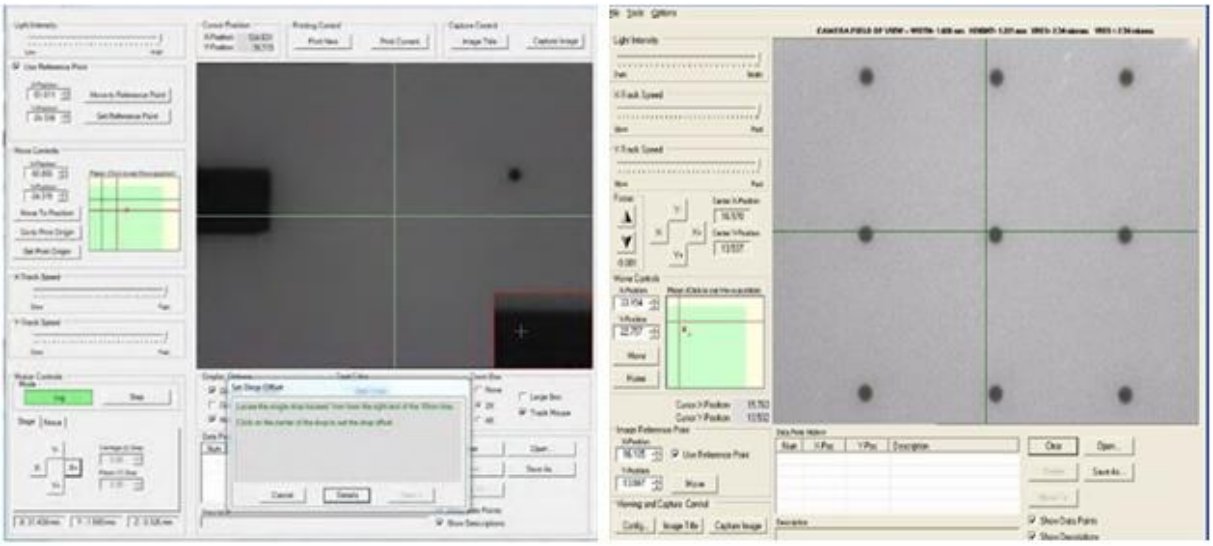

Figure 4.8: Flucial Camera Screen.

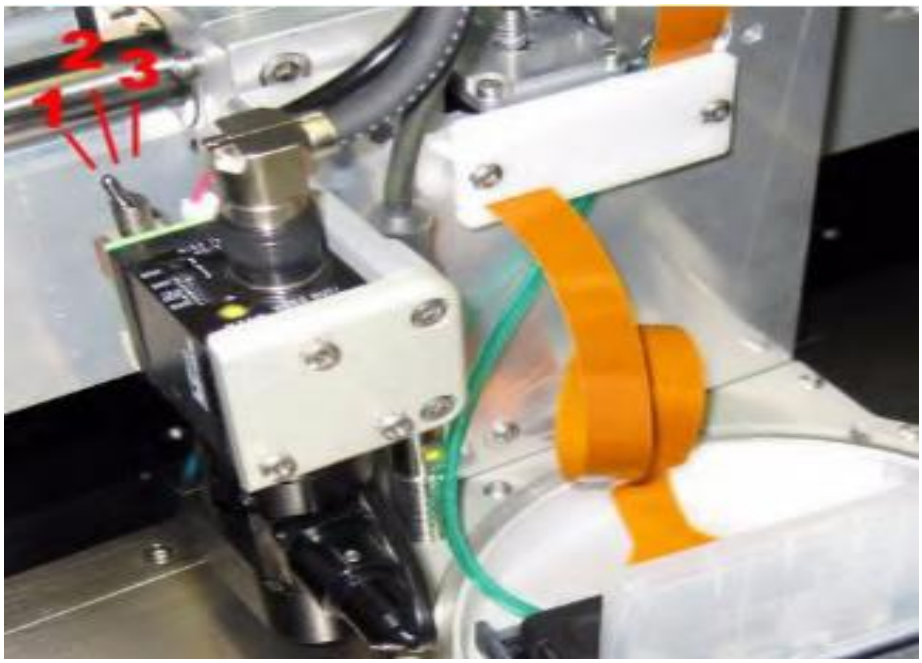

Figure 4.9: Camera switch for different field mode of view. Switch at position 1: corresponds to the Bright field mode, Switch at position 2: means both light sources are switched on, switch at position 3: corresponds to the Dark Field mode.

4.2 Printing Process: Process Steps of Inkjet Printing

The additive fabrication technique of inkjet printing depends on a phenomena called piezoelectricity. Figure 4.10 shows the working principle of inkjet printing which can be simply summarized into:

- Ink Acquisition
- Pre-dosing
- Dosing of the ink
- Ink transfer to the substrate
- Fluid dynamics on the substrate
- Solidification

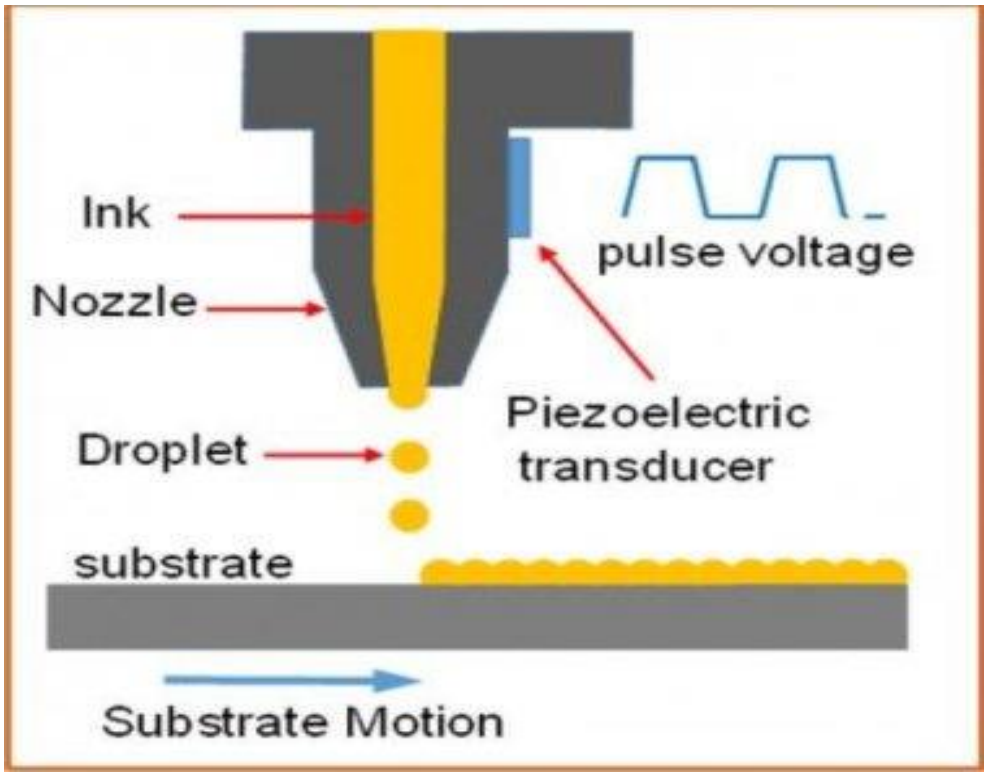

Figure 4.10: The working principle of inkjet printing [153].

4.2.1 Ink Acquisition

The ink is placed in a fluid bag with thermoplastic and wax materials. The fluid bag is a part of the cartridge which installs on print carriage as discussed before in section 4.1.4. In this step

the ink is pressured by the ink supply pump and flows from the fluid bag under the capillary force.

4.2.2 Pre-dosing Ink

The Pre-dosing step depends mainly on piezoelectricity which is generated because of application of a voltage resulting in a pressure difference in the fluid chamber. The motion of the piezo is the vital process resulting in pressure difference. The step of pre-dosing can be illustrated in Figure 4.11. According to the Figure 4.11, a shear mode deformation occurs to the piezoelectric walls on both sides when voltage is applied resulting in producing pressure waves. Because of this deformation force, the ink drops are delivered from the ink pressure reservoir [155]. The imaging signal of the piezoelectric walls is transmitted during the jetting process by using a piezo element.

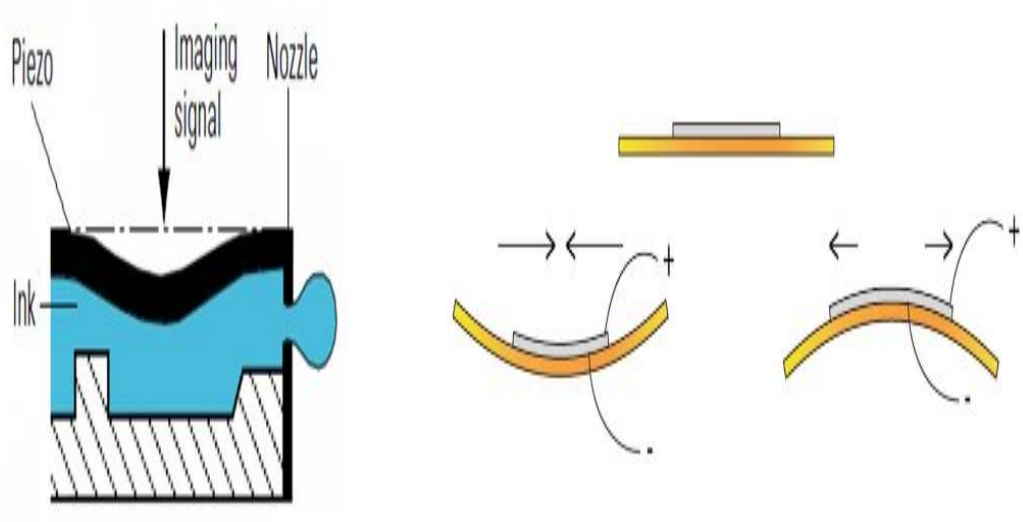

Figure 4.11: The working principle of pre-dosing step [156].

The software of the Fujifilm Dimatix Materials Printer DMP-2831has a standard waveform which can be used as a starting point to understand the jetting process. The typical basic waveform is divided into four segments, as shown in Figure 4.12, each segment has three properties: duration, level, slew rate.

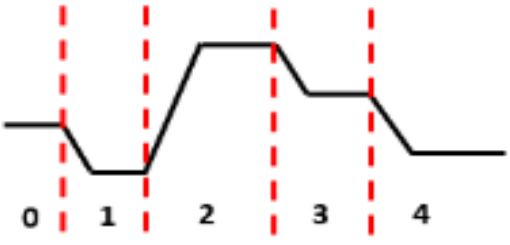

Figure 4.12: Basic Waveform.

The pumping chamber of a piezo-electric print head, the piezoelectric crystal of each nozzle chamber is activate by a four-phase voltage wave:

1- ***Standby:*** At the beginning of Jetting, the voltage decreases to zero so the piezo will start from a relaxed position. Through this phase, the fluid is pulled into the chamber via the inlet. The standby Phase can be shown in Figure 4.13.

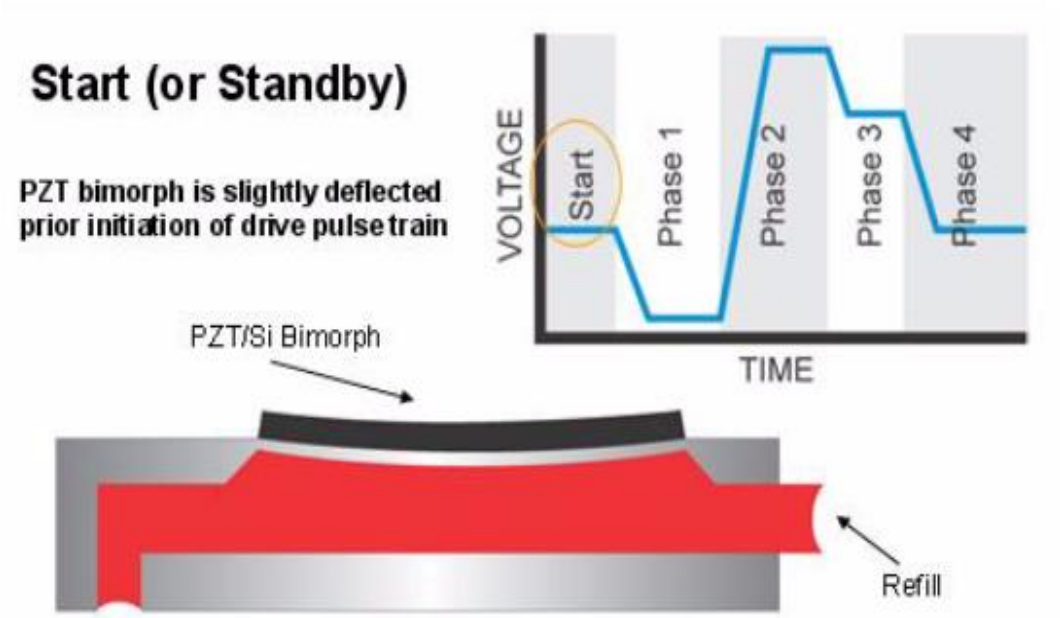

Figure 4.13: Waveform of piezoelectric print head at standby phase [153].

2- ***Phase 1:*** An electric field is generated and the nozzle walls open. The fluid is drawn into the pumping chamber as shown in Figure 4.14.

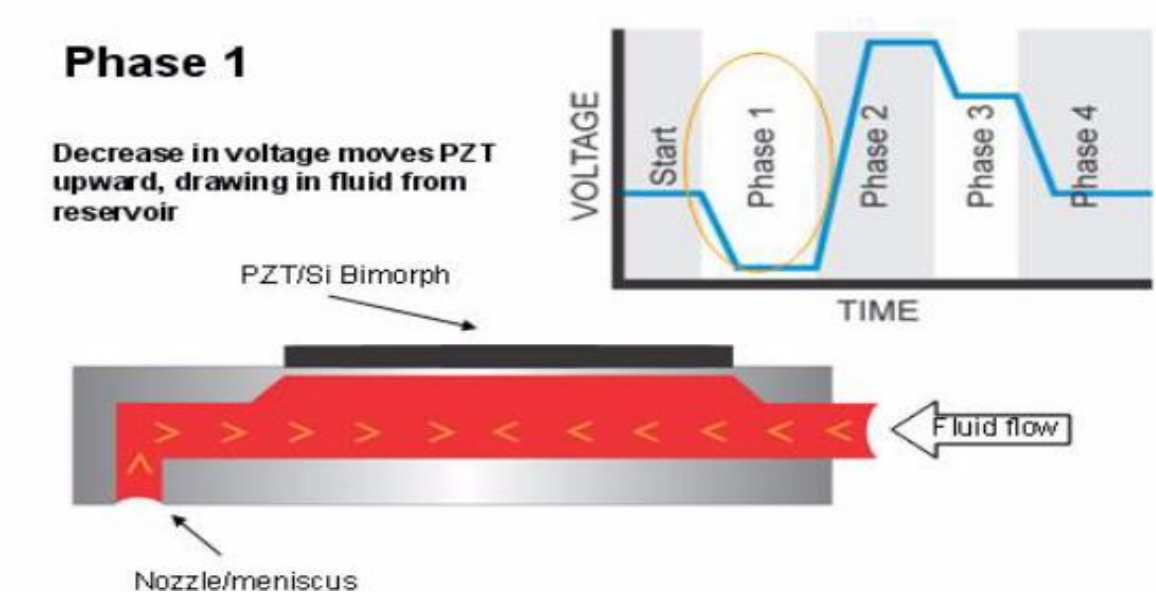

Figure 4.14: Waveform of piezoelectric print head at phase 1 [153].

3- ***Phase 2:*** It is the drop ejection phase. In this phase, the voltage is increased to an extent of compressing of the chamber and generating the pressure. The steepness of the slope provides the energy for the initial ejection as sown in Figure 4.15. It is followed by a hold period.

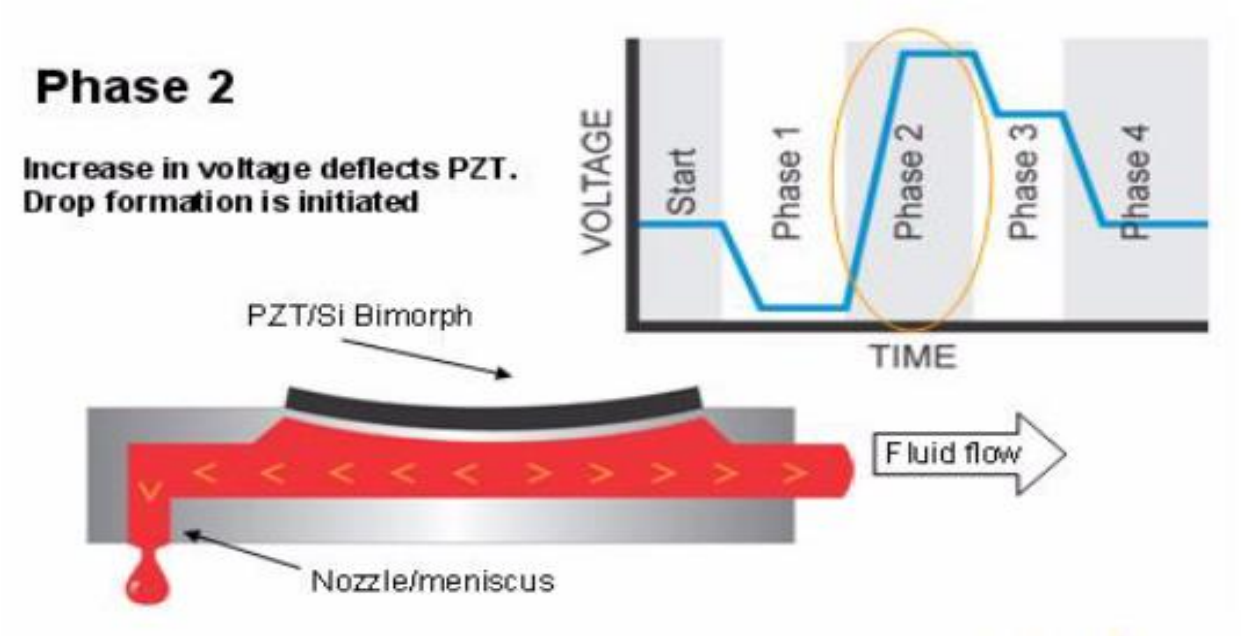

Figure 4.15: Waveform of piezoelectric print head at phase 2 [153].

4- ***Phase 3 & Phase 4:*** In this section, the piezo voltage is decreased to its bias-level returning back to a position "zero" as shown in Figure 4.16.

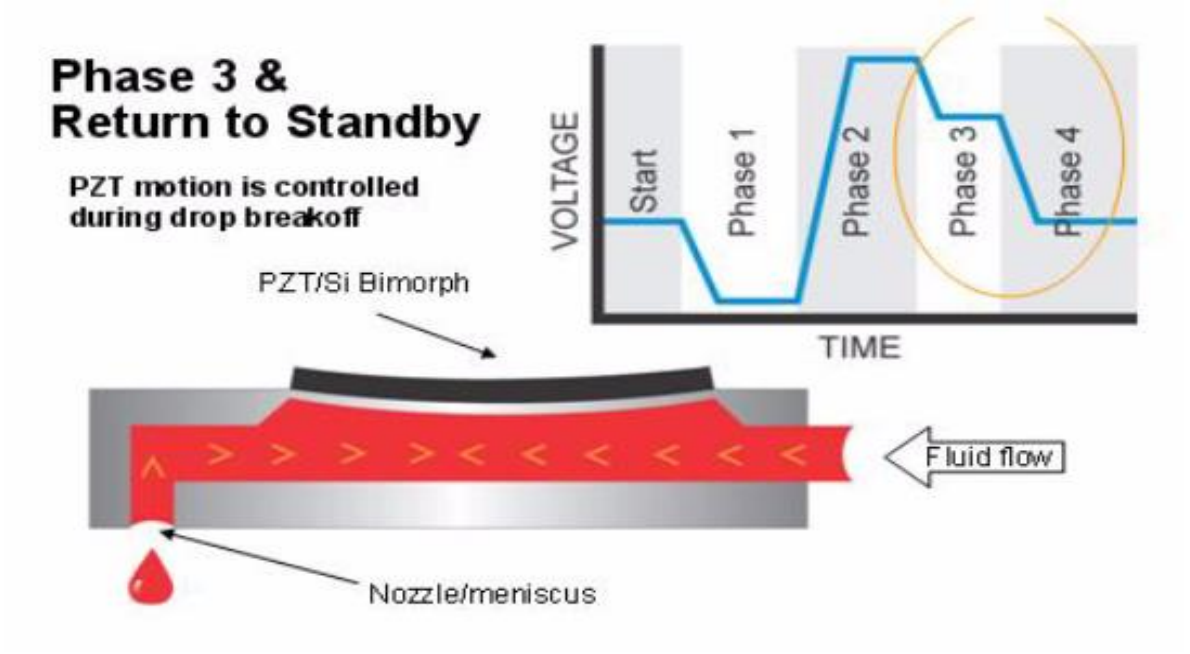

Figure 4.16: Waveform of piezoelectric print head at phase 3 [153].

The manufacturers of the Fujifilm Dimatix Materials Printer DMP-2831 provide the user with a standard waveform which suitable for most of fluid. But different adjustment is needed for different fluids since every fluid has its characteristics pressure waves which depend on the properties of the fluid.

4.2.3 Dosing of the ink

To simulate the formation of liquid drops of incompressible Newtonian fluids from a simple capillary tube, Xu and Basaran carried out computational analysis by imposing a transient flow rate upstream of the nozzle exit. According to their analysis, the formation of the liquid drops depends on the nozzle geometry, drop velocity and the volume of the fluid [156]. According to them, the slow emission of a liquid from a nozzle leads to the formation of a pendant droplet which grow slowly and at the same time it characterized by a balance between inertial and surface tension forces. The size of the droplets can be influenced by the shape of the nozzle opening. A continuous liquid jet is formed when the kinetic energy overcomes the surface energy and this can be happened if the drop velocity is sufficiently large, the dosing of the ink can be illustrated by Figure 4.17. Thus, the fluid flow in the nozzle can be expressed by this equation:

$$\mathbf{Q = \pi \frac{\sqrt{W_e}}{2} \sin \Omega t} \tag{4.1}$$

Where (Ω) is the firing frequency, (t) is the time required for jetting, and (W_e) is the Weber number and it is used to express the lower critical velocity for jetting formation, where:

$$\boldsymbol{W_e = \frac{\rho_l r v^2}{\gamma} > 4} \tag{4.2}$$

r is the radius of the jet, γ is the surface tension, and ρ_l is the liquid density. The initial velocity of the formed drop in the fluid is given by:

$$\mathbf{v = (1\text{-}R^2)\sqrt{W_e} \sin \Omega t} \tag{4.3}$$

The volume of the fluid is given by:

$$\mathbf{V_{MAX} = \pi \frac{\sqrt{W_e}}{\Omega}} \tag{4.4}$$

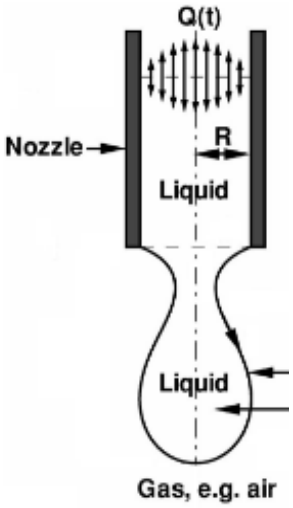

Figure 4.17: The dosing of the ink [156].

4.2.4 Ink Transfer

The Ink transfer is explained in details by Eric R. Lee [158], it depends on three important parameters as the drop's velocity is non linear.

a- Acceleration Force:

The acceleration force of the jetting droplets depends on the acceleration force of the motion of the piezo and the gravity force. Thus, the acceleration force can be expressed by:

$$\mathbf{F_{Acceleration} = F_a + F_g = m*a + m*g = m\,(a + g)} \qquad (4.5)$$

Where (a) is the acceleration due to the piezo motion, (g) is the gravity acceleration, and (m) is the mass of the jetting droplet.

b- Medium Resistance:

The force opposes the motion of the jetting droplets through the medium is expresses by the medium resistance. There are two types of fluid flow; laminar flow and turbulent flow. Laminar flow in air can be expressed by Stokes Law as follows:

$$\mathbf{F_{stockes} = 6\,\pi\eta r\nu} \qquad (4.6)$$

Where ($F_{stockes}$) is the resistance force of the air, (η) is the viscosity of the air, (r) is the droplet's radius, and (ν) is the droplet velocity. On the other hand the turbulent flow in air can be expressed by the following equation:

$$F_{Drag} = \frac{1}{2}\rho C_d A v^2 \quad (4.7)$$

Where (F_{Drag}) is the acceleration force required to move through the air, (C_d) is drag coefficient, (A) is frontal area, and (ρ) is the density of the air. The domination type of flow can be determined by Reynolds Number which is given by:

$$Re = \frac{\rho . v . L}{\eta} \quad (4.8)$$

The laminar flow dominates if the Reynolds Number less than1. Three correction factor should be added to the stockes force:

1- The first correction factor called Cunningham's correction, it is a result of because of the non-continuum effect and can be expressed by:

$$C_c = 1 + \frac{2\lambda}{d}\left[A_1 + A_2 e^{\frac{-A_3 d}{\lambda}}\right] \quad (4.9)$$

Where (λ) is the mean free path, (d) is the droplet diameter, (A_n) are experimentally determined coefficients. This factor significant if droplets become smaller than 15 μm

2- The second factor is a result of the aerodynamic forces or the electric fields which deform the perfect spheres drops, as illustrated in Figure 4.18, and can be expressed by:

$$C_{NS} = \frac{1}{3} + \frac{2d_s}{2_{d_n}} \quad (4.10)$$

Where (d_n) is the circle diameter with the same projected front area in the direction of motion, (d_s) is the diameter of a sphere with an equal surface area to that of the deformed drop. For drops below 100 μm in diameter, this factor is negligible.

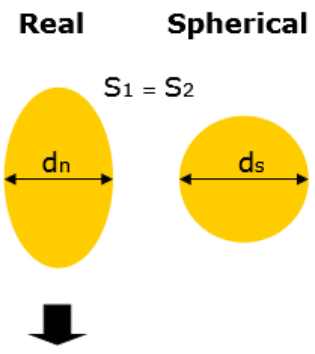

Figure 4.18: The effect of aerodynamic forces or the electric fields on the jetting drops.

3- The third correction is called Buoyancy's correction, it is a result of upward acting force exerted by a medium which opposes an object's weight and can be expressed by:

$$C_B = \frac{4}{3}\pi r^3 g\rho \tag{4.10}$$

Where (r) is the droplet's radius, (g) is the acceleration gravity, (ρ) is the air density. As air has approximately 1/1000 density of fluid, this effect might be neglected for air. So after taken these three correction factors into consideration, the resistance force of the air can be expressed by:

$$F_{RESISTANCE} = \frac{F_{Stokes} C_{NS}}{C_C} + C_B \tag{4.11}$$

The surface resistance to air flow is reduced due to the internal circulate of the fluid in the drop as the fluid drop falls through the air. This action can be illustrated in Figure 4.19.

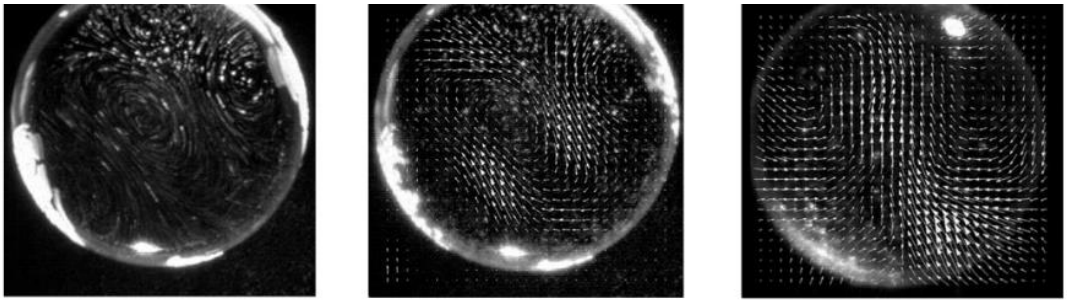

Figure 4.19: Internal Circulating of the fluid in the drop.

c- Acceleration Force:

If the acceleration force is equal to resistance force of the travelling medium (e.g air), the terminal velocity of the droplets is reached.

$$F_{RESISTANCE} = F_{Acceleration} \tag{4.12}$$

$$\frac{F_{Stokes} C_{NS}}{C_C} + C_B = m\,(a + g) \tag{4.13}$$

4.2.5 Fluid dynamics on the substrate

The phenomena of fluid dynamic of liquid drop on solid surface includes bouncing, spreading, and splashing, this can be illustrated in Figure 4.20. In general, two phases can be subdivided from the impact process. An initial impact phase where the droplet hits the substrate. An impact face where a process of rebound occurs leading to the formation of the thin film. The intermolecular forces contribute in the domination of spreading process if the kinetic energy of the drop is extremely small and this usually happens at lower impact velocities. On the other hand, splashing occurs at higher impact velocities as a result of a disintegration of the fluid. The critical velocity is given by:

$$\mathbf{v_{critical}} = \frac{\pi d \sigma}{\rho a} \tag{4.14}$$

Where (d) droplet diameter, (σ) is the surface tension, (ρ) is the density of the fluid, and (a) is the droplet acceleration.

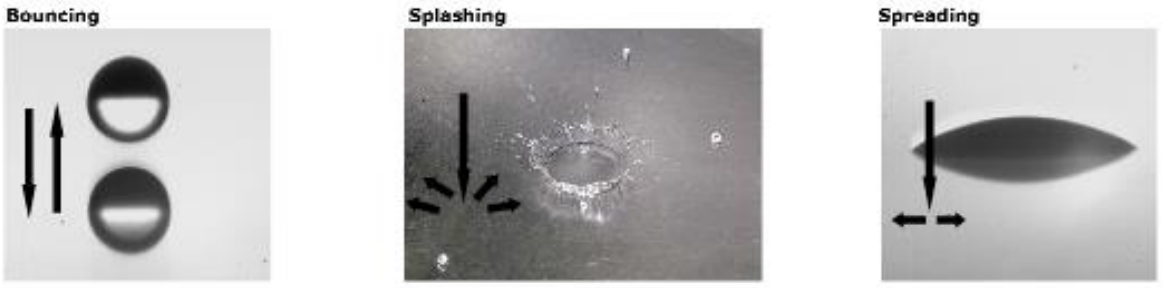

Figure 4.20: The drop impact on the solid surface [8].

When a drop collides with a solid wall, a significance of the shock wave is formed in the drop. Figure 4.21 illustrates this shock and other important parameters. In the ideal case, a point like is the first contact between the wall and the base of the drop leading to develop a contact zone of radius (r_e) then develops. The relationship between contact edge velocity v_c, the initial speeds of the impact velocity v_i and the contact angle (θ) between the drop and the wall is given by:

$$\mathbf{v_e} = \frac{v_i}{\tan \theta} \tag{4.15}$$

With a velocity C_s, which is the same velocity of sound in the term of magnitude, the shock propagates inside the drop. The fluid ahead cannot be disturbed by the impact and the shock remains attached to the contact edge as long as the impact velocity v_i is greater than $C_s \sin \theta$. The shock can only separate from the contact edge and moves up the undisturbed surface of the drop if the contact angle becomes larger than the critical angle:

$$\theta_c = \sin^{-1}\left(\frac{v_i}{C_s}\right) \tag{4.16}$$

The two cases of not disturbed fluid ahead and with shock waves disturbed fluid ahead can be shown in Figure 4.22.

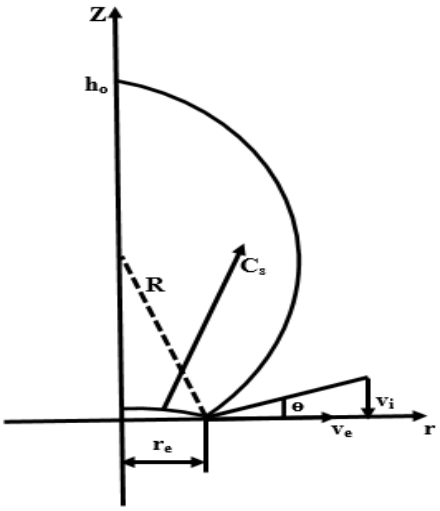

Figure 4.21: The formation of the shock wave in the drop after the collision with a solid wall [159].

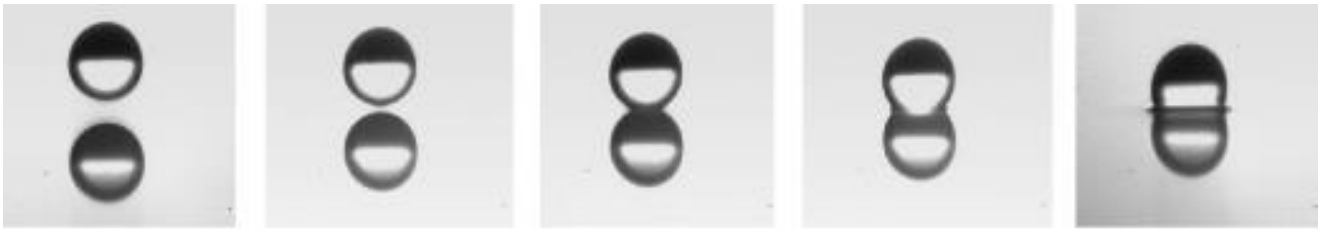

Figure 4.22: Initial phase and contact line propagation [159].

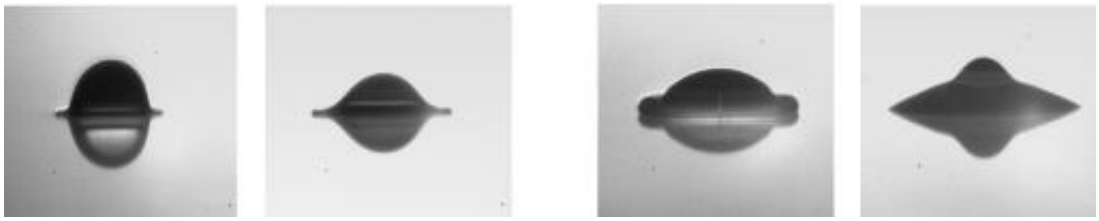

(a) **(b)**

Figure 4.23: (a) Not disturbed fluid ahead (b) with shock waves disturbed fluid ahead [159].

A pressure wave have to put the air below the droplet before a droplet impacts the surface as shown in Figure 4.24. Usually an air bubble is included into the droplet if the contact between the wall and the base of the drop is not point like and the pressure wave velocity is lower than contact edge velocity (v_c). The volume of the air bubble is given by:

$$\mathbf{V_b} = \frac{4}{9}\left(\frac{\eta_{air}}{v_i}\right)\frac{\rho}{\rho_{air}} \tag{4.17}$$

Where (V_b) is the bubble volume, (η_{air}) is the kinetic viscosity of the air, (v_i) is the initial velocity of the drop, (ρ) is the density of the fluid, and (ρ_{air}) is the density of the air.

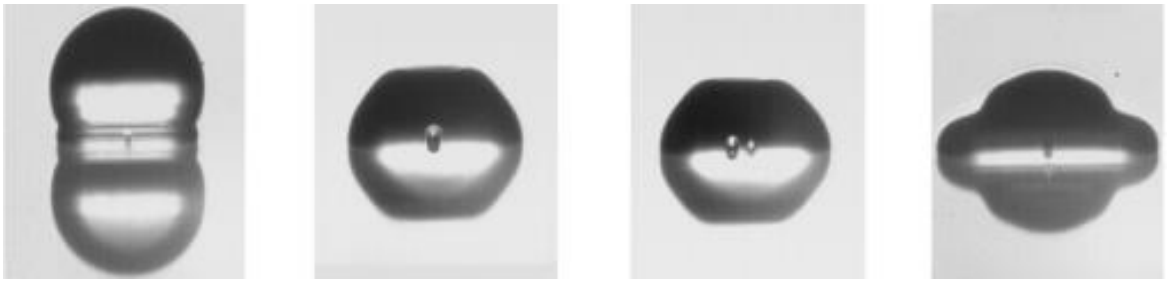

Figure 4.24: The influence of air bubble during a droplet impacts the surface [159].

After the contact line is formed *i.e* initial phase, the second step is the formation of a thin film *i.e.* impact phase. The impact phase can be into two steps for the low surface energy at which the droplet impact onto a solid substrate. The first step there is a rapid radial fluid flow as the radius of the droplet–substrate interface expands and becomes of the order of magnitude of the initial droplet radius (in free flight). The second step, it is the process of rebound where the fluid comes to rest. Figure 4.25 summarizes fluid dynamics on the substrate.

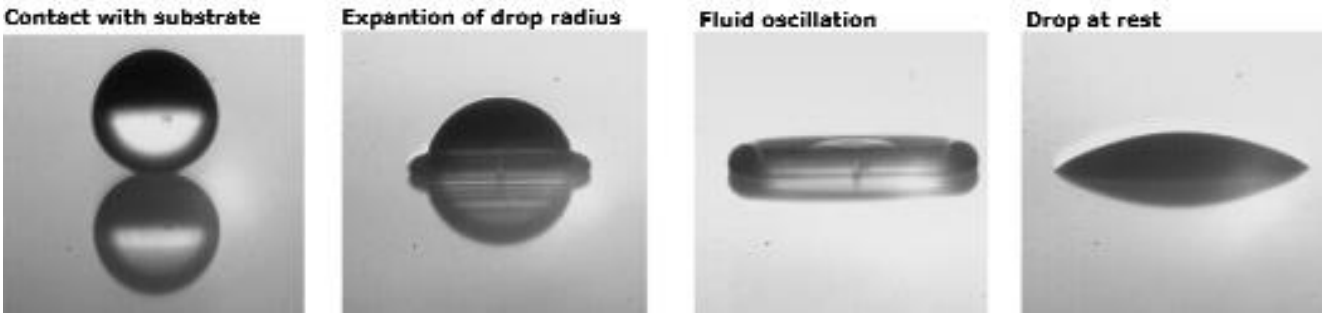

Figure 4.25: The process of fluid dynamics on the substrate [159].

4.2.6 Solidification

The process of solidification is usually called curing reactions can take place via one or combination of several processes such as heating or photonic sintering. These processes are the last step toward the formation of the desired patterns by inkjet printing technique. The solidification step is an important for the deposition and improvement of the printing patterns. The relationship between solidification step and the final morphology and also the electrical resistance of the printed layers have been investigated [160, 161].

The thermal or annealing treatment is a common step toward solidification and it is essential step for each printing process. Several parameters play an important role during the annealing treatment such as drop velocity, substrate temperature and the boiling point of the solvents. There is usually an undesired effect accompanying the evaporation step which is coffee stain effect [162]. This effect mainly is responsible for the electric performance of the printed devices. The different processes involved in the solidification step can be schematized in Figure 4.26. When the solvent starts to evaporate at the drop boundary, an outward capillarity flow of the solvent occurs to transport the undesired amount of the active materials from the interior of the droplet to the periphery. Another flow, called Marangoni flow, can be generated by employing a mixed solvent system with a higher boiling point and a lower surface tension than the main solvent to balance the convective to avoid the formation of coffee stain [163]. Since the direction of the Marangoni flow opposes to the direction of the convective flow. Also, in order to reduce the outward capillary flow, a higher temperature should be applying during the drying process.

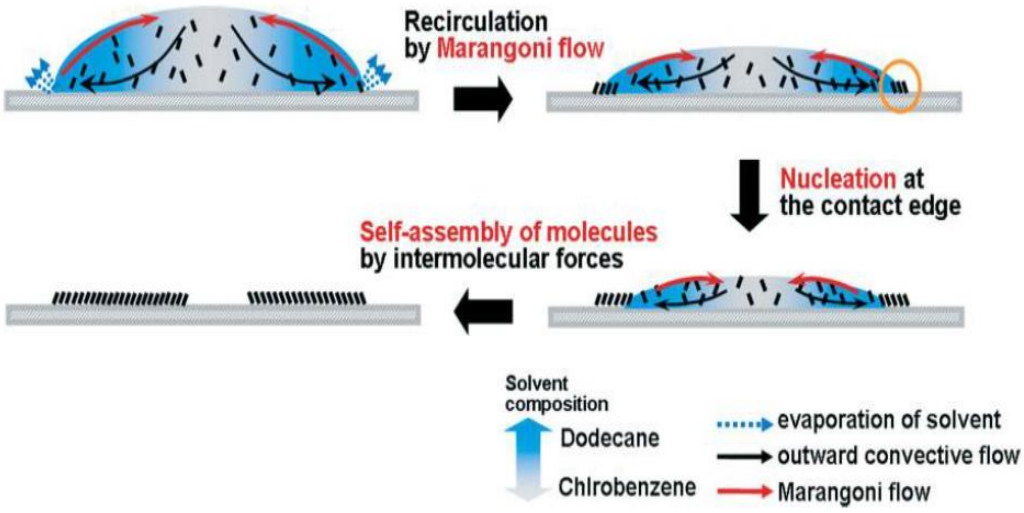

Figure 4.26: The processes involved in the solidification process [160].

Another step toward the curing processes can be followed the annealing step which is photonic sintering. The photonic sintering process is an essential step for nanomaterials as they have significantly larger surface energy, it is a low thermal exposure sintering method. This step depends on high intensity pulse of light, so it is known as intense pulsed light (IPL) sintering [164]. The agglomeration, aggregation, and the non-densifying diffusions are the challenges toward photonic sintering, these phenomena usually occur in nanomaterials. The attractive force between the fine particles size and each other refers to the agglomeration, this type of force is a very weak force such as Van der Waals or electrostatic forces. On the other hand the force results from binding the nanomaterial together through a significant solid necks strength such as metallic force refers to the aggregation [165]. The difference between agglomeration and aggregation can be illustrates in Figure 4.27.

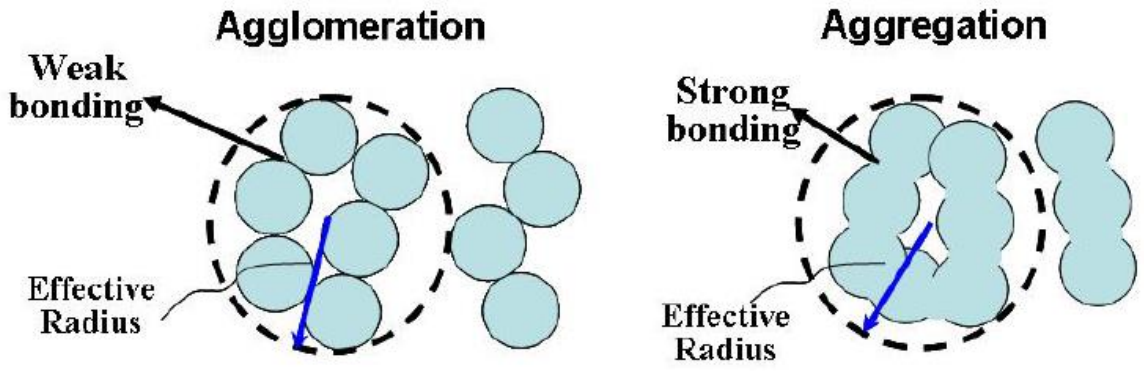

Figure 4.27: The difference between agglomeration and aggregation in nanomaterial [166].

Inhomogeneous distribution of particles over the substrate are a consequence of these two phenomena. So, the photonic sintering is the promising curing step toward creating continuous conductive printing patterns and at the same time mechanical adhesion between the substrate and the neighboring particles. To characterize the degenerated sintering capability of agglomerated and aggregated particles, the concept of effective radius which is much larger than the real radius of particle has been introduced. The advantages of nanoscale particles are lost, when the concept of effective radius reaches the micron size and this can be occurs at higher temperature to overcome the non-densifying diffusions. Since the densification depends on the volume diffusion of the material, so higher temperature is required to diffuse the grain boundaries and neck formation between particles. This can be achieved by photonic sintering whose effect produces minimal damage on low temperature substrates. Densifying and non-densifying diffusions and their sintering results can be illustrated in Figure 4.28.

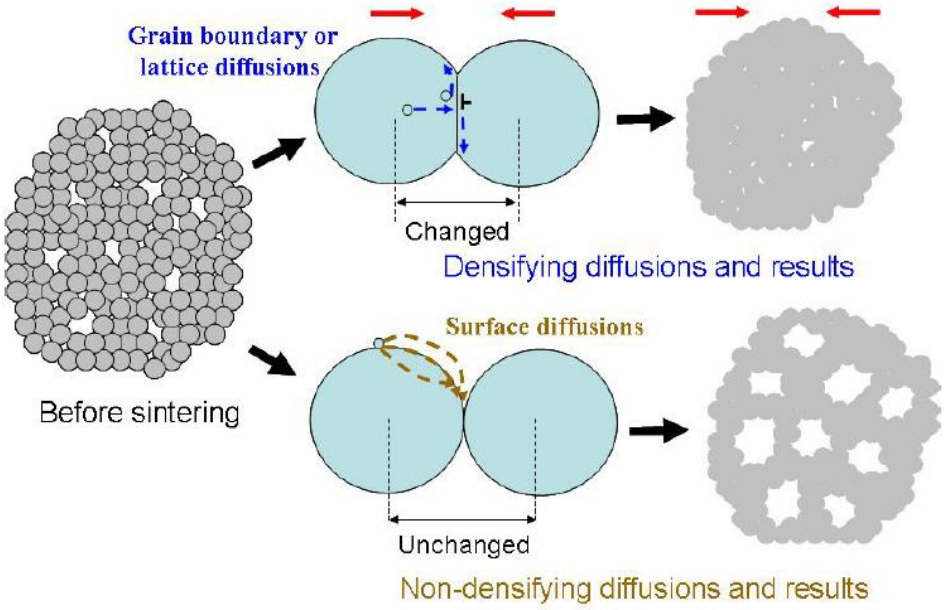

Figure 4.28: Illustration of densifying, non-densifying diffusions and their sintering results [166].

Finally to achieve the ideal condition of printing such as avoiding nozzle clogged, achieving perfect alignment, and also getting rid of drop satellites, several printing parameters should be taken into account:

1- ***Number of Jetting Nozzles:*** As discussed in section 4.1.4, the Fujifilm Dimatix Materials Printer DMP-2831 has a single row of 16 nozzles adjacent to each other. Roughness and precision of the patterns are the factors which determine the number of the nozzles to be used. More than one nozzle can be used for rough patterns. On the other hand, only one nozzles can be used for high precision patterns.

2- ***Cleaning cycles:*** The cleaning cycles depends on the type of the ink and the pattern dimensions. As discussed in section 4.1.2, to prevent nozzle clogging during printing, it is highly recommended to do cleaning cycles before printing. For inks whose particles tend to agglomerate, a frequent cleaning cycles is mostly recommended also for printing wide patterns.

3- ***Jetting or firing Voltage***: It is the voltage required to the drop ejection phase (Phase 2). The range of the jetting voltage of the Fujifilm Dimatix Materials Printer DMP-2831 is from 1-40 V. Each nozzle of the cartridge has its own jetting voltage tab which can be adjusted from the cartridge setting. To prevent the formation of the drop satellites, it is important to adjust the suitable firing voltage. The jetting voltage depends on the viscosity of the fluid. A higher jetting voltage is required for high viscosity inks while

the jetting voltage can be lowered for low viscosity inks. It is important to mention that the drop dimension depends also on the adjutancy value of the jetting voltage. As the lower jetting voltage result in a low drop dimension. On the other hand the higher jetting voltage produce a big drop dimension.

4- ***Drop Spacing:*** It is one of the required resolution of the printed patterns. It refers to the distance between two contiguous from their centers. The resolution of the printed patterns is measured in dot per inch (dpi); where inch = 2.54 cm. Therefore, the relation between the pattern resolution and the drop spacing is given by:

$$Drop\ Spacing\ (\mu m) = \frac{25400}{\text{Resolution (dpi)}}$$

Figure 4.29 shows three basic morphologies when examining printed patterns across a variety of drop spacing. Drop spacing usually varies from 5 µm to 100 µm from the center of one drop to the center of the successive drop. Isolated drops are expected for large spacing whereas an overflowing is expected for low spacing.

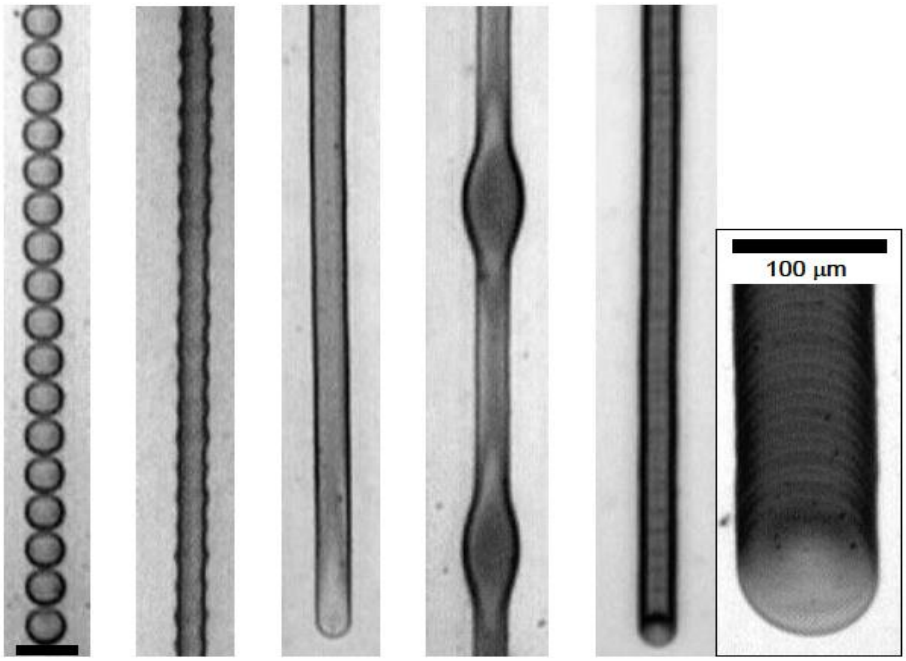

(a) **(b)** **(c)** **(d)** **(e)**

Figure 4.29: Effect of drop spacing on the quality of line printing, drop spacing decreases from left to right (a) individual drops (b) scalloped (c) uniform (d) bulging (e) stacked coins [153].

4.3 Fluid properties of the ink

A range of the chemical and the physical characteristics, within which inks may be successfully printed, is provided by the manufacturers of the Fujifilm Dimatix Materials Printer DMP-2831 as follows:

1- ***Viscosity:*** 10-12 cP at jetting temperature.
2- ***Surface tension:*** 28-33 dyne/cm at jetting temperature.
3- ***Low volatility:*** Boiling points higher than 100 °C are preferred since the highly volatile fluids may start drying at the nozzle leaving residue and therefor preventing it from jetting.
4- ***Density:*** Specific gravity greater than 1 is beneficial.
5- ***Degassing:*** It can be done with a vacuum system before filling a new cartridge, by ultrasonic baths or by spinning to remove any dissolved gas which inhibits jetting.
6- ***Filtration:*** It is recommended to filter the fluids with a 0.2 μm nylon filter before filling a new cartridge.
7- ***Acidity or Alkalinity:*** A pH-value between 4 and 9 is suggested.

These information are the starting point when a new ink is formulated to get an ideal ink. However, appropriate functional ink materials are limited in availability. Inappropriate ink will lead to unstable ink-jetting in which long-lived filaments form, connecting the ejected droplet to the nozzle [167]. The ejecting drops of an ideal inks can be shown in Figure 4.30.

Fluid dynamics involved in the inkjet printing have been studied [168- 171] and an atomistic understanding of ink-jet dynamics is recently emerging [172, 173]. The important physical parameters of printing fluids which strongly influence the final printing performance, with respect to all above mentioned parameters, are viscosity, and surface tension. These fluid properties influence the drop formation mechanism, the spreading of the droplet on the surface and subsequent drop size at a given voltage. For example, a very low surface tension fluid may be flow out of the nozzles. Also a very low viscosity fluid results a very poor control of the droplets and in material waste during the cleaning cycles. Surface tension and viscosity of the ink are important parameters.

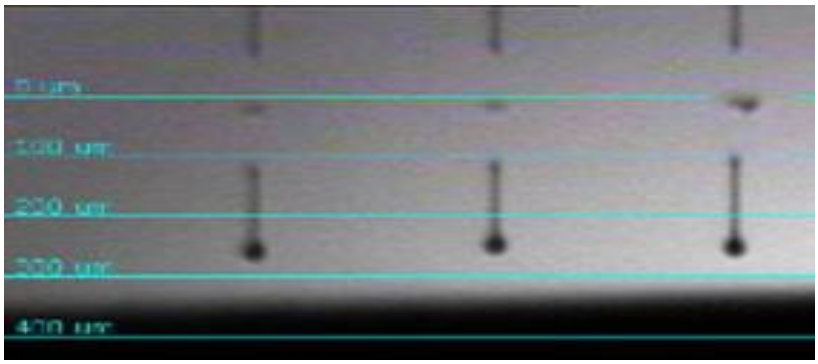

Figure 4.30: The ideal ink ejecting drops [153].

4.3.1 Viscosity Effect

Viscosity data often functions as a “window” through which other characteristics of a material may be observed. Viscosity in general is a measure of a liquid’s ability to resist flow. A thick liquid has a high viscosity so it does not flow easily and a thin liquid that readily flows has low-viscosity. When a fluid starts to flow under the action of a force, another force is produced everywhere which tends to oppose the motion of that liquid, this force is called shearing stress. Because of the successive moving of fluid layer, a transmit momentum from the faster layer to the slower layer trending to resist the relative motion. This behavior can be illustrated in Figure 4.31.

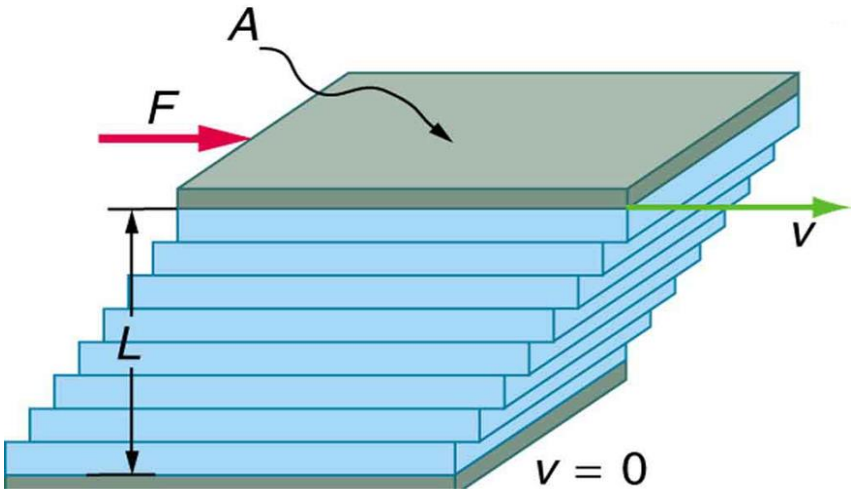

Figure 4.31: Illustration the idea of Viscosity.

According to Figure 4.31, if a shearing force (F) is applied to the top plate (A), this plate will move at a specific velocity (V). The layer of the fluid immediately below the plate will also move with a velocity less than that of the plate. By the same manner, each successively lower layer of the fluid will move at a velocity lower than that of previous layer its immediate predecessor so that the last layer is almost motionless. The force which is applied to the top plate divided by the area (A) of the top plate is defined as shear stress:

$$\text{Shear Stress} = \frac{\text{Force}}{Area} \qquad \text{Newtons/□} \tag{4.18}$$

The velocity gradient, dv/dl, is a differential change in velocity divided by the distance between the top and the bottom plates, it is also called shear rate because it expresses the shearing the liquid experiences. The unit of shear rate is the reciprocal second (sec^{-1}).

$$\text{Shear Rate= Velocity gradient} = \frac{\mathrm{dV}}{dl} \qquad sec^{-1} \tag{4.19}$$

As the force required to maintain this difference in velocity is proportional to the difference in velocity through the liquid, or the velocity gradient, then:

$$\text{Shear Stress } \alpha \text{ Shear Rate} \tag{4.20}$$

$$\frac{\text{Force}}{Area} \quad \alpha \quad \frac{\mathrm{dV}}{dl} \tag{4.21}$$

$$\frac{\text{Force}}{Area} \quad = \quad \eta \frac{\mathrm{dV}}{dl} \tag{4.22}$$

Where η is the proportionality constant between shear stress and the velocity gradient for a given material and is called its viscosity. Equation 4.22 is called the Newton's law of viscosity and states that the shear stress between successive fluid layers is directly proportional to the negative value of the velocity gradient between the two layers. Then, the viscosity of a fluid can be derived from these two properties as a measure of fluid's resistance to gradual deformation by shear stress or shear stress.

$$\text{Viscosity} = \frac{\text{Shear Stress}}{Shear\ rate} \tag{4.23}$$

The cgs physical unit of viscosity is Poise (P), it is more commonly expressed, particularly in ASTM standards, as centipoise (cP). Since:

$$1 \text{ mPa·s} = 1 \text{ cP.}$$

The viscosity of fluids is affected by some factors such as:

1- ***Time:*** The change in viscosity of many inks can occur over time.
2- ***Temperature:*** One of the most obvious factors affecting viscosity of the ink. As the temperature of the ink increases, the viscosity decreases. Printing inks are sensitive to temperature, so the temperature must be carefully controlled.
3- ***Physical/Chemical Properties:*** The composition of fluid is an important factor of its viscosity. When this composition is altered either by changing the properties of the

component or by the addition of other materials. For example, the addition of solvent to printing inks will lower the viscosity.

For the Fujifilm Dimatix Materials Printer DMP-2831, it is suggested that the v viscosity of the ink employed should be in the range of 10-12 cP at jetting temperature. In some cases that range can be higher than 12 cP but should not exceed 30 cP as the filament of the droplet in that case can be broken. Also another challenge is raised if the viscosity of the ink is in the range of 2-4 cP, in that case the formation of the satellite droplets is produced.

4.3.2 Surface Tension Effect

The fundamental principle that enables the operation of inkjet printers is the tendency of a continuous stream of fluid to break apart and form droplets. Droplets form due to the surface tension of the liquid. One striking and interesting property of all liquids is surface tension. In any liquid, intermolecular forces cause attraction between the liquid molecules to each other. These forces that pull liquid molecules towards each other are known as "cohesive" forces. In the body of a liquid, a molecule is surrounded by the other liquid's molecules in all directions, so there is no overall force as the attractive forces cancel each other as illustrated in Figure 4.32. On the other hand the surface interface between the liquid and air, a molecule in the surface of the liquid has attractive forces resulting from the other molecules within the liquid. This causes the outer layer of the liquid to act like a stretched membrane and minimize the surface area. Surface tension simply is described as a phenomenon that results directly from intermolecular forces between molecules of liquids. In other words, the tension of the liquid surface is a result of the molecules at the surface of the liquid which experience a net force drawing them to the interior. The surface tension of a liquid is measured in Dynes/cm.

The surface tension considers one of the important factors of printing industry because the ink that is squirted out of the cartridge and sticks onto the substrate needs to be a steady stream and not stick together. After leaving the nozzle, the column of ink separates into spherical droplets. As these ink spherical droplets are charged, thus they directed into position by charged deflection plates. The principle of this process to work depends mainly on the surface tension of the ink, more surface tension the ink has may clog the nozzle or not adhere properly to the substrate. On the other hand, too low surface tension of the ink, it can cause leak or bleeding of the ink everywhere.

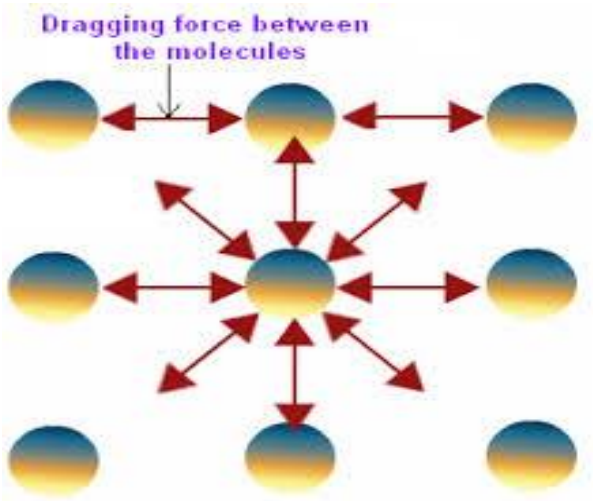

Figure 4.32: Diagram of how water surface tension works [174].

It is important to assure that the inks wets out on the substrate evenly in order to obtain good adhesion and print quality. The possibility to achieve a sufficient bonding between the liquid and the substrate depends on the interfacial area between them. The more the interfacial area, the greater is the possibility of sufficient bonding [174]. The contact angle is an important parameter to achieve good adhesion and good printing quality.

4.3.2.1 Contact angle

The contact angle is a function of energy of adhesion (between molecules in the liquid and solid) and cohesive energy (between the molecules in the liquid in a specific environment [175]. The contact angle is a measure of how the liquid wets the surface, it is defined as the angle formed by the intersection of the liquid-solid interface. When a droplet hits a surface, the contact angle goes from larger values to smaller values until state of equilibrium has been reached. Figure 4.33 shows the state of liquid droplets on the surface regarding to the contact angle. The liquid spreads on the surface if the contact angle is small, the liquid beads on the surface if the contact angle is large. More specifically, a desirable wetting of the surface is achieved if the contact angle is less than 90°. While the fluid will spread over a large area on the surface; while contact angle is greater than 90° generally means that wetting of the surface is unfavorable so no wetting of the surface will occur. Therefore, Strong adhesion and weak cohesion leads to a low surface tension and small contact angle, resulting in a high wetting. For example, complete wetting occurs when the contact angle is 0°, as the droplet turns into a flat puddle.

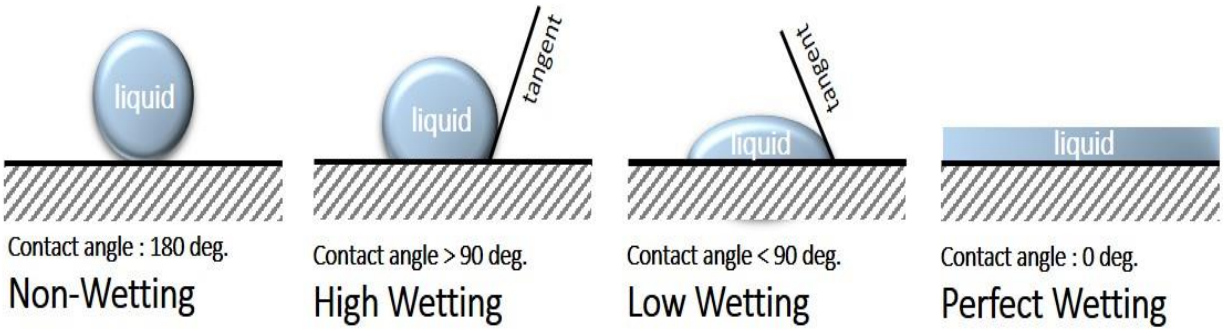

Figure 4.33: Contact angle is a measure of how the liquid wets the surface [175].

4.4 Ink Formation and Characterization

As previously mentioned, reliable inkjet printing requires fine-tuned ink formulations consisting of a certain viscosity and surface tension. In order to allow for structural versatility, device miniaturization, and purely selective system deposition, multilayer inkjet-printed devices require the use of high conductivity metallic inks. The Ag ink DGP-40LT-15C of Advanced Nano Products (ANP) (Sejong, Korea) contains 35% silver nanoparticles in TGME (triethylene glycol monoethyl ether) and has a density of 1.45 ± 0.05 g.cm^{-3} is the main ink used during this thesis.

4.4.1 Silver Nanoparticle-Based Ink

For inkjet-printed conductive materials, one of the most popular options is a silver nanoparticle-based solution. Silver nanoparticles based conductive inks are usually produced by many companies. Table 4.1 summarizes some of commercially available silver nanoparticles inks and their properties.

Concerning this thesis, the commercial Ag ink DGP-40LT-15C of ANP is was the best printable ink, whose physical parameters matched perfectly the Fujifilm Dimatix Materials Printer DMP-2831 requirements. The ink is composed of a dispersion of 30-35 wt. % in triethylene glycol monomethyl ether. The silver NPs have a diameter of approximately 30 nm. Its formulation is engineered for reliable piezoelectric inkjet printing of excellent conductivity, long-term stability, a good adhesion, a high-resolution, and low-resistivity conductive patterns on a variety of flexible substrates. Its durability was high as well as the pattern resolution achievable, photography of some of the printed test-patterns can be shown in Figure 4.34. Its main physical properties provided by the company are listed below:

Solid Content (%): 30-35 %.

Viscosity: 10-17 cP at 22 °C.

Surface tension: 35-38 dyne/cm at 25 °C.

Specific Resisitvity: 11~7 μΩ-cm.

density: 1.23-1.24 g/mL.

Sympol	**Company**	**Size**	**Content (wt %)**	**color**	**Solvent**
NPS-J	Harima	3-7 nm	57-62	Dark Blue	Tetradecane
NPS-J-HTB	Harima	3-7 nm	53-58		Tetradecane
NPFS	Harima	1-10 nm	30		Toluene
AX NJP-6F	Amepox	4-8 nm	40-60	Dark brown	
DGP-40-LT-15C	ANP	5-11 nm	30-35	Dark brown	TGME(Triethylene glycol monoethyl ether
DGP 40TE-20C	ANP	5-11 nm	30-35	Dark brown	TGME(Triethylene glycol monoethyl ether
DGP 45HTG	ANP	5-11 nm	30-35	Dark brown	TGME(Triethylene glycol monoethyl ether
DGH 55LT-25C	ANP	5-11 nm	50-60	Dark brown	Tetradecane
DGH 55-HTG	ANP	5-11 nm	50-60	Dark brown	Tetradecane
TEC-IJ-060	InkTec	< 1 nm	50	Transparent	

Table 4.1: Some of commercially available silver nanoparticles inks and their properties [176, 177].

Figure 4.34: Photography of some of the printed test-patterns.

4.4.2 The Effect of Plasma Treatment

Most of the surface of the employed substrates in this thesis are hydrophobic and do not provide good wettability for polar solvents. To modify the substrate's surface various treatments can be used to become hydrophilic. In this work, Oxygen plasma treatment is the chosen method to obtain hydrophilic surface. Figure 4.35, illustrates the effect of plasma treatment on deposition of Ag-NPs on PDMS substrate. According to the figure, a continuous silver pattern is formed on the plasma-treated hydrophilic surface and on the other hand isolated ink droplets are appeared on the plasma-untreated hydrophobic surface. Also some observations are recorded during the printing such as the drying time for the isolated ink droplets on the plasma-untreated hydrophobic surface is so long while for plasma-treated hydrophilic surface can be done in a few minutes resulting in a continuous silver lines. Hence, plasma treatment is an essential step for surface modification of the substrates prior to printing process for successful printing patterns. The printing process should be done no more than two hours after doing plasma.

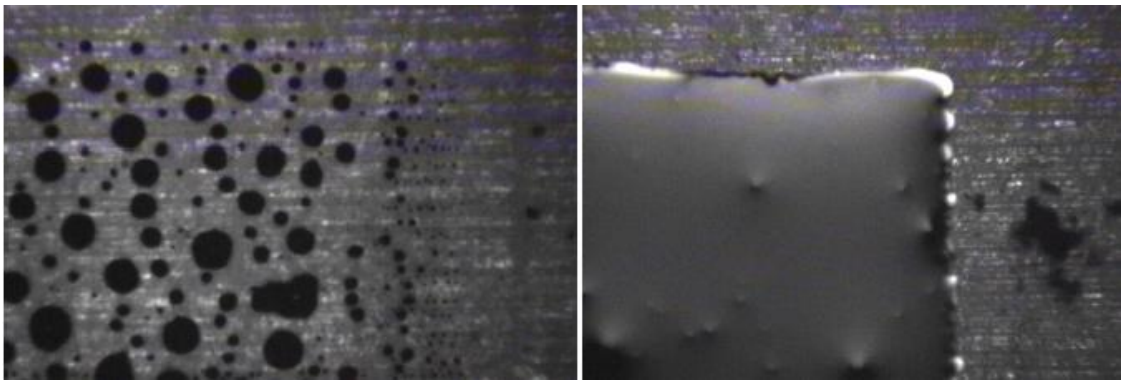

Figure 4.35: The Ag-ANP ink deposited on PDMS (a) without plasma treatment (b) and after plasma treatment.

4.4.3 The Effect of Drop Spacing

The drop spacing is based on the drop diameter of the droplets, as it is set to be half of the drop diameter. For Fujifilm Dimatix Materials Printer DMP-2831, the drop spacing can be varied from 5 to 254 µm. The microscopic pictures of printed silver lines at different drop spacing can be shown in Figure 4.36. According to the figure, obtaining continuous printed lines highly depend on drop spacing.

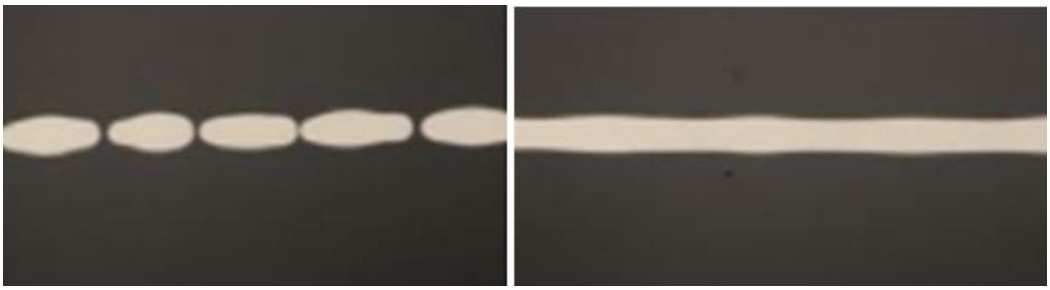

Figure 4.36: Microscopic images of the printed Ag-NPs line at different drop spacing.

4.4.4 The Relationship between the Drop Spacing, Line width and Resistance

As the continuous printed lines highly depend on drop spacing, the printed lines width also depend on the drop spacing. The relationship between the drop spacing, the line width and the electrical resistance can be shown in Figure 4.37. The drop spacing is directly proportional to electrical resistance, as it increase the electrical resistance is also increase. On the other hand, line width is inversely proportional to drop spacing.

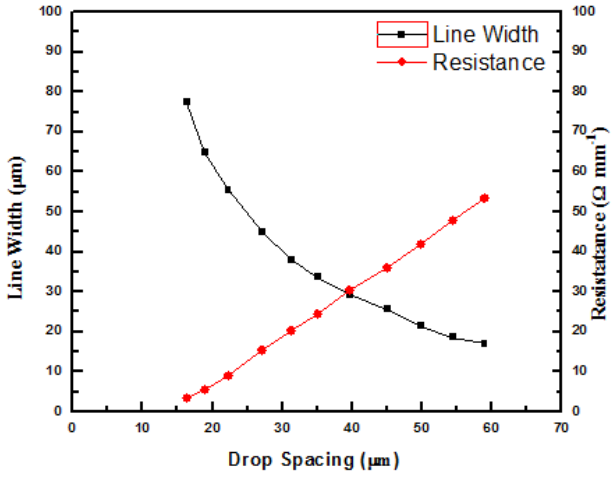

Figure 4.37: The relationship between the drop spacing, line width and the electrical resistance.

4.4.5 The Effect of Photonic Sintering

Figure 4.38 shows microscopic images of printed silver lines after drying under two case: (a) before photonic sintering and (b) after photonic sintering. According to the figure, both cases are homogenous and there is no visible cracks. But there is few droplet borders in the sample before sintering and on the other hand the droplet borders vanished completely in the sample after photonic sintering and also the line width increases. This result is also confirmed by Scanning Electron Microscope (SEM) images before sintering and after sintering as shown in Figure 4.39.

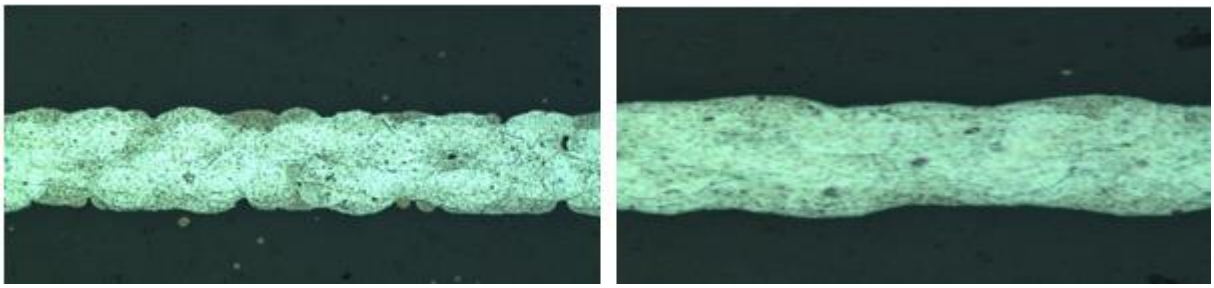

Figure 4.38: Microscopic images of the printed Ag-NPs line (a) before Photonic sintering. (b) after photonic sintering.

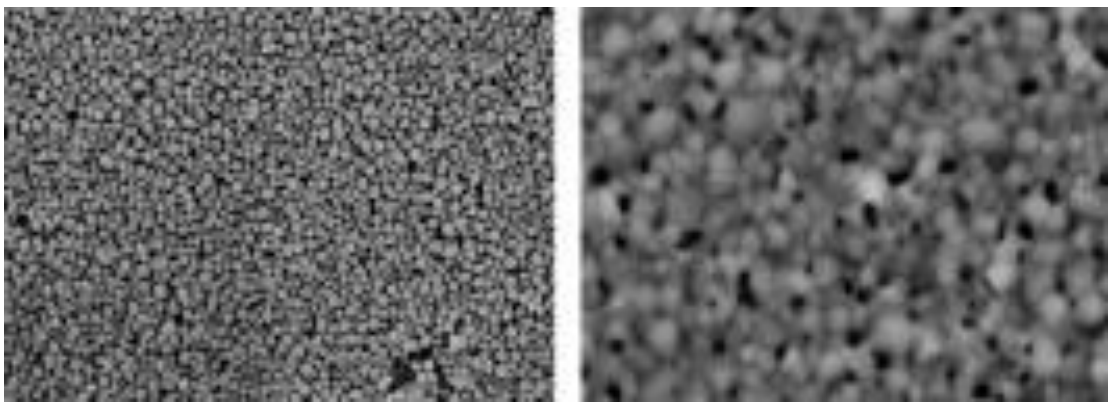

Figure 4.39: SEM images of silver NP ink (a) without Photonic sintering and (b) after Photonic sintering.

During the experimental work of this thesis, both 10 pL and 1 pL cartridges were employed depending on the specific pattern to be printed. Ag-NPs ink has been printed over different flexible substrate. The effect of drop spacing, relation between line width and resistance and also the effect of photonic sintering of each substrate have been studied. The obtained results of each substrate are in agreement with aforementioned results but with the specific printing parameters of each substrate. Table 4.2 summarizes the most important parameters for different substrates as obtained from the experimental work toward high quality printing pattern. It is

important to note that the number of nozzles of Fujifilm Dimatix Materials Printer DMP-2831 is 16 nozzles, the typical number of nozzles during the experimental work of this thesis are 3 nozzles. But higher number of nozzles can be employed also according to the type of the pattern as discussed before. In general, it is not recommended to use more than 5-6 nozzles to avoid nozzle clogging.

Parameter/Substrate	**PET**	**Kapton**	**Silicone**	**PVDF**	**PDMS**
Plasma Treatment	30s, 30%	30s, 30%	30s, 30%	30s, 30%	30s, 30%
Drop spacing	35-40 μm	35-40 μm	35-40 μm	35-40 μm	40 μm
Firing voltage	30-40 V	30-40 V	30-40 V	30-40 V	30-40 V
Maximumjetting frequency	5-20 KHZ	5-20 KHZ	5-20 KHZ	5-20 KHZ	5-20 KHZ
Printing nozzles	2-5	2-5	2-5	2-5	2-5
Platen temperature	60^{o}C	60^{o}C	60^{o}C	40-45◦C	60◦C
Thermal Sintering	60^{o}C for 15-60 minutes	60^{o}C for 1 hour	60^{o}C for 10 minutes	100^{o}C for 1 hour	80◦C for 10 min
Photonic sintering	2.1 kV and 5 pulse of 500 us	2.5 kV and 15 pulses of 500us.	2.5 kV and 7 pulses of 500us.	2.5 kV and 15 pulses of 500us.	2.5kV and 15 pulses of 500μs.

Table 4.2: The most important parameters for different substrates.

4.5 Summary

To achieve high quality printing patterns, the physical and chemical properties of the each ink for the dimatix printer should be studied. Oxygen plasma treatment is an essential step for surface modification of the substrates prior to printing process for successful printing patterns. It is used to modify the substrate's surface from hydrophobic to become hydrophilic. By studying the effect of plasma treatment on substrates, it is observed that a continuous silver pattern is formed on the plasma-treated hydrophilic surface and on the other hand isolated ink droplets are appeared on the plasma-untreated hydrophobic surface. Also some observations are recorded during the printing such as the drying time for the isolated ink droplets on the plasma-untreated hydrophobic surface is so long while for plasma-treated hydrophilic surface can be done in a few minutes resulting in a continuous silver lines. The drop spacing is another important parameter as obtaining continuous printed lines highly depend on drop spacing. By studying the relationship between drop spacing, electrical resistance and the width of the printed lines, it is found that the drop spacing is directly proportional to electrical resistance, as it increase the electrical resistance is also increase. On the other hand, line width is inversely proportional to drop spacing. Microscopic images of printed silver lines after drying under two case: (a) before photonic sintering and (b) after photonic sintering is also studied, in both cases the printed silver lines are homogenous and there is no visible cracks. But there is few droplet borders in the sample before sintering and on the other hand the droplet borders vanished completely in the sample after photonic sintering and also the line width increases. This result is also confirmed by Scanning Electron Microscope (SEM) images before sintering and after sintering.

Chapter 5

Inkjet Printing of Capacitive Tactile Sensors

Creating an inexpensive skin-like flexible and stretchable surface that is covered with sensors have been under particular attention to be employed in many different disciplines [178], such as in human-computer interaction design [179- 181], in biomedical materials science research [182, 183], in robotics for surface tactile sensing and navigation [184- 186], and in wearable computing as e-textiles [187, 188]. A complete new generation of electronic devices with remarkable new characteristics can be achieved by employing the inkjet printing technique.

In this chapter, an overview on the tactile sensing for robotic application will be presented. In addition to a short review of the tactile sensing technologies for robotic application, especially the capacitive tactile sensors, will be presented. A capacitive sensor based on a polydimethylsiloxane (PDMS) film integrated into a printed circuit board (PCB) on a flexible substrate whose layout is defined by inkjet printing will be introduced; as the main application of this thesis. A full description of the fabrication and characterization of capacitive tactile sensor will be involved. In the terms of sensitivity and dynamic response, the influence of the dielectric thickness of the PDMS on the sensor behavior has been studied. From the result, it has been found that PDMS film of thickness of about 100 μm is the best thickness for our application as it shows about 1.1 pF/N and less than 15 s of recovery time. Whereas The PDMS film with about 45 μm thickness presents a sensitivity of about 3 pF/N or a change in capacitance of about 45%, whereas when the thickness increases the sensitivity is reduced drastically. The dynamic response of thinner films is penalized and more time is required to recover the initial value although these films result in higher

sensitivities. The evaluation of the fabricated sensor will be also investigated by integration of the film into a flexible PCBs including a microcontroller. The inkjet printing technique is employed to define interconnects of the circuit by silver nanoparticles. This work demonstrates the feasibility of this simple approach to be used for artificial skin applications.

5.1 Overview on the Tactile Sensing for Robotic Application

In recent years, an extensively interested toward the field of robotics is increased as robots are required to be able to perform human-like manipulation tasks. To achieve that task, robots need an interface to be able to manipulate objects while simultaneously reasoning and sensing about their environment. All information about positions and the forces at all points of contact between robots and the objects, they are interacting with, can be provided through the suggested interface. Development of artificial skin interfaces with fully distributed tactile sensing is the key issue in the robotics community. In 1980s, along with a realization of the importance of computers and robotics, the importance of tactile sensor technology was recognized. The simplest definition of the tactile sensing in robotics is the continuous sensing of variable contact forces [189] which provide information about force feedback for the control of the robot, the contact configuration, if the robot is in contact with an object, and the stability of the grasp [190]. Such information can be used to better understand and optimize handling techniques to increase the performance, skills, and versatility of the robot through analyzing object manipulation [191].

There is a great interest to understand the human sense physiology of touch and perception, as well as the human hand ergonomics activity and movements during grasping and handing manipulation of objects to achieve the tendency in the robotics community to be look to human movements, as well as the human skin and sense of touch, for inspiration. The functional requirements for a robotic tactile sensing system are detecting the force and the shape distribution of a contact region for object recognition, detecting the contact, release, lift, and replacement of an object, detecting the direction and the contact force magnitude for maintaining a stable grasp during manipulation, tracking the variation of contact points during manipulation, detecting the magnitude and the force of contact forces due to the motion of the hand during manipulation, detecting tangential forces due to the shape and the weight of the object, detecting the difference between actual and predicted

actual grip forces necessary for manipulation, and finally detecting both static and dynamic contact forces.

Research, development trends and advancements from emerging applications to commercialization of tactile sensors has been presented. For over 30 years, the maturation of tactile sensing technology has been expected. Huge potential and application of tactile sensing in areas of robotics have been taken into account starting with Harmon who considered because of technical difficulties and low return on investment, tactile sensing unfit for areas such as medicine and agriculture [192- 195]. But, Nevins and Whitney in the same time announced that passive monitoring will eliminate the need of tactile sensing [196]. The importance of the tactile sensing technology increased around the start of the 21st century to support the development of more intelligent systems and products such as medical robotics and industrial automation and hence improve the quality of human life [195, 197]. In 2000, review on tactile sensing technology has been published by Lee who analyzed the causes of delayed acceptance of this technology among industrial and consumer markets [195]. Lumelsky et al. firstly demystified the technological requirements and the benefits of having sensitive skin devices as consequence a new paradigm in sensing and control were envisioned by them [184]. For minimally invasive surgery, tactile sensing systems has been examined by Eltaib and Hewitin 2003 who reasserted the importance of the technology for this particular field [198]. To cover the area of tactile sensors in details, it is advisable to read the book of Wettels [199] who demonstrated how sensor can mimic human skin. Also Najarian and Dargahi's book which encompasses the human tactile sensing basics, the technologies and applications of biomedical engineering in terms of intrinsic sensing [200].

Some common tactile sensing transduction techniques are based on optical, capacitive, piezoresistive, magnetic, thermoresistive, piezoelectric, and inductive methods. A short review of the tactile sensing technologies for robotic application will be introduced in the next section.

5.2 Tactile Transduction Techniques

5.2.1 Optical Tactile sensors

Previously the optical sensors suffered from the rigidity and the wiring complexity when electrical signals are used due to using huge number of sensors. Employing fibre optic cables are the solution to overcome these limitation [201] which in turn gives the introduction of plastic optical fibres (POFs) presented by Heo et al. [202]. Figure 5.1 represents an example of fabricated POF-based microbend optical fibre sensor which is embedded in a silicone elastomer. LED light source and a charge-coupled device (CCD) detector are the essential requirements of the optical measuring system. When the force is applied, a modification of light intensity occurs owing to the bending of POFs. Up to 15N applied force with a resoultion of 0.05 N, the sensor shows a linear response despite of some hysteresis errors resulting from the material properties of the silicone rubber.

Figure 5.1: Fabricated prototype of optical fiber tactile sensors [202].

Due to bending or misalignment, signal attenuation and alteration are produced which considered the main disadvantage of the optical sensors. On the other hand, several benefits of Optical sensors such as:

- Low-cost.
- No cross-talk between wiring.

- It is insensitive to electromagnetic radiation.
- Having high spatial resolution.
- It can be used both as transmitter and detector.
- Flexibility and durability.

5.2.2 Piezoelectric Sensors

Conversion of an applied force or stress into an electric voltage can be done by piezoelectric sensors [87]. The most common piezoelectric materials in tactile sensing applications is Polyvinylidene fluoride (PVDF) films due to their high piezoelectric coefficients, mechanical flexibility, low weight and chemical inertness, dimensional stability [204, 205]. Figure 5.2 is an example of robotic fingertip embedded with strain gauges and PVDF film receptors which was presented by Hosoda et al. [206]. During pushing and rubbing of different textures, the PVDF sensors gives an output of around 1V and that of the strain gauges have an output between 0.5 and 1V. The piezoelectric sensors are suitable for biomimetic artificial skin with the ability to sense texture, and possibly with further development, forces. Despite of the advantages of the piezoelectic sensor which are:

- High outputs and sensitivities.
- Well suited for dynamic applications.
- Thin films and low weights possible.
- Mechanically flexible.
- Robust and chemically resistant.
- Simplified wiring.

There are some disadvantages associated with this type of sensor such as:

- Drift of sensor output.
- Charge amplifier required.
- Not suitable for static applications.
- Not stretchable.

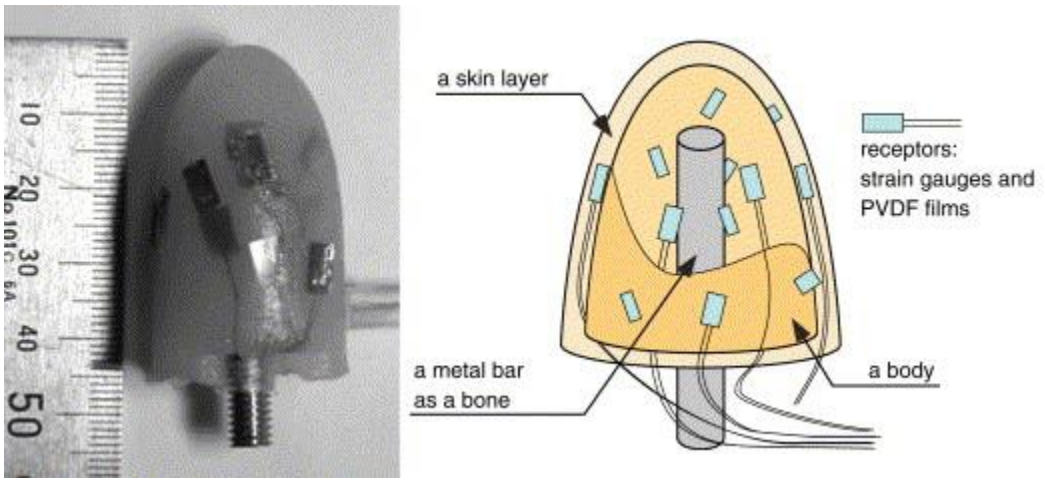

Figure 5.2: A schematic example of robotic fingertip embedded with strain gauges and PVDF film receptors [206].

5.2.3 Resistive Sensors

Resistive sensors are considered the largest family of tactile sensors. There are many types of resistive sensors such as strain gauges, piezoresistors, conductive polymers and conductive elastomer composites, each type of them will be discussed briefly in the next sections.

5.2.3.1 Strain Gauges

A long winding snake is the structure of strain gauges. When a force is applied, the cross section of the strain gauge decreases and its conduction length increases due to the elastic deformation and finally leading to a change in its resistance. Huang et al. studied the behavior of strain gauges when placed on orthogonally placed silicon-based microcantilevers embedded in a layer of PDMS [207]. The structure and operation of such sample can be illustrated in Figure 5.3. They recorded that a linear response to the applied stress of the sensors covered with PDMS is achieved with a sensitivity of about 0.02%/N normal stress.

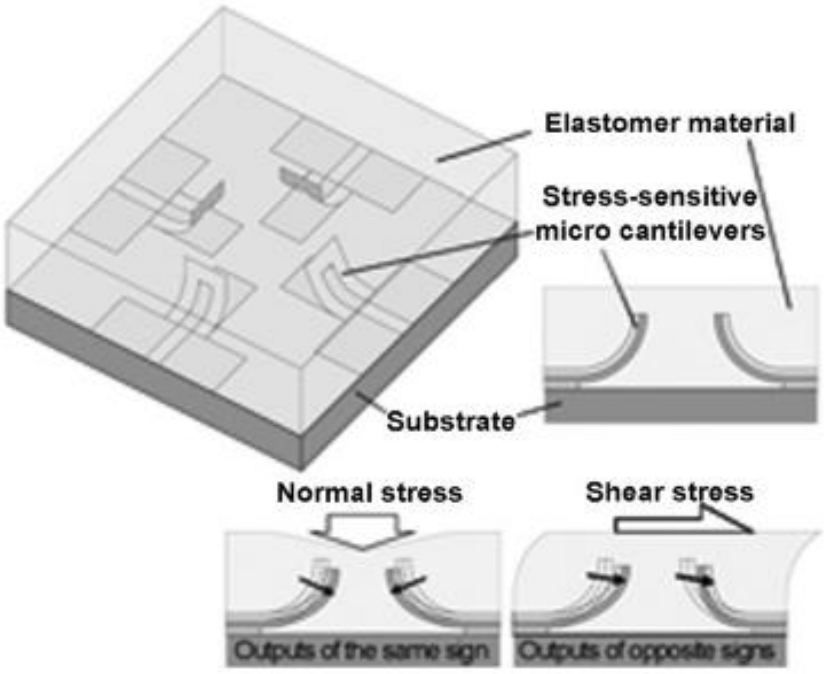

Figure 5.3: Structure and operation of embedded tilted cantilevers [207].

The advantages of Strain gauges are:

- High sensitivity.
- Small sizes and high spatial resolution.
- Well established design and fabrication techniques.
- 3D force sensing possible.
- Ease of integration with other microelectromechanical systems (MEMS) and electronics.
- Ease of integration with flex PCB/fabric for flexibility.

The disadvantages of this type of sensors are:

- Fragile sensor element.
- Relatively costly materials and fabrication techniques.
- When integrated with flex PCB/fabric, not stretchable.
- Even if sensor is small, total package size can be large.

5.2.3.2 Piezoresistive Sensors

The change in resistance of the piezoresistive material itself is the key to detect the mechanical stress. Figure 5.4 shows an example of 3D force sensor array based on the piezoresistive effect.

The advantages of piezoresistive sensors:

- High sensitivity
- Small sizes and high spatial resolution
- Well established design and fabrication techniques
- Integration easily with other MEMS and electronics.
- Elastomer as protective layer
- Elastomer is stretchable
- The grasping quality increased grasping.
- Soft material mimics human skin.
- .Possibility for 3D force sensing.

The disadvantages of the piezoresistive sensors are:

- Loss of sensor sensitivity.
- Even if sensor is small, total package size can be large.
- Relatively costly materials and fabrication techniques.
- Creep.
- Fragile sensor element.
- Ambiguity (transverse inverse problem).

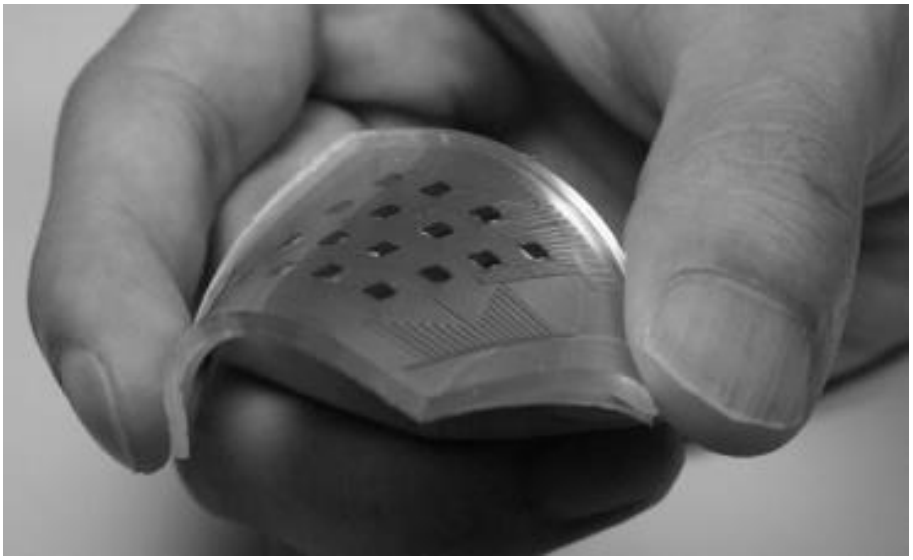

Figure 5.4: An example of 3D force sensor array based on the piezoresistive effect [208].

5.2.3.3 Conductive Polymers Sensors

A porous nylon matrix which is filled with electrodeposited polypyrrole is the sensing material of the conductive polymers sensors. By applying applied compressive load, the conductivity of the composite material increases. Within the applied pressure range of 20–600 kPa, a flexible tactile sensor is presented with a stable sensitivity of 0.023% / kPa. A schematic of an ion-polymer metal composite used as the sensing layer in a 3D tactile sensor can be illustrated in Figure 5.5.

The advantages of piezoresistive sensors:

- Mechanically flexible.
- Robust and chemically resistant.
- Large-area low-cost fabrication techniques.

The disadvantages of the piezoresistive sensors are:

- Not stretchable.
- Low sensitivity.
- Applications often restricted to pressure sensing/imaging because the conduction occurs in all directions.

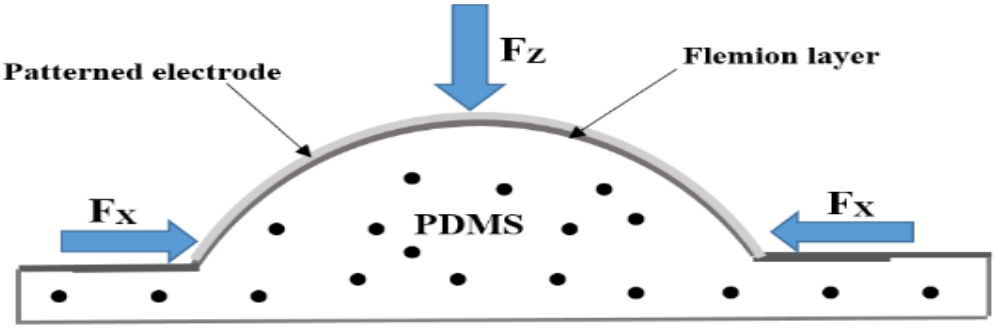

Figure 5.5: A schematic of an ion-polymer metal composite used as the sensing layer in a 3D tactile sensor [209].

5.2.3.4 Conductive Elastomers Composites

Because of the unique characteristic elastomers as materials are enriched with conductive filler, they are commonly used as pressure sensitive materials. The elastomer composite layer of the sensor can be deformed if the sensor is subjected to an external applied force. As a consequence, its resistivity changes depending on the type of conductive particles, the volume percentage and the type of conductive particles in the elastomer and the resulting material stiffness. Elastomers are highly stretchable and thus they are considered suitable materials on curved surfaces and moving parts applications. An application of conductive elastomers can be shown in Figure 5.6.

The advantages of conductive elastomers composites sensors are:

- Simple structures and fabrication techniques possible
- Thin films and low weights possible

The disadvantages of conductive elastomers composites sensors are:

- Hysteresis of composite material.
- Low sensing range.
- Restricted to pressure sensing/imaging.

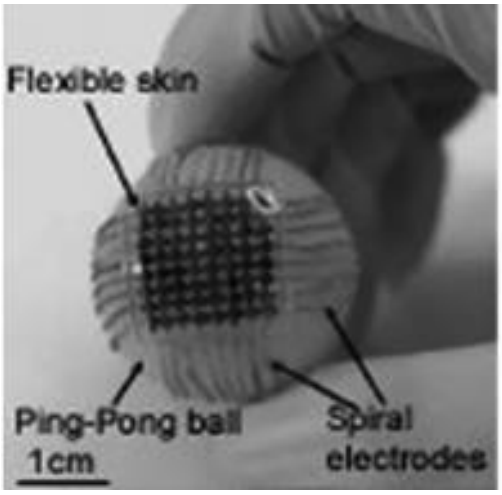

Figure 5.6: An application of the conductive elastomers sensors at which the sensor array stretched over a ping pong ball [210].

5.2.4 Capacitive Tactile Sensors

Capacitive tactile sensors are the main application of the inkjet printing technique which developed during the experimental work of this thesis. Without direct temperature, it is possible to detect any small deflections of structures via the capacitive tactile sensing which considered one of the most sensitive techniques [211]. Tactile sensor matrices or arrays have been developed by several groups [212, 213] also several attempts have been made to completely cover a humanoid with artificial skin [214- 216]. Directly on flexible thin films of polyimide with thicknesses down to 25µm, arrays of capacitive sensors have been fabricated by Pritchard et al [217]. Two circular evaporated gold plates with an intermediate parylene dielectric layer are the constituents of each capacitive sensor. When pressure is applied to the fabricated sensors, the sensors show a linear response. Also, Cannata et al. presented mechanically flexible modules containing a complete sensor and communication system [218] and they reported large areas can be covered such as a body of robot by combining several modules together. Schmitz et al. used the prototype principle to build a prototype finger where the sensors are fabricated as a cover for fingertips not fabricated in modules [219]. They incorporated in the bottom side of the fingertip a rigid PCB at which the sensor electronics can be integrated in. At the same time the same structure can be used to cover the entire circumference of a finger by placing the rigid substrate with a flexible one. Under applied pressure, sensors show a nonlinear response with higher sensitivity even for lower pressures. For

detection of normal and shear applied forces, Lee et al. presented a configuration of parallel plate capacitors embedded in flexible layer of PDMS where each sensor consists of four pairs of plates [220], as shown in Figure 5.7. Between the capacitor plates, A PDMS spacer layer with air gaps is found where these air gaps are deformed when an external force is applied leading to a change in capacitance which in turn gives a measure of the magnitude and direction of the applied force.

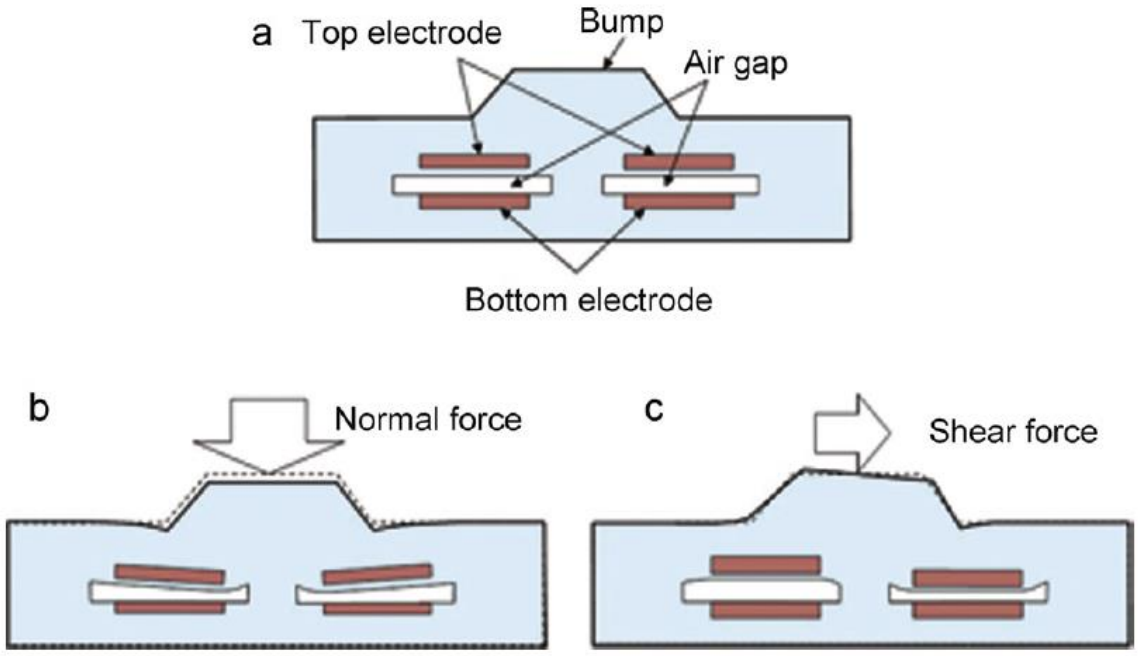

Figure 5.7: (a) Schematic design of capacitive tactile sensors to measure normal and shear stress. (b) represents their response to normal force. (c) represents their response to shear force [220].

On the other hand, for measuring both vertical and horizontal contact forces, da Rocha et al. present another configuration of plates where each sensor also comprises of four variable capacitors [221]. For that configuration, the same top electrode is common between the four capacitors. A change of capacitance of each capacitor occurs as a result of deformation the dielectric material by applying an external force leading to variation of the area of each of the bottom electrodes. The magnitude and direction of the applied forces can be determined by reading out capacitances of the system of capacitors. Hoshi and Shinoda proposed a configuration to reduce wiring in tactile skins by introducing the cell-bridge system which is a network of signal transmission devices [222]. Each capacitive sensor is a cell which consists of two capacitors forming by alternating

layers of conductive fabric and dielectric material with embedded bridges. So, the working principle of such configuration depends on the communication between the embedded bridges with each other via the conductive layer and hence reducing wiring. Shinoda and Oasa presented a completely wireless capacitive based pressure sensor where a layer of silicone rubber embedded with passive resonators was used [223]. Each capacitive sensor is a resonator which comprises of a capacitor and a coil. On the outside layer of the sensor, a ground coil is located which is inductively coupled to the coil of the embedded resonator. A change of capacitance of each embedded capacitor occurs as a result of applying external stress leading to a shift in the resonance frequency of the LC resonator reading by the ground coil. Flexible capacitive pressure sensors based on microstructured thin PDMS films have been developed by Mannsfeld et al. and by using different microstructured patterns, such as lines and pyramids, they are capable of tuning the pressure sensitivity [224]. By using silicone elastomer Ecoflex between two transparent elastic films of carbon nanotube (CNT) and PDMS, acting as electrodes, skin-like capacitive pressure and strain sensors have been introduced by Lipomi et al. [225]. A flexible capacitive pressure sensor based on PDMS, capable of detecting up to 945 kPa, has been developed by Lei et al. for plantar pressure measurement in biomechanical applications [226].

The advantages of capacitive tactile sensors are:

- Small sizes devices.
- Its fabrication process is very simple.
- Possibility of High spatial resolution.
- Minimized wiring
- Suitable for large-area applications
- Low cost per area compared to IC transistors
- Well established design and fabrication techniques
- Ease of integration with other flexible MEMS
- 3D force sensing possible
- High sensitivity
- Temperature independent

The disadvantages of capacitive tactile sensors are:

- Parasitic capacitances
- Sensitive to electromagnetic interference
- Relatively complex circuitry
- Cross-talk between sensor elements

So in next section, a full description of the fabrication of capacitive tactile sensors will be presented in details.

5.3 Fabrication of Capacitive Tactile Sensors for Robotic Application

An exciting future in surface tactile sensing, wearable computing and smart object manufacturing is expected through research in materials and mechanics for flexible and stretchable electronics. A capacitive sensor based on a polydimethylsiloxane (PDMS) film integrated into a printed circuit board (PCB) on a flexible substrate whose layout is defined by inkjet printing is the main application of inkjet printing technique. In the following section the fabrication steps of the capacitive force sensor will be presented in details. Figure 5.8 shows a cross-sectional view of the capacitive sensor involved in this thesis.

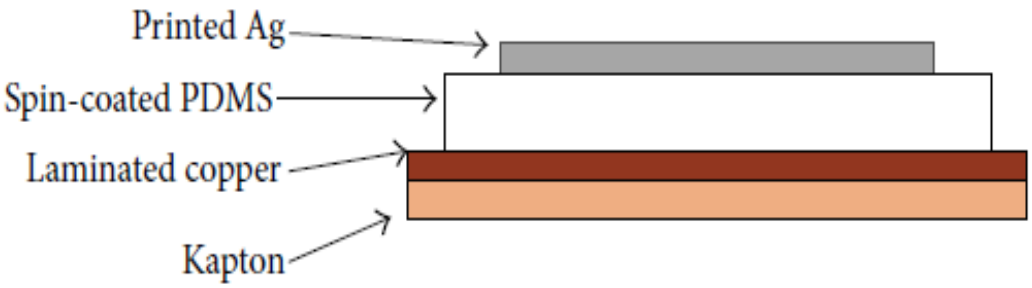

Figure 5.8: Cross-sectional view of the capacitive sensor [227].

5.3.1 Fabrication of Dielectric Layer

Polydimethylsiloxane (PDMS) is the chosen dielectric layer for our capacitive sensor as it has been chosen before by several authors as mentioned in section 5.2.4 due to its mechanical characteristics and its relative ease of manufacturing. By mixing the base and the curing agent in a weight ratio of 10 of the base to 1 of the curing agent, the PDMS films were prepared. A continuous mechanical stirring was applied for 10 min to the mixture. Then, the mixture is desiccated for 30 min to remove entrapped air bubbles resulting from stirring. Onto the surface of copper face of Kapton, the viscous PDMS mixture was directly deposited. The substrte with the PDMS were spin-coated to reach the desired thickness of PDMS and get a uniform thin film at the same time. Spin coating at 10 rps for 30 s and 25 rps for 60 s resulted in a layer thickness of about 100 μm and 45μm, respectively. Thicker films were composed of multiple spin-coated layers. Then, the film was desiccated again for 10min to remove any enclosed air bubbles. Afterwards the PDMS is cured by placing the sample on a hotplate at 100°C for 60min.

5.3.2 Inkjet Printing of Capacitive Tactile Sensors Structures

A capacitive sensor consists of two conductive plates with a dielectric material sandwiched between them. So, two conductive plates are needed in our device. One of them is copper electrode which is laminated onto the top of Kapton as a flexible substrate. The second electrode was inkjet-printed on the top layer of PDMS with a Dimatix printer-2831 by using electrically conductive ink (DGP 40LT-15C from ANP Co., USA) with about 30–35% of silver nanoparticles and triethylene glycol monoethyl ether (TMGE) as solvent. The top electrode consisted of two consecutive printed layers. The substrate temperature was fixed at 60°C during printing. A drop space of 40 μm was settled in the printer for 80 μm landed diameter drops. The printed structure of the second electrode was designed with contacts of (3mm × 3 mm) and (1mm× 1mm), where the distance between contacts was 1 cm with 1mm width. Figure 5.9 illustrates the layers that composed this sensor.

.

Figure 5.9: Layout of the printed top electrode [227].

5.3.3 Sintering Treatment of Printed Structure

Two type of sintering treatment are involved, thermal sintering and photonic sintering. Thermal sintering is occurred to dry the printed structure to decrease or avoid the coffee stain effect and to obtain a high quality printed patterns. A drying step at 80°C for 10 min is followed the printing process of the desired structure. On the other hand to achieve a good resistivity of the printed patterns, it is preferable to perform the photonic sintering. During our experimental work, a photonic sintering was conducted with a voltage of 2.5kV and 15 pulses of 500μs. An optical microscope image of the printed layer on top of the PDMS is depicted in Figure 5.10.

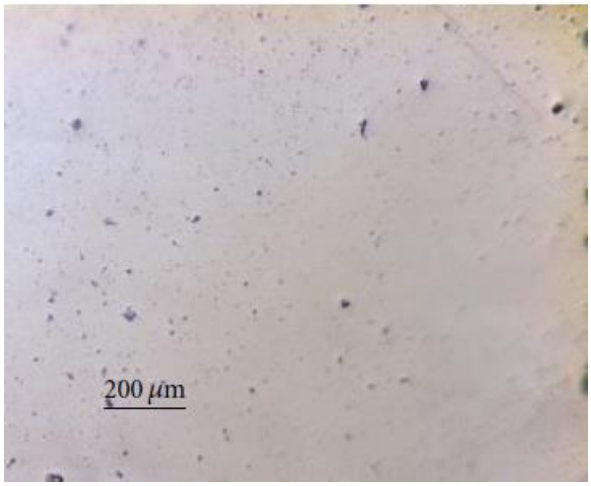

Figure 5.10: Microscopic image of silver NPs over PDMS [227].

After performing the photonic sintering process, the sheet resistance of the printed electrode was measured to be about 19.2 ± 2.2Ω/□. Sheet resistance measurements were conducted on the printed electrode with a self-made linear four-point probe in combination with a Keithley ACS 2600 (Germering, Germany). A correction factor of 0.651 was calculated and applied to remove the effect of limited boundaries according to Smits [228].

The thicknesses of the PDMS films and silver electrodes were measured with a Dektak XT™ Stimulus Surface Profiling System (Bruker Corporation, Coventry, UK). The thickness of the printed silver on the PDMS film is shown in Figure 5.10. The typical coffee ring effect of printed layers can also be seen in the same figure. Surface profilometer measurements revealed the thickness of the printed silver layer on PDMS to be about 4290 ± 200 nm. This is about one order of magnitude higher than silver layers on other substrates printed with the same drop spacing and drop waveform [229, 230]. This huge difference in height cannot be explained with a reduced packing density of the silver nanoparticles. The only other material in direct contact with the PDMS is the solvent of the ink. The used ink possesses around 95% (vol) of TGME that leads to a wet ink layer of approximately 6-7 μm after printing [231], which is close to the thicknesses we measured. Thus, we could assume that the increased height of the printed silver tracks on PDMS is related to a swelling of the PDMS after solvent absorption. Among others, Lee et al. investigated the effect of many solvents on swelling using an immersed piece of PDMS [232] and found a swelling behavior for almost all tested solvents with a Hansen total solubility parameter close to PDMS. According to Dow Chemical [233] and the calculation method of Lee et al. this parameter is 10.1 for TGME. Other solvents having this parameter have a swelling ratio between 103% and 121%. The higher ratio leads to the swelling of the PDMS of about 4 μm already if the top 20 μm of PDMS is saturated with solvent. The swelling of the PDMS also explains the small increase in height next to the printed layers in Figure 5.11 between 0.5 and 0.6 mm.

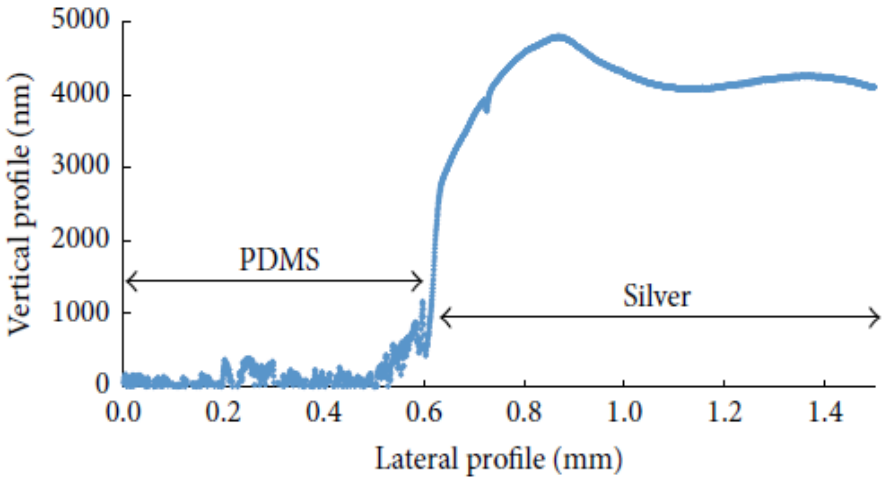

Figure 5.11: Profile of the printed silver layer on top of the PDMS [227].

Finally, two wires were glued to the copper electrode and the printed silver NPs electrode using silver-filled epoxy EPO-TEK H20E (Epoxy Technology, Inc., Billerica, USA). The fabricated device as shown in Figure 5.12 was dried at 60°C for 60min.

Figure 5.12: An image of the fabricated sensor [227].

5.4 Characterization of Capacitive Tactile Sensors for Robotic Application

Different PDMS films were prepared with different thickness values. Figure 5.13 illustrates the sensitivity (S) of the device defined as the change in capacitance ΔC in pF divided by the change in force ΔF in N:

$$S\ (\mathrm{pF/N}) = \frac{\Delta C}{\Delta F} \tag{5.1}$$

In all cases, we measured ΔC at 1N force (ΔF) and looked at ΔC after applying the force for 1min. As can be seen from Figure 5.13, the sensor sensitivity decreases exponentially with the increase in the PDMS thickness. This result is in agreement with previous reports in literature [224, 234-237]. Our objective here is to achieve a simple force sensor that can be easily integrated into a flexible PCB. Therefore, our sensor must be sensitive enough to be measured by a standard microcontroller and fast enough to do tracking of the applied force. At first glance, a thinner dielectric film leads to a higher sensitivity and, thus, a better performance.

However, when we analyzed the dynamic response of the thinnest film (~45 μm), the time required to recover its initial capacitance value was much higher than the time required by the film of about 100 μm thickness. The thinnest layer requires more time to recover, while the 100 μm film needs less than 15 s. Furthermore, the 100 μm thick PDMS film used in this work has lower hysteresis

in comparison to the one with a lower thickness. The reason behind is the fact that unstructured films, which are thinner than several hundred micrometers, are subject to significant viscoelastic creep. On the other hand, thicker unstructured PDMS films are nearly fully elastic under pressures lower than 100 kPa. As a result, thin PDMS films have higher relaxation times compared to thick films, which accounts for a higher hysteresis during device operation [224]. For this reason, we selected the device with a PDMS film thickness of 100 μm, which presents the best compromise between nominal capacitance (~5 pF) and change under applied force (>20%).

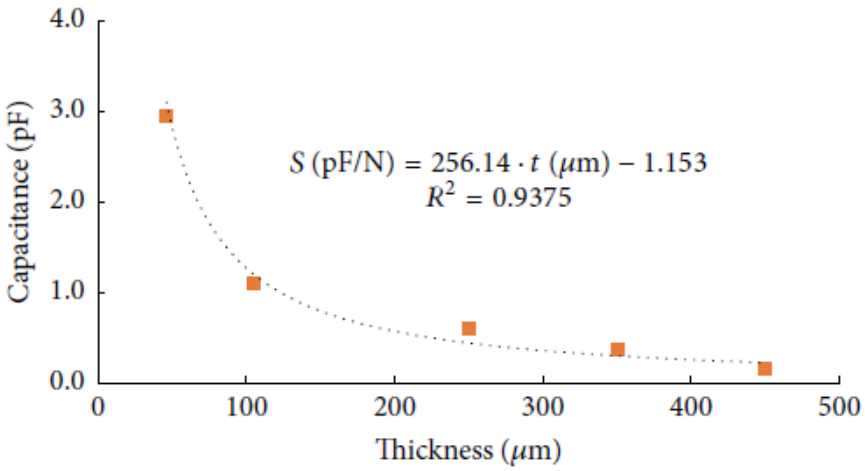

Figure 5.13: The relation between capacitance and different thickness of PDMS [227].

Figure 5.14 illustrates the response of the selected sensor (~100 μm) when applying an increasing force of 50mN every 30 s. This behavior can be approximated by a rational function with one zero and one pole. In particular, the parameters are a = 5.81pF, b = 331.70, and c = 66.55 with R^2 = 0.9843. The response can also be approximated by linearization when we define the suitable force ranges. For instance, in 30–150mN force range the sensitivity is about 3.7 fF/mN, while this sensitivity decreases to 0.7 fF/mN in 150–450mN range and to 0.06 fF/mN at higher forces

$$(\text{pF}) = \frac{a.F(mN) + b}{F\,(mN) + c} \tag{5.2}$$

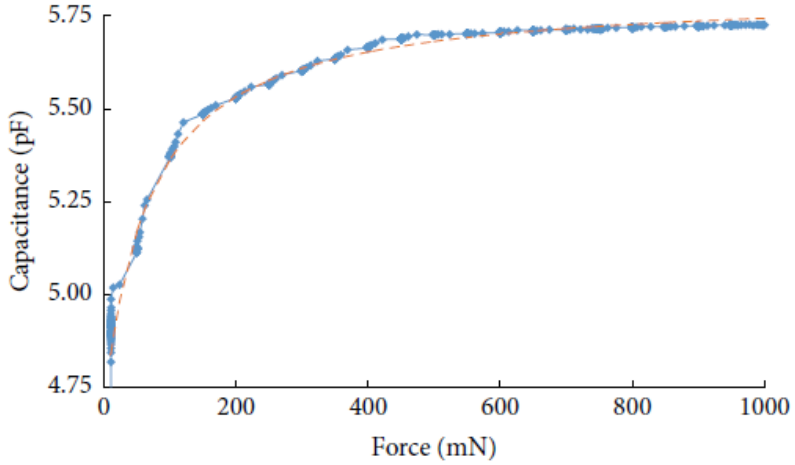

Figure 5.14: Capacitance versus applied force for about 100 μm PDMS thickness where the blue curve is the experimental data and the dashed-red curve is the fitting [227].

In order to observe the dynamic response of this sensor and its hysteresis and reproducibility, we performed different tests presented in Figure 5.15 and Figure 5.16. Figure 5.15 illustrates the high reproducibility of the sensor as well as its fast time response to the force applied, although the recovery time is slightly longer than the response time.

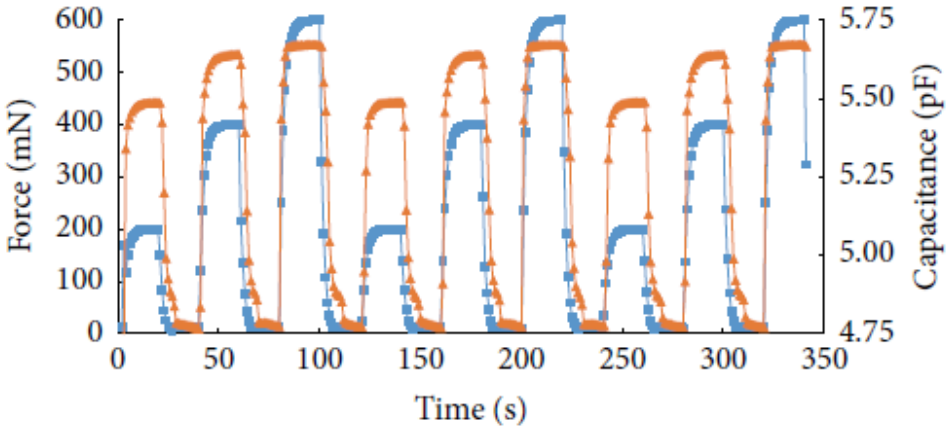

Figure 5.15: Dynamic response of the selected sensor (about 100 μm PDMS thickness) [227].

As can be seen in Figure 5.16, the sensor goes back to its initial capacitance value if there is no force applied with an error less than 3% at the different force steps applied. If we compare this response with the one reported by Cagatay et al. [238] for a PDMS film of about 110μm and pillar

of about 30 μm, we observe similar capacitance values under no force. The sensitivity is about 10% lower in the sensor described here, but the fabrication procedure and the integration on a final system are much easier.

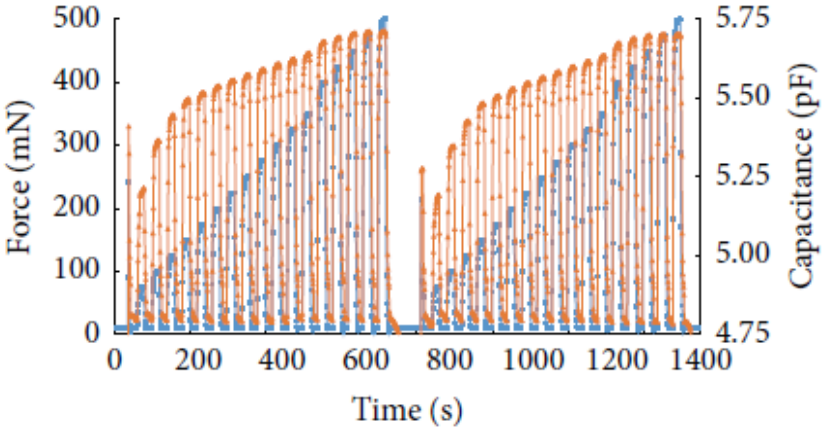

Figure 5.16: Dynamic response of the selected sensor (about 100 μm PDMS thickness) there is no force applied where the blue line represented force and the red line represented Capacitance [227].

5.5 Integration of Capacitive Tactile Sensors into Printed Circuit Board (PCB)

After showing the performance of the standalone sensor, we integrated it into a hybrid system of an inkjet-printed circuit board assembled with conventional surface mount components. Figure 5.17 is a schematic and photograph of hybrid integrated system with inkjet-printed silver layers. The mount devices (SMD) and PDMS film can be shown in Figure 5.18. The circuitry was printed with silver nanoparticle inkjet ink on a coated polyethylene terephthalate (PET) based substrate (Novele from Novacentrix, USA). From top left to bottom right, it contains a connector for programming the microcontroller (μC) and retrieving the measured values, four light emitting diodes (LEDs) with their corresponding serial resistor (R), and the sensor electrode. Above the sensor electrode, a piece of a 100 μm thick PDMS film was placed. Although we have demonstrated the possibility of direct printing the electrode on the PDMS, after pressing several times the silver layer on PDMS without any protection, this layer starts to show cracks. In order to avoid this issue and ensure longer durability of the system, we decided to employ another PET substrate with an inkjet-printed electrode on top of the PDMS film with the electrode facing down.

These two electrodes touching the PDMS layer on each side form the capacitive sensor. All electrical connections were done with electrically conductive epoxy.

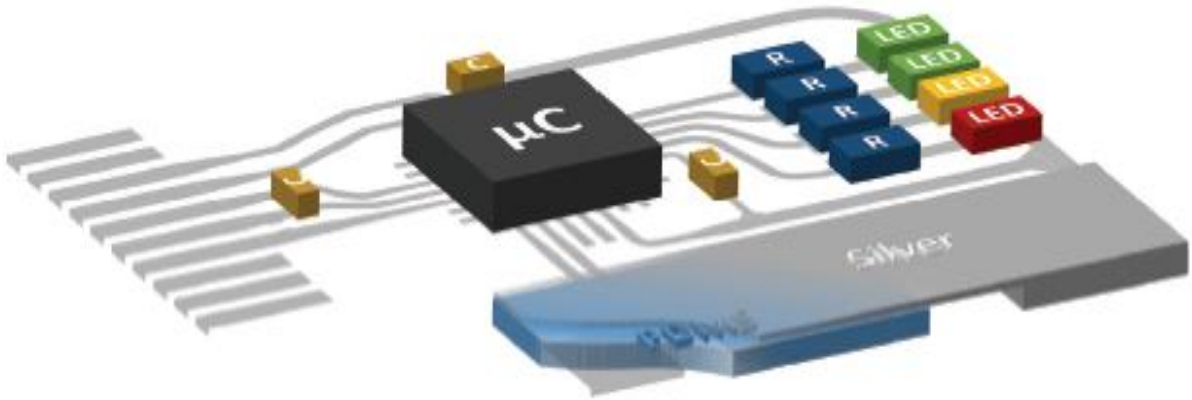

Figure 5.17: Schematic and photograph of hybrid integrated system with inkjet-printed silver layers [227].

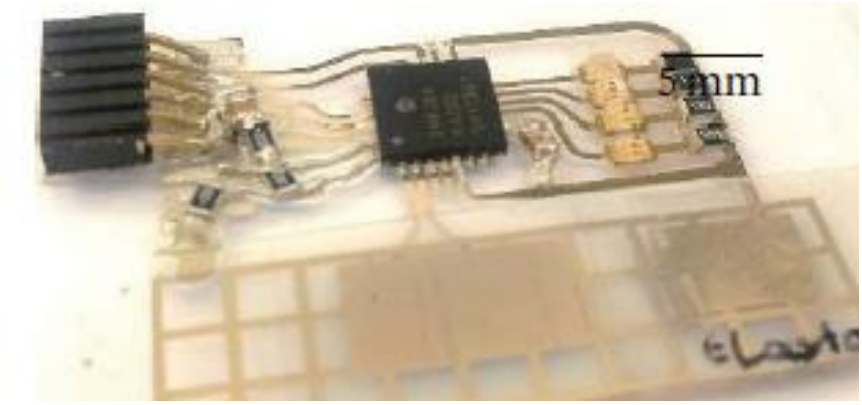

Figure 5.18: The Surface Mount Devices (SMD) and PDMS film [227].

The microcontroller PIC24FJ64GA202 (Microchip) is equipped with a charge time measurement unit (CMTU), which was used to measure the capacitive sensor. We used a current (I) of 55μA to charge the capacitor for 1.5μs (t) with the charge Q. The resulting voltage V at the electrodes was then converted to a digital value D using the internal 12-bit analog-to-digital converter of the microcontroller with the reference voltage (Vref) at 3.25V. This procedure allows us to calculate the measured capacitance following the equation:

$$C = \frac{Q}{V} = \frac{I \,.\, t}{D \,.\, V_{Ref.}/2^{12}} \tag{5.3}$$

The measured force profile consists of a ramp with increasing force. Every 30 s the force was increased by 20% from 5mN to 1000mN. Force and average capacitance values were taken 25 s after each step to allow both values to stabilize. We measured the voltage 100 times and averaged it to increase the signal-to-noise ratio. Figure 5.19 shows a very small change of capacitance and a clear trend to higher capacitance at higher force. The relation between the capacitance C and the force F can be approximated by equation 5.3, where the parameter values are a = 28.83 pF, b = 126.1, and c = 4.414 at R^2= 0.9938. In comparison to direct capacitive measurements of the sensor, the microcontroller includes the parasitic capacitances of its input pins and the wires to the sensor. Based on the presented results above, this parasitic capacitance is in the order of 24 pF.

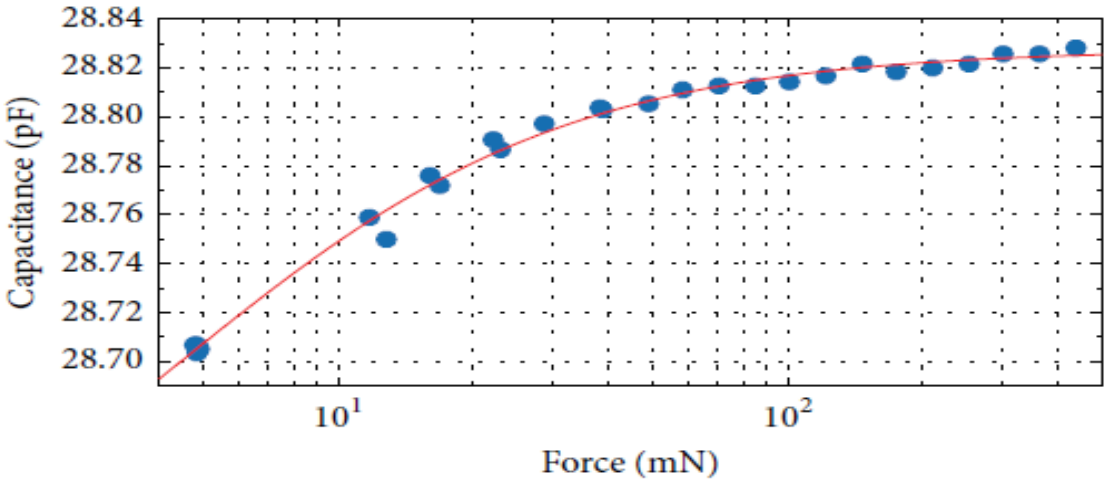

Figure 5.19: Capacitance between sensor electrodes versus applied force (blue dots) and fitted curve (red line) [227].

The relative change in the capacitance in this experiment is very small and touches the limits of the measurement capabilities of the microcontroller. One reason is the small sensor capacitance compared to the parasitic capacitance. This drawback could be overcome by using a strategy similar to the one presented by Toth and Meijer [239]. As another possibility of improving the system performance, it is to enhance the sensor capacitance to raise sensitivity. It is suggested to increase the electrode area to the maximum size suitable for the application and/or use microstructured PDMS films that present higher sensitivities. The relative change in the sensor

capacitance may be improved by using microstructured PDMS films that achieve a higher sensitivity by changing the average dielectric constant between the sensor electrodes.

5.6 Summary

In this chapter, a capacitive force sensor based on polydimethylsiloxane (PDMS) is presented. We have prepared different PDMS films by varying the film thickness. These films have been placed on a polyimide foil with copper layer, acting as bottom electrode, and a silver electrode has been printed on the other side of the PDMS, acting as top electrode. It has been observed that the thickness of the printed silver is 10 times higher than the one achieved in other substrates for the same ink with the same drop spacing and drop waveform. This increased height of the printed silver tracks on PDMS can be attributed to swelling of the PDMS after solvent absorption. The PDMS film with about 45 μm thickness presents a sensitivity of about 3 pF/N or a change in capacitance of about 45%, whereas when the thickness increases the sensitivity is drastically reduced. Although thinner films result in higher sensitivities, the dynamic response is penalized and more time is required to recover the initial value. We found that the best compromise between the sensor sensitivity and its dynamic response is for thicknesses about 100 μm. For this kind of PDMS films, a nonlinear sensitivity of about 1.1 pF/N is achieved with a response time less than 15s and no substantial hysteresis in its response. The best candidate ($\sim$100 μm) has been characterized and integrated together with a microcontroller and other components on a flexible substrate, where interconnects are defined by inkjet printing of silver nanoparticles, proving the suitability of this technology to integrate those sensors in more complex printed circuits for artificial skin applications.

Chapter 6

Conclusion and Outlook

The main goal of this thesis was divided into two main parts. The first part was to study, optimize, and highlight the basic knowledge and the challenges associated with the burgeoning and exciting field of innovative processing techniques suitable for scalable manufacturing of solution processable thin-film electronics. The other part was concerned with employing the one of the promising fabrication technique to fabricate a reliable capacitive force sensor based on a flexible substrate.

To help realization of flexible electronics potential and their importance, this thesis started with introducing an overview of flexible electronics technology research in details in addition to a comparison between the characteristics of inorganic and organic electronics. Also, the challenges of materials used in flexible devices were also mentioned. Most of the scalable manufacturing of solution-processable thin-film electronics, describing the basic working principles, the main advantages and disadvantages of each technique was presented to highlight the reasons for choosing inkjet printing and spray deposition technique as the main techniques used during the experimental work of this thesis.

As carbon nanotubes (CNTs) are the suitable materials for stretchable and flexible electronic applications, chapter three started with an overview on CNT thin-films on different substrates. A high quality CNT thin-films through a reproducible, reliable, and low cost spray deposition technique was investigated. Also the preparation method for fabrication of SWCNT films using sodium dodecyl sulfate (SDS) as dispersive agents was explained in details. The performance of

CNT thin-films deposition on different rigid substrates such as glass, ITO-coated glass, and spectrosil substrates) including at the same time a comparison of the morphological features of the thinnest CNT films on the different substrates was demonstrated. A high transparency with a mean transmittance of 97% at 550nm was achieved. Also, SWCNT thin-films with a sheet resistance of 165 Ω/ with a mean transmittance of 83% without any further doping were presented. The work function values for CNT films deposited on different rigid substrates was studied and it is proved that the surface treatment and layer thickness have no effect on the work function. And the presence of exposed regions of ITO is the reason of the small variation observed in the work function's values owing to its effect during the measurement. Additionally, a Schottky model can be used to describe the electronic level matching at the interface with ITO. Assuming that, as for conjugated polymers, the depletion length is in the order of few micrometers for carbon nanotubes and much bigger than the thickness of our films. Thus, by using a Schottky model, the work function of ITO itself was possible to be measured.

On the Other hand, CNT thin-films deposition on flexible substrates such as ITO-PET and PET substrates where two films with high and low CNT density were prepared on PET substrate and analyzed. A significantly higher roughness, especially for thicker films, was observed on CNT films deposited onto the flexible substrates in accordance with the mean value for bare flexible ITO film and bare flexible PET which are 3 nm and 9 nm, respectively. The thick CNT film on ITO coated PET has a mean value of roughness equals to 54 nm, on the other hand the thin film's mean value of roughness is 16 nm. The roughness mean values observed for CNT films on bare PET are 29 nm for thick films and 15 nm for thin films. The work function of CNT films on flexible substrate was also studied and the obtained result is similar to the observed results for the rigid substrates, work function remains nearly constant with some fluctuation independent on the substrates and thickness. On the other, it does not observe any influence of the ITO on the work function of the CNTs. The bare flexible substrates are promising candidate for replacing ITO, this result is concluded by making a comparison between the work function of CNT films on rigid as well as flexible substrates with the one of untreated ITO. Finally by using time-resolved THz spectroscopy, the photogenerated carrier dynamics and frequency resolved complex photoconductivity were studied for a CNT film on a PET substrate. It was observed changing in transmission of the main peak of the THz pulse allows monitoring dynamics of the photoinduced conductivity and relaxation of photogenerated carriers. Thus, it is concluded that

the photoconductivity of the CNT films is short-lived, with photoexcited carrier relaxation occurring on picosecond time scales, similar to previously reported data for other CNT systems. The complex photoinduced conductivity of the CNT film at a specific time after optical excitation was determined by analyzing the changes in the transmitted THz pulse waveform.

In chapter four, an overview of Fujifilm Dimatix Materials Printer DMP-2831 as the main technique in this thesis was introduced including system identification, working principle and parameters of printer employed in the work. The inkjet printing process step by step was explained including the ideal printing parameters to achieve high quality printing patterns. The physical and chemical properties of the suitable ink for the dimatix printer will be mentioned. As viscosity and surface tension are the most important physical parameters of printing fluids which strongly influence the final printing performance, the effect of these two parameters was also presented. In order to allow for structural versatility, device miniaturization, and purely selective system deposition, the Ag ink DGP-40LT-15C was employed as the main conductive ink during this thesis for Fujifilm Dimatix Materials Printer DMP-2831. The effect of plasma treatment of different substrates was studied introduced and as a consequence, it is proved that plasma treatment is an essential step for surface modification of the substrates prior to printing process for successful printing patterns. The relationship between the drop spacing, continuous printed lines, line width and electrical resistance was studied, it is found that the continuous printed lines and printed line width highly depend on drop spacing. It is proved that the drop spacing is directly proportional to electrical resistance, as it increase the electrical resistance is also increase. On the other hand, line width is inversely proportional to drop spacing. Finally, the effect of photonic sintering of the printed patterns had been investigated thoroughly by using the optical microscopy and the result is confirmed by Scanning Electron Microscope (SEM). Through which the obtained images of printed silver lines after drying before photonic sintering and after photonic sintering, it was observed that both cases are homogenous and there is no visible cracks. But there was few droplet borders in the sample before sintering and on the other hand the droplet borders vanished completely in the sample after photonic sintering and hence the line width increases.

Creating an inexpensive skin-like flexible and stretchable surface that is covered with sensors have been under particular attention to be employed in many different disciplines. So, an

overview on the tactile sensing for robotic application was presented in chapter 5 in addition to a short review of the tactile sensing technologies for robotic application, especially the capacitive tactile sensors. A capacitive sensor based on a polydimethylsiloxane (PDMS) film integrated into a printed circuit board (PCB) on a flexible substrate whose layout is defined by inkjet printing was presented as the main application of this thesis. A full description of the fabrication and characterization of capacitive tactile sensor was involved. From studying the influence of the dielectric thickness of the PDMS on the sensor behavior in the terms of sensitivity and dynamic response, it is found that PDMS film of thickness of about 100 μm is the best thickness for our application as it shows about 1.1 pF/N and less than 15 s of recovery time. Whereas The PDMS film with about 45 μm thickness presents a sensitivity of about 3 pF/N or a change in capacitance of about 45%, whereas when the thickness increases the sensitivity is reduced drastically. The dynamic response of thinner films is penalized and more time is required to recover the initial value although these films result in higher sensitivities. The evaluation of the fabricated sensor was also investigated by integration of the film into a flexible PCBs including a microcontroller and using a current (I) of 55μA to charge the capacitor for 1.5μs (t) with the charge Q. The resulting voltage V at the electrodes was then converted to a digital value D using the internal 12-bit analog-to-digital converter of the microcontroller with the reference voltage (Vref) at 3.25V. A very small change of capacitance and a clear trend to higher capacitance at higher force was observed by increasing the applied force by 20% from 5mN to 1000mN every 30 s. Finally, because of the relative change in the capacitance was very small and touches the limits of the measurement capabilities of the microcontroller, it is suggested to suggested to increase the electrode area to the maximum size suitable for the application and/or use microstructured PDMS films that present higher sensitivities to improve the system performance and to enhance the sensor capacitance to raise sensitivity. This work demonstrates the feasibility of this simple approach to be used for artificial skin applications.

Finally, the next generation of flexible electronic devices technologies needs to be significantly lower in costs and higher in performance. The first step toward all approaching possible novel applications are with employing the suitable innovative processing techniques.

REFERENCES

[1] M. Billinghurst, and T. Starner, "Wearable devices. New ways to manage information," IEEE Computer, vol. 32, pp. 57–64, 1999. DOI: 10.1109/2.738305.

[2] A. Sedra, and K. Smith, "Microelectronic circuits," Oxford University Press, Oxford, 1997.

[3] D. Mentley, "State of flat panel display technology and future trends," Proc. IEEE, vol. 90(4), pp. 453-459, 2002. DOI: 10.1109/JPROC.2002.1002520.

[4] R. Jaeger, and T. Balock, "Microelectronic circuit design," McGraw-Hill, New York, 2003.

[5] W. O'Mara, R. Herring, and L. Hunt, "Handbook of semiconductor silicon technology," William Andrew Publishing, Norwich, 1990.

[6] S. Magdassi, "The chemistry of inkjet inks," World Scientific Publishing, Singapore, 2010.

[7] S. R. Forrest, "The path to ubiquitous and low-cost organic electronic appliances on plastic," Nature, vol. 428, pp. 911–918, 2004. DOI: 10.1038/nature02498.

[8] R. H. Friend, R. W. Gymer, A. B. Holmes, J. H. Burroughes, R. N. Marks, C. Taliani, D. D. C. Bradley, D. A. Dos Santos, J. L. Bredas, M. Logdlund, and W. R. Salaneck, "Electroluminescence in conjugated polymers," Nature, vol. 397, pp. 121–128, 1991. DOI: 10.1038/16393.

[9] S. R. Forrest, "Active optoelectronics using thin-film organic semiconductors," IEEE Journal of Selected Topics Quantum Electronics, vol. 6, pp. 1072–1083, 2000. DOI: 10.1109/2944.902156.

[10] C. W. Tang, “Two-layer organic photovoltaic cell,” Applied Physics Letters, vol. 48. pp. 183–185, 1986. DOI: 10.1063/1.96937.

[11] G. Yu, J. Gao, J. Hummelen, F. Wudl, and A. J. Heeger, “Polymer photovoltaic cells: Enhanced efficiencies via a network of internal donor–acceptor heterojunctions,” Science, vol. 270, pp. 1789–1791, 1995. DOI: 10.1126/science.270.5243.1789.

[12] J. J. M. Halls, C. A. Walsh, N. C. Greenham, E. A. Marseglia, R. H. Friend, S. C. Moratti, and A. B. Holmes, “Efficient photodiodes from interpenetrating polymer networks,” Nature, vol. 376, pp. 498–500, 1995. DOI: 10.1038/376498a0.

[13] J. A. Rogers, Z. Bao, K. Baldwin, A. Dodabalapur, B. Crone, V. R. Raju, V. Kuck, H. Katz, K. Amundson, J. Ewing, and P. Drzaic, “Paper-like electronic displays: Large-area, rubber-stamped plastic sheets of electronics and microencapsulated electrophoretic inks,” Proceedings of the National Academy of Sciences of the United States of America (PNAS), vol. 98. pp. 4835–4840. 2001. DOI: 10.1073/pnas.091588098.

[14] E. S. Snow, J. P. Novak, P. M. Campbell, and D. Park, “Random networks of carbon nanotubes as an electronic material,” Applied Physics Letters, vol. 82, pp. 2145–2147, 2003. DOI: http://dx.doi.org/10.1063/1.1564291.

[15] X. Duan, C. Niu, V. Sahl, J. Chen, J. W. Parce, S. Empedocles, and J. L. Goldman “Highperformance thin-film transistors using semiconductor nanowires and nanoribbons,” Nature, vol. 425, pp. 274–278, 2003. DOI: 10.1038/nature01996.

[16] D. B. Mitzi, L. L. Kosbar, C. E. Murray, M. Copel, and A. Afzali, “High-mobility ultrathin semiconducting films prepared by spin coating,” Nature, vol. 428, pp. 299–302, 2004. DOI: 10.1038/nature02389.

[17] P. T. Kazlas, and M. D. McCreary, “Paperlike microencapsulated electrophoretic materials and displays,” MRS Bulletin, vol. 27, pp. 894–897, 2002. DOI: https://doi.org/10.1557/mrs2002.279.

[18] S. Park, and S. Jayaraman “Smart textiles: Wearable electronic systems,” MRS Bulletin, vol. 28, pp. 585–591, 2003. DOI: https://doi.org/10.1557/mrs2003.170.

[19] A. N. Jansen, K. Amine, A. E. Newman, D. R. Vissers, and G. L. Henriksen, "Low-cost, flexible battery packaging materials," Journal of the Minerals, Metals and Materials Society, vol. 54, pp. 29–54, 2002. DOI: 10.1007/BF02822616.

[20] M. J. B. Robshaw, "An overview of RFID tags and new cryptographic developments," Information Security Technical Report, vol. 11, pp. 82–88, 2006. DOI: http://dx.doi.org/10.1016/j.istr.2006.03.006.

[21] S. Tung, S. R. Witherspoon, L. A. Roe, A. Silano, D. P. Maynard, and N. Ferraro, "A MEMS based flexible sensor and actuator system for space inflatable structures," Smart Materials and Structures, vol. 10, pp. 1230–1239, 2001. DOI: stacks.iop.org/SMS/10/1230.

[22] B. K. Crone, A. Dodabalapur, R. Sarpeshkar, A. Gelperin, H. E. Katz, and Z. Bao "Organic oscillator and adaptive amplifier circuits for chemical vapor sensing," Journal of Applied Physics, vol. 91, pp. 140–146, 2002. DOI: 10.1063/1.1476084.

[23] W. Fix, A. Ullmann, J. Ficker, and W. Clemens, "Fast polymer integrated circuits," Applied Physics Letters, vol. 81, pp. 1735–1737, 2002. DOI: http://dx.doi.org/10.1063/1.1501450.

[24] G. Gelinck, H. E. A. Huitema, E. V. Veenendaal, E. Cantatore, L. Schrijnemakers, J. B. P. H. Van Der Putten, T. C. T. Geuns, M. Beenhakkers, J. B. Giesbers, B. Huisman, E. J. Meijer, E. M. Benito, F. J. Touwslager, A. W. Marsman, B. J. E. Van Rens, and D. M. De Leeuw, "Flexible activematrix displays and shift registers based on solution-processed organic transistors," Nature Materials, vol. 3, pp. 106–110, 2004. DOI: 10.1038/nmat1061.

[25] M. Berggren and A. Richter-Dahlfors, "Organic bioelectronics," Advanced Materials, vol. 19, no. 20, pp. 3201–3213, 2007. DOI: 10.1002/adma.200700419.

[26] K. Deisseroth, "Optogenetics," Nature Methods, vol. 8, no. 1, pp. 26–29, 2011. DOI: 10.1038/nmeth.f.324.

[27] T. A. Finland, "The Millennium Technology Prize 2010," www.technologyacademy.fi, 2010.

[28] E. J. M. Kendall, "Transistors," Pergamon Press, New York, 1969.

[29] J. T. Wallmark, "Field-effect Transistors: Physics, Technology, and Applications," Prentice-Hall, Englewood Cliff, 1966.

[30] J. J. Liou, and F. Schwierz, "RF MOSFET: recent advances, current status and future trends," Solid State Electronics, vol. 47, pp. 1881-1895, 2003. DOI: http://dx.doi.org/10.1016/S0038-1101 (03)00225-9.

[31] D. R. Gamota, P. Brazis, K. Kalyanasundaram, and J. Zhang, "Printed Organic and Molecular Electronics," Kluwer Academic Publishers, Boston (2004).

[32] K. Yoshino, K. Tada, A. Fujii, E. M. Conwell, and A. A. Zakhidov, "Novel photovoltaic devices based on donor-acceptor molecular and conducting polymer systems," IEEE Transactions on Electron Devices, vol. 44, pp. 1315-1324, 1997. DOI: 10.1109/16.605474.

[33] K. Tada, R. Hidayat, M. Hirohata, T. Kawai, S. B. Lee, L. U. Bakhadirov, A. A. Zakhidov, and K.Yoshino, "Conducting polymer-fullerene D-A photocell with decreased serial resistance: ITO/PAT(C60)y/C60/Al structure," Synthetic Metals, vol. 85, pp. 1349-1350, 1997. DOI: http://dx.doi.org/10.1016/S0379-6779 (97)80266-4.

[34] B. Adhikari, and S. Majumdar, "Polymers in sensor applications," Progress in Polymer Science, vol. 24, pp. 699–766, 2004. DOI: http://dx.doi.org/10.1016/j.progpolymsci.2004.03.002.

[35] D. I. Bower, "An Introduction to Polymer Physics," Cambridge University Press, New York, 2002.

[36] H. S. Nalwa, "Handbook of Organic Conductive Molecules and Polymers," John Wiley and Sons, New York, vol. 3, 1997.

[37] J. Mort, G. Pfister, "Electronic Properties of Polymers," John Wiley and Sons, New York, 1982.

[38] L. F. Thompson, C. G. Willson, and S. Tagawa, "Polymers for Microelectronics: Resists and Dielectrics," American Chemical Society, Washington, 1994.

[39] D. T. Grubb, I. Mita, and D. Y. Yoon, "Materials Science of High Temperature Polymers for Microelectronics," Materials Research Society, Pittsburg, 1991.

[40] K. Gilleo, “Polymer Thick Film,” Van Nostrand Reinhold, New York, 1996.

[41] E. R. Salmon, “Encapsulation of Electronic Devices and Components,” Marcel Dekker Inc., New York, 1987.

[42] M. T. Goosey, “Plastics for Electronics,” Elsevier Applied Science Publishers, London (1985).

[43] H. Ito, S. Tagawa, K. Horie, “Polymeric Materials for Microelectronic Applications: Science and Technology,” American Chemical Society, Washington, 1994.

[44] C. P. Wong, “Polymers for Electronic and Photonic Applications,” Academic Press Inc., Harcout Brace Jovanovich Publishers, Boston, 1993.

[45] S. Fakirov, “Handbook of Condensation Thermoplastic Elastomers,” Weinheim: Wiley-VCH, 2005.

[46] M. J. Howard, “Plastics for Electronics: desk-top data bank,” The International Plastic Selector Inc., San Diego, 1979.

[47] http://www.dupont.com.

[48] http://www.microchem.com/products/su_eight.htm.

[49] D. S. Soane, and Z. Martynenko, “Polymers used in Microelectronics: Fundamentals and Applications,” Elsevier, New York, 1989.

[50] Y. S Liu, R. J. Wojnarowski, W. A. Hennessy, P. A. Piacente, J. Rowlette, M. Kadar-Kallen, J. Stack, Y. Liu, A. Peczalski, A. Nahata, and J. Yardley, “Plastic VCSEL array packaging and high density polymer waveguides for board and backplane optical interconnect,” Proceedings - Electronic Components and Technology Conference, pp. 999 –1005, 1998. DOI: 10.1109/ECTC.1998.678832.

[51] T. M. Long, and T. M. Swager, “Molecular design of free volume as a route to low-k dielectric materials,” Journal of the American Chemical Society, vol. 125 (46), pp. 14113-14119, 2003. DOI: 10.1021/ja0360945.

[52] H. R. Kricheldorf, “Progress in Polyimide Chemistry,” Springer, New York, 1999.

[53] D. S. Soane, and Z. Martynenko, “Polymers in Microelectronics,” Elsevier, New York, 1989.

[54] http://www.rogerscorporation.com.

[55] A. Facchetti, “Semiconductors for organic transistors,” Materials Today, vol. 10 (3), pp. 28–37, 2007. DOI: http://dx.doi.org/10.1016/S1369-7021 (07)70017-2.

[56] W. J. Feast, J. Tsibouklis, K. L. Pouwer, L. Groenendaal, and E. W. Meijer, “Synthesis, processing and material properties of conjugated polymers,” Polymers, vol. 37 (22), pp. 5017–5047, 1996. DOI: http://dx.doi.org/10.1016/0032-3861 (96)00439-9.

[57] T. Kawase, T. Shimoda, C. Newsome, H. Sirringhaus, and R. H. Friend, “Inkjet printing of polymer thin film transistors,” Thin Solid Films, vol. 438-439, pp. 279–287, 2003. DOI: http://dx.doi.org/10.1016/S0040-6090 (03)00801-0.

[58] J. E. Mark, J. E. Mark, C. C.-Y Lee, and P. A. Bianconi, “Hybrid Organic-Inorganic Composites,” American Chemical Society, Washington, 1995.

[59] G. Horowitz, “Organic Field-Effect Transistors,” Advanced Materials, vol. 10, pp. 365-377, 1998. DOI: 10.1002/ (SICI) 1521-4095(199803)10:5<365: AID-ADMA365>3.0.CO;2-U.

[60] H. Klauk, D. J. Gundlach, J. A. Nichols, and T. N. Jackson, “Pentacene organic thin-film transistors for circuit and display applications,” IEEE Transactions on Electron Devices, vol. 46, pp. 1258-1263, 1999. DOI: 10.1109/16.766895.

[61] S. Mandal, D. Roy, R. V. Chaudhari, and M. Sastry, “Pt and Pd Nanoparticles Immobilized on Amine-Functionalized Zeolite: Excellent Catalysts for Hydrogenation and Heck Reactions,” Chemistry of Materials, vol. 16, pp. 3714-3724, 2004. DOI: http://dx.doi.org/10.1021/cm0352504.

[62] H. Bönnemann and W. Brijoux, “The preparation, characterization and application of organosols of early transition metals,” NanoStructured Materials, vol. 5, pp. 135-140, 1995. DOI: http://dx.doi.org/10.1016/0965-9773 (95)00023-2.

[63] S. Nie, and S. R. Emory, “Probing Single Molecules and Single Nanoparticles by Surface-Enhanced Raman Scattering,” Science, vol. 275, pp. 1102-1106, 1997. DOI: 10.1126/science.275.5303.1102.

[64] D. Yu, X. Sun, J. Bian, Z. Tong, and Y. Qian, “Gamma radiation synthesis, characterization and nonlinear optical properties of highly stable colloidal silver nanoparticles in suspensions,” Physica E, vol. 23, pp. 50-55, 2004. DOI: http://dx.doi.org/10.1016/j.physe.2003.12.128.

[65] H. Wang, X. Qiao, J. Chen, X. Wang, and S. Ding, “Mechanisms of PVP in the preparation of silver nanoparticles,” Materials Chemistry and Physics, vol. 94, pp. 449–453, 2005. DOI: http://dx.doi.org/10.1016/j.matchemphys.2005.05.005.

[66] J. C. Lin, and J. Y. Chan, “On the resistance of silver migration in Ag-Pd conductive thick films under humid environment and applied d.c. field,” Materials Chemistry and Physics, vol. 43, pp. 256− 265, 1996. DOI: http://dx.doi.org/10.1016/0254-0584 (95)01642-8.

[67] D. Deng, Y. Jin, Y. Cheng, T. Qi, and F. Xiao, “Copper Nanoparticles: Aqueous Phase Synthesis and Conductive Films Fabrication at Low Sintering Temperature,” ACS Applied Materials and Interfaces, vol. 5, pp. 3839−3846, 2013. DOI: 10.1021/am400480k@proofing.

[68] K. Kudo, M. Iizuka, S. Kuniyoshi, and K. Tanaka, “Device characteristics of lateral and vertical type organic field effect transistors,” Thin Solid Films, vol. 393, pp. 362-367, 2001. DOI: http://dx.doi.org/10.1016/S0040-6090 (01)01120-8.

[69] T. Dobbertin, E. Becker, T. Benstem, G. Ginev, D. Heithecker, H.-H. Johannes, D. Metzdorf, H. Neuner, R. Parashkov, and W. Kowalsky, “OLED matrix displays: in-line process technology and fundamentals,” Thin Solid Films, vol. 442, pp. 132-139, 2003. DOI: http://dx.doi.org/10.1016/S0040-6090 (03)00960-X.

[70] J. H. Sung, S. J. Kim, and K. H. Lee, “Fabrication of microcapacitors using conducting polymer micro-electrodes,” Journal of Power Sources, vol. 124, pp. 343-350, 2003. DOI: 10.1016/S0378-7753(03)00669-4.

[71] I. M. Thomas, “High laser damage threshold porous silica antireflective coating,” Applied Optics, vol. 25, pp. 1481–1483, 1986. DOI: 0003-6935/86/091481-03$02.00/0.

[72] P. Maraghechi, and A.Y. Elezzabi, "The design of a reversible wafer holder for uniform photoresist coatings of deeply etched cavities," Measurement Science and Technology, vol. 19: pp. 1–5, 2008. DOI: stacks.iop.org/MST/19/087003.

[73] B. Menaa, M. Takahashia, Y. Tokudaa, and T. Yoko, High optical quality spin-coated polyphenylsiloxane glass thick films on polyethyleneterephtalate and silica substrates," Materials Research Bulletin, vol. 41, pp. 1925–1934, 2006. DOI: http://dx.doi.org/10.1016/j.materresbull.2006.03.008.

[74] T. J. Rehg, and B. G. Higgins, "Spin coating of colloidal suspensions," American Institute of Chemical Engineers Journal, vol. 38, pp. 489–501, 1992. DOI: 10.1002/aic.690380403.

[75] A. Mihi, M. Ocana, and H. Miguez, "Oriented colloidal-crystal thin films by spin-coating microspheres dispersed in volatile media," Advanced Materials, vol. 18, pp. 2244–2249, 2006. DOI: 10.1002/adma.200600555.

[76] B. D Washo, "Rheology and modeling of the spin coating process," IBM Journal of Research and Development, vol. 21, pp. 190–198, 1977. DOI: 10.1147/rd.212.0190.

[77] K. Gilleo, "Polymer Tick Film", Van Nostrand Reinhold, New York, 1996.

[78] Z. Bao, Y. Feng, A. Dodabalapur, V. R. Raju, and A. J. Lovinger, "High-Performance Plastic Transistors Fabricated by Printing Techniques," Chemistry of Materials, vol. 9, pp. 1299-1301, 1997. DOI: 10.1021/cm9701163.

[79] A. Knobloch, A. Bernds, and W. "Clemens, Printed Polymer Transistors," First International IEEE Conference on Polymers and Adhesives in Microelectronics and Photonics, pp. 84-90, 2001. DOI: 10.1109/POLYTR.2001.973262.

[80] J. Y. Park, L. K. Lagorce, and M. G. Allen, "Ferrite-based integrated planar inductors and transformers fabricated at low temperature," IEEE Transactions on Magnetics, vol. 33, pp. 3322-3324, 1997. DOI: 10.1109/20.617931.

[81] K. I. Arshak, D. McDonagh, and M. A, Durcan, "Development of new capacitive strain sensors based on thick film polymer and cermet technologies," Sensors and Actuators A, vol. 79, pp. 102-114, 2000. DOI: http://dx.doi.org/10.1016/S0924-4247 (99)00275-7.

[82] M. Albareda-Sirvent, A. Merkoçi, and S. Alegret, "Configurations used in the design of screen-printed enzymatic biosensors," Sensors and Actuators B, vol. 69, pp. 153-163, 2000. DOI: http://dx.doi.org/10.1016/S0925-4005 (00)00536-0.

[83] N. G. Patel, S. Meier, K. Cammann, and G.-C. Chemnitius, "Screen-printed biosensors using different alcohol oxidases," Sensors and Actuators B, vol. 75, pp. 101-110, 2001. DOI: http://dx.doi.org/10.1016/S0925-4005 (01)00545-7.

[84] D. Vincenzi, M. A. Butturi, V. Guidi, M. C. Carotta, G. Martinelli, V. Guarnieri, S. Brida, B. Margesin, F. Giacomozzi, M. Zen, G. U. Pignat el, A. A. Vasiliev, and A.V. Pisliakov, "Development of a low-power thick-film gas sensor deposited by screen-printing technique onto a micromachined hotplate," Sensors and Actuators B, vol. 77, pp. 95-99, 2001. DOI: http://dx.doi.org/10.1016/S0925-4005 (01)00679-7.

[85] B. Riviere, J.-P. Viricelle, C. Pijolat, "Development of tin oxide material by screen-printing technology for micro-machined gas sensors," Sensors and Actuators B, Vol. 93, 531-537, 2003. DOI: http://dx.doi.org/10.1016/S0925-4005 (03)00173-4.

[86] J. Szlufcik, F. Duerinckx, J. Horzel, E. V. Kerschaver, H. Dekkers, S. De Wolf, P. Choulat, C. Allebe, and J. Nijs, "High-efficiency low-cost integral screen-printing multi crystalline silicon solar cells," Solar Energy Materials and Solar Cells, vol. 74, pp. 155-163, 2002. DOI: http://dx.doi.org/10.1016/S0927-0248 (02)00060-0.

[87] T. Aramoto, F. Adurodija, Y. Nishiyama, T. Arita, A. Hanafusa, K. Omura, and A. Morita, "A new technique for large-area thin film CdS/CdTe solar cells," Solar Energy Materials and Solar Cells, vol. 75, pp. 211-217, 2003. DOI: http://dx.doi.org/10.1016/S0927-0248 (02)00161-7.

[88] T. C. Rohner, N. Lion, and H. H. Girault, "Electrochemical and theoretical aspects of electrospray ionisation," Phys. Chem. Chem. Phys. vol. 6, pp. 3056-3068, 2004. DOI: 10.1039/B316836K.

[89] L. Rayleigh, "On the equilibrium of liquid conducting masses charged with electricity," Philosophical Magazine Series 5, vol. 14, pp. 184-186, 1882. DOI: http://dx.doi.org/10.1080/14786448208628425.

[90] D. S. Kim, J. S. Kim, and M. C. Lee, "Thin film forming technique based on hybrid spray coating using electrostatic force and air pressure," Japanese Journal of Applied Physics, vol. 53, pp. 05HC08-1–05HC08-8, 2014. DOI: http://dx.doi.org/10.7567/JJAP.53.05HC08.

[91] B. J. de Gans, P. C. Duineveld, and U. S. Schubert, "Inkjet Printing of Polymers: State of the Art and Future Developments," Advanced Materials, vol. 16 (3), pp. 203–213, 2004. DOI: 10.1002/adma.200300385.

[92] G. G. Rozenberg, E. Bresler, S. P. Speakman, C. Jeynes, and J. H. G. Steinke, "Patterned low temperature copper-rich deposits using inkjet printing," Applied Physics Letters, vol. 81, pp. 5249-5251, 2002. DOI: http://dx.doi.org/10.1063/1.1481985.

[93] Z. Bao, J. A. Rogers, H. E. Katz, "Printable organic and polymeric semiconducting materials and devices," Journal of Materials Chemistry, vol. 9, pp. 1895-1904, 1999. DOI: 10.1039/A902652E.

[94] E. P. Furlani, "Fluid Mechanics for Inkjet Printing, Fundamentals of Inkjet Printing: The Science of Inkjet and Droplets," Edition S. D. Hoath, Wiley-VCH Verlag GmbH and Co. KGaA, Weinheim, Germany, pp. 13-56, 2016. DOI: 10.1002/9783527684724.ch2.

[95] S. Wagner, H. Gleskova, J. C. Sturm, and Z. Suo Z, "Novel processing technology for macro-electroics," R. A. Street (edition), Technology and Applications of Hydrogenated Amorphous Silicon, Springer, Berlin, pp 222–251, 2000. DOI: 10.1007/978-3-662-04141-3_5.

[96] B. A. Ridley, B. Nivi, J. M. Jacobson, "All-inorganic field effect transistors fabricated by printing," Science, vol. 286, pp.746–749, 1999. DOI: 10.1126/science.286.5440.746.

[97] T. Shimoda, Y. Matsuki, M. Furusawa, T. Aoki, I. Yudasaka, H. Tanaka, H. Iwasawa, D. Wang, M. Miyasaka, and Y. Takeuchi, "Solution-processed silicon films and transistors," Nature vol. 440, pp. 783–786, 2006. DOI: 10.1038/nature04613.

[98] F. Garnier, R. Hajlaouir, A. Yassar, and P. Srivastava, "All-polymer field-effect transistor realized by printing techniques," Science, vol. 265, pp. 1684–1686, 1994. DOI: 10.1126/science.265.5179.1684.

[99] H. Sirringhaus, T. Kawase, R. H. Friend, T. Shimoda, M. Inbasekaran, W. Wu, and E. P. Woo, "High-resolution inkjet printing of all-polymer transistor circuits," Science, vol. 290: pp. 2123–2126, 2000. DOI: 10.1126/science.290.5499.2123.

[100] H. Gleskova, S. Wagner, and D. S. Shen, "Electrophotographic patterning of thin-film silicon on glass foil," IEEE Electron Device Letters, vol. 16, pp. 418–420, 1995. DOI: 10.1109/55.464803.

[101] W. S. Wong, S. E. Ready, R. Matusiak, S. D. White, J. P. Lu, J. Ho, and R. A. Street, "Amorphous silicon thin-film transistors and arrays fabricated by jet printing," Applied Physics Letters, vol. 80, pp. 610-612, 2002. DOI: http://dx.doi.org/10.1063/1.1436273.

[102] N. Rouhi, D. Jain, and P. J. Burke, "High-Performance Semiconducting Nanotube Inks: Progress and Prospects," ACS Nano, vol. 5, pp. 8471–8487, 2011. DOI: 10.1021/nn201828y.

[103] L. Hu, D. S. Hecht, and G. Gruner, "Carbon Nanotube Thin Films: Fabrication, Properties, and Applications," Chem. Rev, vol. 110, pp. 5790–5844, 2010. DOI: 10.1021/cr9002962.

[104] Q. Cao, and J. A. Rogers, "Ultrathin Films of Single-Walled Carbon Nanotubes for Electronics and Sensors: A Review of Fundamental and Applied Aspects," Adv. Mater., vol. 21, pp. 29–53, 2009. DOI: 10.1002/adma.200801995.

[105] R. Saito, M. Fujita, G. Dresselhaus, and M. S. Dresselhaus, "Electronic structure of graphene tubules based on C60," Phys. Rev. B, vol, 46, pp. 1804, 1992. DOI:https://doi.org/10.1103/PhysRevB.46.1804.

[106] T. G. Durkop, E. Cobas, and M. S. Fuhrer, "Extraordinary Mobility in Semiconducting Carbon Nanotubes," Nano Lett., vol. 4, pp. 35-39, 2004. DOI: 10.1021/nl034841q.

[107] C. M. E. Kane, "Size, Shape, and Low Energy Electronic Structure of Carbon Nanotubes," Phys. ReV. Lett., vol. 78, pp. 1932, 1997. DOI:https://doi.org/10.1103/PhysRevLett.78.1932.

[108] J. Li, Y. Lu, Q. Ye, M. Cinke, J. Han, and M. Meyyappan, "Carbon Nanotube Sensors for Gas and Organic Vapor Detection," Nano Lett., vol. 3 (7), pp. 929–933, 2003. DOI: 10.1021/nl034220x.

[109] M. Penza, R. Rossi, M. Alvisi, G. Cassano, and E. Serra, "Functional characterization of carbon nanotube networked films functionalized with tuned loading of Au nanoclusters for gas sensing applications," Sensors Actuators B Chem., vol. 140 (1), pp. 176–184, 2009. http://dx.doi.org/10.1016/j.snb.2009.04.008.

[110] M. Ha, Y. Xia, A. a Green, W. Zhang, M. J. Renn, C. H. Kim, M. C. Hersam, and C. D. Frisbie, "Printed, sub-3V digital circuits on plastic from aqueous carbon nanotube inks," ACS Nano, vol. 4 (8), pp. 4388–95, 2010. DOI: 10.1021/nn100966s.

[111] C. Wang, J. Zhang, and C. Zhou, "Macroelectronic Integrated Circuits Using High-Performance Separated Carbon Nanotube Thin Film Transistors," ACS Nano, vol. 4 (12), pp. 7123–7132, 2010. DOI: 10.1021/nn1021378.

[112] D. Zhang, K. Ryu, X. Liu, E. Polikarpov, J. Ly, M. E. Tompson, and C. Zhou, "Transparent, Conductive, and Flexible Carbon Nanotube Films and Their Application in Organic Light-Emitting Diodes," Nano Lett., vol. 6 (9), pp. 1880–1886, 2006. DOI: 10.1021/nl0608543.

[113] Y.-M. Chien, F. Lefevre, I. Shih, and R. Izquierdo, "A solution processed top emission OLED with transparent carbon nanotube electrodes," Nanotechnology, vol. 21, (13), pp. 134020, 2010. DOI: https://doi.org/10.1088/0957-4484/21/13/134020.

[114] R. C. Tenent, T. M. Barnes, J. D. Bergeson, A. J. Ferguson, B. To, L. M. Gedvilas, M. J. Heben, and J. L. Blackburn, "Ultrasmooth, Large Area, High-Uniformity, Conductive transparent Single-Walled-Carbon-Nanotube Films for Photovoltaics Produced by Ultrasonic Spraying," Adv. Mater., vol. 21 (31), pp. 3210–3216, 2009. DOI: 10.1002/adma.200803551.

[115] A. K. K. Kyaw, H. Tantang, T. Wu, L. Ke, C. Peh, Z. H. Huang, X. T. Zeng, H. V. Demir, Q. Zhang, and X. W. Sun, "Dye-sensitized solar cell with a titanium-oxide-modified carbon nanotube transparent electrode," Appl. Phys. Lett., vol. 99 (2), pp. 021107, 2011. DOI: http://dx.doi.org/10.1063/1.3610488.

[116] A. K. K. Kyaw, H. Tantang, T. Wu, L. Ke, J. Wei, H. V. Demir, Q. Zhang, and X. W. Sun, "Dye-sensitized solar cell with a pair of carbon-based electrodes," J. Phys. D. Appl. Phys., vol. 45 (16), pp. 165103, 2012. DOI: https://doi.org/10.1088/0022-3727/45/16/165103.

[117] R. A. Hatton, N. P. Blanchard, L. W. Tan, G. Latini, F. Cacialli, and S. R. P. Silva, "Oxidised carbon nanotubes as solution processable, high work function hole-extraction layers for organic solar cells," Org. Electron., vol. 10 (3), pp. 388–395, 2009. DOI: http://dx.doi.org/10.1016/j.orgel.2008.12.013.

[118] M. Kaempgen, C. K. Chan, J. Ma, Y. Cui, and G. Gruner, "Printable Thin Film Supercapacitors Using Single-Walled Carbon Nanotubes, " Nano Letters., vol. 9, pp. 1872-1876, 2009. DOI: 10.1021/nl8038579.

[119] J. Vaillancourt, H. Y. Zhang, P.Vasinajindakaw, H. T. Xia, X. J. Lu, X. L. Han, D. C. Janzen, W. S. Shih, C. S. Jones, M. Stroder, M. Y. H. Chen, H. Subbaraman, R. T. Chen, U. Berger, and M. Renn, "All ink-jet-printed carbon nanotube thin-film transistor on a polyimide substrate with an ultrahigh operating frequency of over 5 GHz," Applied Physics Letters, vol. 93, pp. 243301, 2008. DOI: http://dx.doi.org/10.1063/1.3043682.

[120] C. F. Zhou, S. Kumar, C. D. Doyle, and J. M. Tour, "Functionalized Single Wall Carbon Nanotubes Treated with Pyrrole for Electrochemical Supercapacitor Membranesm," J. M. Chem. Mater, vol. 17, pp. 1997-2002, 2005. DOI: 10.1021/cm047882b.

[121] T. Fukao, S. Nakamura, H. Kataura, and M. Shiraishi, "Solution-Processed Single-Walled Carbon Nanotube Transistors with High Mobility and Large On/Off Ratio," Jpn. J. Appl. Phys., Part 1, Vol. 45, pp. 6524, 2006. DOI: https://doi.org/10.1143/JJAP.45.6524.

[122] Y. V. Gulyaev, N. I. Sinitsyn, G. V. Torgashov, S. T. Mevlyut, A. I. Zhbanov, Y. F. Zakharchenko, Z. Y. Kosakovskaya, L. A. Chernozatonskii, O. E. Glukhova, and I. G. Torgashov, "Work function estimate for electrons emitted from nanotube carbon cluster films," J. Vac. Sci. Technol., B, vol. 15, pp. 422, 1997. DOI: 10.1109/IVMC.1996.601808.

[123] J. W. Cheah, Y. M. Shi, H. G. Ong, C. W. Lee, L. J. Li, and J. L. Wang, "N-type behavior of ferroelectric-gate carbon nanotube network transistor," Appl. Phys. Lett., vol. 93, pp. 082103, 2008. DOI: http://dx.doi.org/10.1063/1.2975158.

[124] E. Artukovic, M. Kaempgen, D. S. Hecht, S. Roth, and G. Gruner, "Transparent and Flexible Carbon Nanotube Transistors," Nano Lett., vol. 5, pp. 757-760, 2005. DOI: 10.1021/nl050254o.

[125] R. N. Das, B. Liu, J. R. Reynolds, and A. G. Rinzler, "Engineered Macroporosity in Single-Wall Carbon Nanotube Films," Nano Lett., vol. 9, pp. 677-783, 2009. DOI: 10.1021/nl803168s.

[126] J. Y. Lee, K. Liang, K. H. An, and Y. H. Lee, "Nickel oxide/carbon nanotubes nanocomposite for electrochemical capacitance," Synth. Met., vol. 150, pp. 153-157, 2005. DOI: http://dx.doi.org/10.1016/j.synthmet.2005.01.016.

[127] P. Ramesh, M. E. Itkis, J. M. Tang, and R. C. Haddon, "SWNT−MWNT Hybrid Architecture for Proton Exchange Membrane Fuel Cell Cathodes," J. Phys. Chem. C, vol. 112, pp. 9089-9094, 2008. DOI: 10.1021/jp711280j.

[128] J. M. Tang, K. Jensen, M. Waje, W. Li, P. Larsen, K. Pauley, Z. Chen, P. Ramesh, M. E. Itkis, Y. Yan, and R. C. Haddon, "High Performance Hydrogen Fuel Cells with Ultralow Pt Loading Carbon Nanotube Thin Film Catalysts," J. Phys. Chem. C, vol. 111, pp. 17901-19704, 2007. DOI: 10.1021/jp071469k.

[129] J. E. Trancik, S. C. Barton, and J. Hone, "Transparent and Catalytic Carbon Nanotube Films," Nano Lett., vol. 8, pp. 982-987, 2008. DOI: 10.1021/nl071945i.

[130] D. Liu, M. Fina, J. H. Guo, X. B. Chen, G. Liu, S. G. Johnson, and S. S. Mao, "Organic light-emitting diodes with carbon nanotube cathode-organic interface layer," Appl. Phys. Lett., vol. 94, pp. 013110, 2009. DOI: http://dx.doi.org/10.1063/1.3049605.

[131] C. S. Du, and N. Pan, "High power density supercapacitor electrodes of carbon nanotube films by electrophoretic deposition," Nanotechnology, vol. 17, pp. 5314, 2007. DOI https://doi.org/10.1088/0957-4484/17/21/005.

[132] V. Krstic, G. S. Duesberg, J. Muster, M. Burghard, and S. Roth, "Langmuir−Blodgett Films of Matrix-Diluted Single-Walled Carbon Nanotubes," Chem. Mater., vol. 10, pp. 2338-2340, 1998. DOI: 10.1021/cm980207f.

[133] Y. Maeda, S. Kimura, M. Kanda, Y. Hirashima, T. Hasegawa, T. Wakahara, Y. F. Lian, T. Nakahodo, T. Tsuchiya, T. Akasaka, J. Lu, X. W. Zhang, Z. X. Gao, Y. P. Yu, S. Nagase, S. Kazaoui, N. Minami, T. Shimizu, H. Tokumoto, and R. Saito, "Large-Scale Separation of Metallic

and Semiconducting Single-Walled Carbon Nanotubes," J. Am. Chem. Soc., vol. 127, pp. 10287-10290, 2005. DOI: 10.1021/ja051774o.

[134] I. Mukhopadhyay, and H. Touhara, "Different methods of preparing electrode from single-wall carbon nanotubes and their effect on the Li ion insertion process," J. Solid State Electrochem., vol. 12, pp. 715-720, 2008. DOI: 10.1007/s10008-007-0414-1.

[135] A. Behnam, and G. Bosman, A. Ural, "Percolation scaling of 1/f noise in single-walled carbon nanotube films," Phys. ReV. B, vol. 78, pp. 085431, 2008. DOI: https://doi.org/10.1103/PhysRevB.78.085431.

[136] P. L. Taberna, G. Chevallier, P. Simon, D. Plee, and T. Aubert, "Activated carbon–carbon nanotube composite porous film for supercapacitor applications," Mater. Res. Bull., vol. 41, pp. 478-484, 2006. DOI: http://dx.doi.org/10.1016/j.materresbull.2005.09.029.

[137] E. Bekyarova, M. E. Itkis, N. Cabrera, B. Zhao, A. Yu, J. Gao, and R. C. Haddon, "Electronic Properties of Single-Walled Carbon Nanotube Networks," J. Am. Chem. Soc., vol. 127 (16), pp. 5990–5995, 2005. DOI: 10.1021/ja043153l.

[138] S. Kim, J. Yim, X. Wang, D. D. C. Bradley, S. Lee, and J. C. DeMello, "Spin-and Spray-Deposited Single-Walled Carbon- Nanotube Electrodes for Organic Solar Cells," Adv. Funct. Mater. vol. 20 (14), pp. 2310–2316, 2010. DOI: 10.1002/adfm.200902369.

[139] T. Sekitani, Y. Noguchi, K. Hata, T. Fukushima, T. Aida, and T. Someya, "A rubberlike stretchable active matrix using elastic conductors," Science, vol. 321, pp. 1468-1472, 2008. DOI: 10.1126/science.1160309.

[140] C. Yu, C. Masarapu, J. Rong, B. Wei, and H. Jiang, "Stretchable Supercapacitors Based on Buckled Single-Walled Carbon-Nanotube Macrofilms," Advanced Materials, vol. 21, pp. 4793-4797, 2009. DOI: 10.1002/adma.200901775.

[141] T. Yamada, Y. Hayamizu, Y. Yamamoto, Y. Yomogida, A. Izadi-Najafabadi, D. N. Futaba, and K. Hata, "A stretchable carbon nanotube strain sensor for human-motion detection," Nature nanotechnology, vol. 6, pp. 296-301, 2011. DOI: 10.1038/nnano.2011.36.

[142] K. Liu, Y. Sun, P. Liu, X. Lin, S. Fan, and K. Jiang, "Cross-Stacked Superaligned Carbon Nanotube Films for Transparent and Stretchable Conductors," Advanced Functional Materials, vol. 21, pp. 2721-2728, 2011. DOI: 10.1002/adfm.201100306.

[143] T. Chen, H. Peng, M. Durstock, and L. Dai, "High-performance transparent and stretchable all-solid supercapacitors based on highly aligned carbon nanotube sheets," Scientific reports, vol. 4, pp.1-7, 2014. DOI: doi: 10.1038/srep03612.

[144] J. P. Issi, L. Langer, J. Heremans, and C. H. Olk, "Electronic properties of carbon nanotubes: Experimental results," Carbon, vol. 33, pp. 941-948, 1995. DOI: http://dx.doi.org/10.1016/0008-6223 (95)00023-7.

[145] A. Abdellah, B. Fabel, P. Lugli, and G. Scarpa, "Spray deposition of organic semiconducting thin-films: Towards the fabrication of arbitrary shaped organic electronic devices," Org. Electron., vol. 11, pp. 1031–1038, 2010. DOI: http://dx.doi.org/10.1016/j.orgel.2010.02.018.

[146] V. Robbiano, A. Abdellah, L. Santarelli, A. Falco, S. El-molla, L. V. Titova, D. N. Purschke, F. A. Hegmann, F. Cacialli, and P. Lugli, "Analysis of Sprayed Carbon Nanotube Films on Rigid and Flexible Substrates", Nanotechnology, 2014 IEEE Conference on Nanoelectronics, 2014. DOI: 10.1109/NANO.2014.6968021.

[147] T. M. Brown, G. M. Lazzerini, L. J. Parrott, V. Bodrozic, L. Bürgi, and F. Cacialli, "Time dependence and freezing-in of the electrode oxygen plasma-induced work function enhancement in polymer semiconductor heterostructures," Org. Electron., vol. 12 (4), pp. 623–633, 2011. DOI: http://dx.doi.org/10.1016/j.orgel.2011.01.015.

[148] P. U. Jepsen, D. G. Cooke, and M. Koch, "Terahertz spectroscopy and imaging - Modern techniques and applications," Laser Photon. Rev., vol. 5 (1), pp. 124–166, 2011. DOI: 10.1002/lpor.201000011.

[149] L. V. Titova, T. L. Cocker, D. G. Cooke, X. Wang, A. Meldrum, and F. A. Hegmann, "Ultrafast percolative transport dynamics in silicon nanocrystal films," Phys. Rev. B, vol. 83 (8), pp. 085403, 2011. DOI: https://doi.org/10.1103/PhysRevB.83.085403.

[150] M. C. Beard, J. L. Blackburn, and M. J. Heben, “Photogenerated free carrier dynamics in metal and semiconductor single-walled carbon nanotube films,” Nano Lett., vol. 8 (12), pp. 4238–4242, 2008. DOI: 10.1021/nl801913y.

[151] S. A. Jensen, R. Ulbricht, A. Narita, X. Feng, K. Müllen, T. Hertel, D. Turchinovich, and M. Bonn, “Ultrafast photoconductivity of graphene nanoribbons and carbon nanotubes,” Nano Lett., vol. 13 (12), pp. 5925–5930, 2013. DOI: 10.1021/nl402978s.

[152] Q. Zhang, E. H. Hároz, Z. Jin, L. Ren, X. Wang, R. S. Arvidson, A. Lüttge, and J. Kono, “Plasmonic nature of the terahertz conductivity peak in single-wall carbon nanotubes,” Nano Lett., vol. 13 (12), pp. 5991–5996, 2013. DOI: 10.1021/nl403175g.

[153] “Fujifilm Dimatix Materials Printers DMP-2800 Series,” UserManual, (2008).

[154] Nicholas A. Vacirca and Timothy P. Kurzweg, “Inkjet printing techniques for the fabrication of polymer optical waveguides,” conference Advanced Fabrication Technologies for Micro/Nano Optics and Photonics III, vol. 75910A, (2010). DOI:10.1117/12.841436.

[155] Kotaro YOSHIMURA, Mitsura KISHIMOTO, and Toshiro SUEMUNE, "Inkjet Printing Technology," OKI Technical Review, vol. 64, pp. 41-44, (1998). Available at: http://www.oki.com/en/otr/downloads/otr-161-10.pdf.

[156] H. Kipphan, “Handbook of print Media,” spring, pp. 1027-1111, (2000). DOI: 10.1007/978-3-540-29900-4_13.

[157] Q. Xu, and O. A. Basaran, “Computational analysis of drop-on-demand drop formation,” Physics of Fluids, vol. 19, pp. 102111-12, (2007). DOI: http://dx.doi.org/10.1063/1.2800784.

[158] E. R. Lee, “Microdrop Generation,” CRC Press, p. 272, (2002). Available at: https://play.google.com/store/books/details?id=gn7LBQAAQBAJ&rdid=bookgn7LBQAAQBAJ&rdot=1&source=gbs_vpt_read&pcampaignid=books_booksearch_viewport.

[159] M. Rein, “Phenomena of Liquid Drop Impact on Solid and Liquid Surfaces,” Fluid Dynamics Research, vol. 12, pp.61-93, (1993). DOI: 10.1016/0169-5983(93)90106-K.

[160] J. A. Lim, W. H. Lee, H. S. Lee, J. H. Lee, Y. D. Park, and K. Cho, "Self-Organization of Ink-jet-Printed Triisopropylsilylethynyl Pentacene via Evaporation-Induced Flows in a Drying Droplet," Adv. Funct.Mater., vol. 18, pp. 229–234, (2008). DOI: 10.1002/adfm.200700859.

[161] C. Kim, M. Nogi, and K. Suganuma, "Electrical conductivity enhancement in inkjetprinted narrow lines through gradual heating," J. Micromech. Microeng., vol. 22, p. 035016 (5pp), (2012). DOI: https://doi.org/10.1088/0960-1317/22/3/035016.

[162] R. D. Deegan, O. Bakajin, T. F. Dupont, G. Huber, S. R. Nagel, and T. A. Witten, "Capillary flow as the cause of ring stains from dried liquid drops," Nature, vol. 389, pp. 827–829, (1997). DOI: 10.1038/39827.

[163] H. Hu and R. G. Larson, "Marangoni Effect Reverses Coffee-Ring Depositions," J. Phys. Chem. B, vol. 110, pp. 7090–7094, (2006). DOI: 10.1021/jp0609232.

[164] H. S. Kim, S. R. Dhage, D. E. Shim, and H. T. Hahn, "Intense pulse light sintering of copper nanoink for printed electronics," Applied Physics A, vol. 97, pp. 791-798, (2009). DOI: 10.1007/s00339-009-5360-6.

[165] J. C. Kim, K. H. Auh, and D. M. Martin, "Multi-level particle packing model of ceramic agglomerates," Modeling and Simulation of Materials of Science and Engineering, vol. 8, pp. 159-168, (2000). DOI: https://doi.org/10.1088/0965-0393/8/2/306.

[166] M. J. Mayo, "Processing of nanocrystalline ceramics from ultrafine particles," International Materials Reviews, vol. 41, pp. 85-115, (1996). DOI: http://dx.doi.org/10.1179/imr.1996.41.3.85.

[167] B.-J. Gans, E. Kazancioglu, W. Meyer, U. S. Schubert, "Ink-jet Printing Polymers and Polymer Libraries Using Micropipettes," Macromol. Rapid Commun. vol. 25, pp. 292–296, (2004). DOI: 10.1002/marc.200300148.

[168] H. Dong, W. W. Carr, J. F. Morris, "Visualization of drop-on-demand inkjet: Drop formation and deposition," Phys. Fluids, vol. 77 (2006), pp. 085101-8. DOI: http://dx.doi.org/10.1063/1.2234853.

[169] Q. Xu, O. A. Basaran, "Computational analysis of drop-on-demand drop formation," Phys. Fluids, vol. 19, pp. 102111–12, (2007). DOI: http://dx.doi.org/10.1063/1.2800784.

[170] X. Zhang, O. A. Basaran, "An experimental study of dynamics of drop formation," Phys. Fluids, vol. 7, pp. 1184–1203, (1995). DOI: http://dx.doi.org/10.1063/1.868577.

[171] P. K. Notz, A. U. Chen, O. A. Basaran, "Satellite drops: Unexpected dynamics and change of scaling during pinch-off," Phys. Fluids, vol. 13, pp. 549–552, (2001). DOI: http://dx.doi.org/10.1063/1.1343906.

[172] F. I. Li, P. H. Leo, J. A. Barnard, "Dendrimer Pattern Formation in Evaporating Drops: Solvent, Size, and Concentration Effects," J. Phys. Chem. C, vol. 112, pp. 14266–14273, (2008). DOI: 10.1021/jp802850y.

[173] F. Lugli, F. Zerbetto, "Atomistic Simulation of "Drop-on-Demand," Inkjet Dynamics" J. Phys. Chem. C, vol. 112, pp. 10616–10621 (2008). DOI: 10.1021/jp075482g.

[174] A.W. Adamson, A. P. Gast, "Physical chemistry of surfaces 6th edition", John Wiley & Sons, ISBN: 978-0-471-14873-9, p.808 (1997). [Online]. Available at: http://eu.wiley.com/WileyCDA/WileyTitle/productCd-0471148733.html.

[175] J. H. Snoeijer, B. Andreotti, "A microscopic view on contact angle selection", Phys. Fluids, vol. 20, pp. 057101-11, (2008). DOI: http://dx.doi.org/10.1063/1.2913675.

[176] Y. Neuvo and S. Ylönen, "Bit Bang Rays to the Future," ISBN (pbk) 978-952-248-078-1, (2009). Available at: http://lib.tkk.fi/Reports/2009/isbn9789522480781.pdf.

[177] M. Pudas, N. Halonen, P. Granat, and J. Vähäkangas, "Gravure printing of conductive particulate polymer inks on flexible substrates," Prog. Org. Coatings, vol. 54, pp. 310–316, (2005). DOI: http://dx.doi.org/10.1016/j.porgcoat.2005.07.008.

[178] W. S. Wong. And A. Salleo, Flexible Electronics: Materials and Applications, Springer, vol. 11, pp.1-462, (2009). DOI: 10.1007/978-0-387-74363-9.

[179] J. Rekimoto, "Smartskin: an infrastrcture for freehand manipulation on interactive surfaces," SIGCHI conference on Human Factors in Computing Systems: Changing Our World, Changing Ourselves, vol. 4, pp. 113-120, (2002). DOI>10.1145/503376.503397.

[180] I. Rosenberg and K. Perlin, "The UnMousePad: an interpolating multi-touch force-sensing input pad," ACM Trans. Graph, vol. 28, pp. 65:1-65:9, (2009). DOI: 10.1145/1531326.1531371.

[181] C. Rendl, P. Greindl, M. Haller, M. Zirkl, B. Stadlober and P. Hartmann, "PyzoFlex: Printed Piezoelectric Pressure Sensing Foil," UIST '12: Proceedings of the 25th Symposium on User Interface Software and Technology, pp. 509-518, (2012). DOI: 10.1145/2380116.2380180.

[182] Z. Ma, "An Electronic Second Skin," Science, vol. 333 (6044), pp. 830-831, (2011). DOI: 10.1126/science.1209094.

[183] Dae-Hyeong Kim et al., "Epidermal Electronics," Science, vol. 333 (6044), pp. 838-843, (2011). DOI: 10.1126/science.1206157.

[184] V. J. Lumelsky, M. S. Shur and S. Wagner, "Sensitive Skin," IEEE Sensor Journal, vol. (1), pp. 41-51, (2001). DOI: 10.1109/JSEN.2001.923586.

[185] D. Um and V. Lumelsky, "Fault tolerance via component redundancy for a modularizaed sensitive skin," IEEE Internation Conference on Robotics and Automation, pp. 722-727, (1999). DOI: 10.1109/ROBOT.1999.770060.

[186] M. Hakozaki, A. Hatori and H. Shinoda, "A sensitive skin using wireless tactile sensing elements," Technical Digest of the 18th Sensor Symposium, vol. 18, pp.147-150, (2001). Available at: http://citeseerx.ist.psu.edu/viewdoc/download?doi=10.1.1.475.3310&rep=rep1&type=pdf

[187] L. Buechley and M. Eisenberg, "Fabric PCBs, electronic sequins, and socket buttons: techniques for e-textile craft," Personal and Ubiquitous Computing, vol. 13 (2), pp. 133-150, (2009). DOI: 10.1007/s00779-007-0181-0.

[188] Pacelli, M., "Sensing Fabrics for Monitoring Physiological and Biomechanical Variables: E-textile solutions," Medical Devices and Biosensors, pp. 1-4, (2006). DOI: 10.1109/ISSMDBS.2006.360082.

[189] K. E. Pennywitt, "Robotic tactile sensing," Byte, vol. 11 (1), pp. 177–200, (1986).

[190] J. Tegin, and J. Wikander, “Tactile sensing in intelligent robotic manipulation – a review,” Ind. Robot, vol. 32, pp. 64–70, (2005). DOI: http://dx.doi.org/10.1108/01439910510573318.

[191] HANDLE Project Website, (2009), Available at: http://www.handle-project.eu/

[192] L. Harmon, “Automated tactile sensing,” The International Journal of Robotics Research, vol. 1 (2), pp. 3-32, (1982).

[193] L. Harmon, “Tactile sensing for robots,” Robotics and Artificial Intelligence, vol. 11, pp. 109–158, (1984). DOI: 10.1007/978-3-642-82153-0_5.

[194] L. Harmon, “Touch-sensing technology –a review,” Society of Manufacturing Engineers Tech. Rep. No. MSR80–03, p. 58, (1980).

[195] M. Lee, “Tactile sensing: new directions, new challenges,” The International Journal of Robotics Research vol. 19 (7), pp. 636-643, (2000).

[196] J. Nevins, andD. Whitney, “Research on advanced assembly automation,” Computer, vol. 10 (12), pp. 24-38, (1977). DOI: 10.1109/C-M.1977.217597.

[197] M. Lee, and H. Nicholls, “Tactile sensing for mechatronics – a state of the art survey,” Mechatronics, vol. 9 (1), pp. 1-31, (1999). DOI: http://dx.doi.org/10.1016/S0957-4158 (98)00045-2.

[198] M. Eltaib, and J. Hewit, “Tactile sensing technology for minimal access surgery – a review,” Mechatronics vol. 13 (10), pp. 1163–1177, (2003). DOI: http://dx.doi.org/10.1016/S0957-4158 (03)00048-5.

[199] N. Wettels, “Biomimetic Tactile Sensor for Object Identification and Grasp Control,” A Multi-modal Sensor Mimicking the Human Digit, LAP Lambert Acad. Publ., (2011).

[200] S. Najarian, S. Najjarıyan, J. Dargahi, A. Mehrizi, Artificial Tactile Sensing in Biomedical Engineering, McGraw-Hill Biophotonics, McGraw-Hill, (2009).

[201] L. Ascari, P. Corradi, L. Beccai, and C. Laschi, “A miniaturized and flexible optoelectronic sensing system for tactile skin,” J. Micromech. Microeng. vol. 17, pp. 2288–2298 (2007). DOI: https://doi.org/10.1088/0960-1317/17/11/016.

[202] J. S. Heo, J. Y. Kim, and J. J. Lee, "Tactile sensors using the distributed optical fiber sensors," in: Proceedings of the 3rd International Conference on Sensing Technology (ICST), pp. 486–490, (2008). DOI: 10.1109/ICSENST.2008.4757153.

[203] C. Steinem, and A. Janshoff, "Piezoelectric Sensors," Springer-Verlag, Berlin/Heidelberg, Germany, 2007. DOI: 10.1007/b100347.

[204] P. Ueberschlag, "PVDF piezoelectric polymer," Sens. Rev. vol. 21, pp. 118–125, (2001). DOI: http://dx.doi.org/10.1108/02602280110388315.

[205] S. Lang, and S. Muensit, "Review Some Lesser-known applications piezoelectric and pyroelectric polymers," Appl. Phys. A: Mater. Sci. Process., vol. 85, pp. 125–134, (2006). DOI: 10.1007/s00339-006-3688-8.

[206] K. Hosoda, Y. Tada, and M. Asada, "Anthropomorphic robotic soft fingertip with randomly distributed receptors," Robot. Auton. Syst., vol. 54, pp. 104–109, (2006).DOI: http://dx.doi.org/10.1016/j.robot.2005.09.019.

[207] Y. Huang, M. Sohgawa, K. Yamashita, T. Kanashima, M. Okuyama, M. Noda, and H. Noma, "Fabrication and normal/shear stress responses of tactile sensors of polymer/Si cantilevers embedded in PDMS and urethane gel elastomers," IEEJ Trans. Sens. Micromachines, vol. 128, pp. 193–197 (2008). DOI: 10.1541/ieejsmas.128.193.

[208] K. Noda, Y. Hashimoto, Y. Tanaka, andI. Shimoyama, "MEMS on robot applications, in: Proceedings of the Solid-State Sensors," Actuators and Microsystems Conference (TRANSDUCERS). International, pp. 2176–2181, (2009). DOI: 10.1109/SENSOR.2009.5285608.

[209] L.C. Tsao, D.R. Chang, W.P. Shih, and K.C. Fan, "Fabrication and characterization of electro-active polymer for flexible tactile sensing arraym," Key Eng. Mater., vol. 381–382, pp. 391–394 (2008). DOI:10.4028/www.scientific.net/KEM.381-382.391.

[210] M. Y. Cheng, C.-M. Tsao, Y. Lai, and Y.-J. Yang, "A novel highly-twistable tactile sensing array using extendable spiral electrodes," in: Proceedings of the IEEE 22nd International

Conferenceon Micro Electro Mechanical Systems (MEMS), pp. 92–95, (2009). DOI: 10.1109/MEMSYS.2009.4805327.

[211] V. Maheshwari, and R. Saraf, “Tactile devices to sense touch on a par with a human finger,” Angew. Chem. Int. Ed., vol. 47, pp. 7808–7826, (2008). DOI: 10.1002/anie.200703693.

[212] G. Schwartz, B. C.-K.Tee, and J. Mei, “Flexiblepolymer transistors with high pressure sensitivity for application in electronic skin and health monitoring,” Nature Communications, vol. 4, article no. 1859, pp. 1-8, (2013). DOI: 10.1038/ncomms2832.

[213] M. Ying, A. P. Bonifas, and N. S. Lu, “Silicon nanomembranes for fingertip electronics,” Nanotechnology, vol. 23, pp. 1-7, (2012). Online at stacks.iop.org/Nano/23/344004.

[214] R. S. Dahiya, G. Metta, M. Valle, and G. Sandini, “Tactile sensing—from humans to humanoids,” IEEE Transactions on Robotics, vol. 26, pp. 1–20, (2010). DOI: 10.1109/TRO.2009.2033627.

[215] J. Engel, J. Chen, Z. Fan, and C. Liu, “Polymer micromachined multimodal tactile sensors,” Sensors and Actuators A: Physical, vol. 117, pp. 50–61, (2005). DOI: http://dx.doi.org/10.1016/j.sna.2004.05.037.

[216] T. Someya, T. Sekitani, S. Iba, Y. Kato, H. Kawaguchi, and T. Sakurai, “A large-area, flexible pressure sensor matrix with organic field-effect transistors for artificial skin applications,” Proceedings of the National Academy of Sciences of the United States of America, vol. 101, pp. 9966–9970, (2004). DOI: 10.1073/pnas.0401918101.

[217] E. Pritchard, M. Mahfouz, B. Evans, S. Eliza, and M. Haider, “Flexible capacitive sensors for high resolution pressure measurement,” in: Proceedings of the IEEE 7th Conference on Sensors (IEEE-sensors), pp. 1484–1487, (2008). DOI: 10.1109/ICSENS.2008.4716726.

[218] G. Cannata, M. Maggiali, G. Metta, and G. Sandini, “An embedded artificial skin for humanoid robots,” in: Proceedings of the IEEE International Conference on Multisensor Fusion and Integration for Intelligent Systems (MFI), pp. 434–438, (2008). DOI: 10.1109/MFI.2008.4648033.

[219] A. Schmitz, M. Maggiali, M. Randazzo, L. Natale, and G. Metta, "A prototype fingertip with high spatial resolution pressure sensing for the robot iCub," In: Proceedings of the 8th IEEE-RAS International Conference on Humanoid Robots (Humanoids), pp. 423–428, (2008). DOI: 10.1109/ICHR.2008.4755988.

[220] H. Lee, J. Chung, S. Chang, and E. Yoon, "Normal and shear force measurement using a flexible polymer tactile sensor with embedded multiple capacitors," J. Microelectromech. Syst., vol. 17, pp. 934–942, (2008). DOI: 10.1109/JMEMS.2008.921727.

[221] J. G. V. da Rocha, and S. Lanceros-Mendez, "Capacitive sensor for three-axis force measurements and its readout electronics," IEEE Trans. Instrum. Meas., vol. 58, pp. 2830–2836, (2009). DOI: 10.1109/TIM.2009.2016366.

[222] T. Hoshi, and H. Shinoda, "A Large area robot skin based on cell-bridge system", in: Proceedings of the IEEE 5th Conference on Sensors, pp. 827–830, (2006). DOI: 10.1109/ICSENS.2007.355595.

[223] H. Shinoda, and H. Oasa, "Wireless tactile sensing element using stress-sensitive resonator," IEEE ASME Trans. Mechatron., vol. 5, pp. 258–265, (2000). DOI: 10.1109/3516.868917.

[224] S. C. B. Mannsfeld, B. C.-K. Tee, and R. M. Stoltenberg, "Highly sensitive flexible pressure sensors with microstructured rubber dielectric layers," Nature Materials, vol. 9, pp. 859–864, (2010). DOI: 10.1038/nmat2834.

[225] D. J. Lipomi, M. Vosgueritchian, B. and C.-K. Tee, "Skin-like pressure and strain sensors based on transparent elastic films of carbon nanotubes," Nature Nanotechnology, vol. 6, pp. 788–792, (2011). DOI:10.1038/nnano.2011.184.

[226] K. F. Lei, K.-F. Lee, and M.-Y. Lee, "Development of a flexible PDMS capacitive pressure sensor for plantar pressure measurement," Microelectronic Engineering, vol. 99, pp. 1–5, (2012). DOI: http://dx.doi.org/10.1016/j.mee.2012.06.005.

[227] S. El-Molla, A. Albrecht, E. Cagatay, P. Mittendorfer, G. Cheng, P. Lugli, J. F. Salmeron, A. Rivadeneyra, "Integration of a Thin Film PDMS-Based Capacitive Sensor for Tactile Sensing

in an Electronic Skin," Journal of Sensors, vol. 2016, pp. 1-7, (2016). DOI: http://dx.doi.org/10.1155/2016/1736169.

[228] F. M. Smits, "Measurement of sheet resistivities with the four point probe," Bell System Technical Journal, vol. 37, pp. 711– 718, (1958). DOI: 10.1002/j.1538-7305.1958.tb03883.x.

[229] A. Rivadeneyra, J. Fern´andez-Salmer´on,M. Agudo, J. A. L´opez- Villanueva, L. F. Capitan-Vallvey, and A. J. Palma, "Design and characterization of a low thermal drift capacitive humidity sensor by inkjet-printing," Sensors and Actuators B: Chemical, vol. 195, pp. 123–131, (2014). DOI: http://dx.doi.org/10.1016/j.snb.2013.12.117.

[230] A. Rivadeneyra, J. Fern´andez-Salmer´on, M. Agudo-Acemel, J. A. L´opez-Villanueva, A. J. Palma, and L. F. Capitan-Vallvey, "A printed capacitive-resistive double sensor for toluene and moisture sensing," Sensors and Actuators B: Chemical, vol. 210, pp. 542–549, (2015). DOI: http://dx.doi.org/10.1016/j.snb.2015.01.036.

[231] J. F. Salmer´on, F.Molina-Lopez,D. Briand et al., "Properties and printability of inkjet and screen-printed silver patterns for RFID antennas," Journal of Electronic Materials, vol. 43, pp. 604– 617, (2014). DOI: 10.1007/s11664-013-2893-4.

[232] J. N. Lee, C. Park, and G. M.Whitesides, "Solvent compatibility of poly(dimethylsiloxane)-based microfluidic devices," Analytical Chemistry, vol. 75, pp. 6544–6554, (2003). DOI: 10.1021/ac0346712.

[233] DOW P-Series Glycol Ethers, (2015). http://msdssearch. dow.com/PublishedLiteratureDOWCOM/dh 012d/0901- b8038012d976.pdf.

[234] J. C. L¨otters, W. Olthuis, P. H. Veltink, and P. Bergveld, "The mechanical properties of the rubber elastic polymer polydimethylsiloxane for sensor applications," Journal of Micromechanics and Microengineering, vol. 7, pp. 145–147, (1997). DOI: https://doi.org/10.1088/0960-1317/7/3/017.

[235] I. D. Johnston, D. K. McCluskey, C. K. L. Tan, and M.C.Tracey, "Mechanical characterization of bulk Sylgard 184 for microfluidics and microengineering," Journal of

Micromechanics and Microengineering, vol. 24, Article ID035017 p. 7, (2014). DOI: https://doi.org/10.1088/0960-1317/24/3/035017.

[236] A. Mata, A. J. Fleischman, and S. Roy, "Characterization of polydimethylsiloxane (PDMS) properties for biomedicalmicro/nanosystems," Biomedical Microdevices, vol. 7, pp. 281–293, (2005). DOI: 10.1007/s10544-005-6070-2.

[237] M. Liu, J. Sun, Y. Sun, C. Bock, and Q. Chen, "Thickness dependent mechanical properties of polydimethylsiloxane membranes," Journal of Micromechanics and Microengineering, vol. 19, Article ID 035028 (pp. 4), (2009). DOI: https://doi.org/10.1088/0960-1317/19/3/035028.

[238] E. Cagatay, P. Kohler, P. Lugli, and A. Abdellah, "Flexible capacitive tactile sensors based on carbon nanotube thin films," IEEE Sensors Journal, vol. 15, pp. 3225–3233, (2015). DOI: 10.1109/JSEN.2015.2404342.

[239] F. N. Toth and G. and C. M. Meijer, "A low-cost, smart capacitive position sensor," IEEE Transactions on Instrumentation and Measurement, vol. 41, pp. 1041–1044, (1992). DOI: 10.1109/19.199446.

List of Publications

Peer Reviewed Journals

[1] S. El-Molla, A. Albrecht, E. Cagatay, P. Mittendorfer, G. Cheng, P. Lugli, J. F. Salmeron, A. Rivadeneyra, "Integration of a Thin Film PDMS-Based Capacitive Sensor for Tactile Sensing in an Electronic Skin," Journal of Sensors, vol. 2016, pp. 1-7, 2016. DOI: http://dx.doi.org/10.1155/2016/1736169.

Conference Proceedings

[1] P. Lugli, A. Abdellah, A. Abdelhalim, A. Albrecht, M. Becherer, E. Cagatay, A. Falco, F. Loghin, S. El-molla, J. F. Salmeron, and A. Rivadeneyra "Fabrication , characterization and modeling of flexible electronic components based on CNT networks", 2016 IEEE International Symposium on Circuits and Systems (ISCAS), 2016. DOI: 10.1109/ISCAS.2016.7527502.

[2] V. Robbiano, A. Abdellah, L. Santarelli, A. Falco, S. El-molla, L. V. Titova, D. N. Purschke, F. A. Hegmann, F. Cacialli, and P. Lugli, "Analysis of Sprayed Carbon Nanotube Films on Rigid and Flexible Substrates", Nanotechnology, 2014 IEEE Conference on Nanoelectronics, 2014. DOI: 10.1109/NANO.2014.6968021.

Acknowledgment

First and foremost, I would like to express my sincere gratitude to my supervisor Prof. Dr. Paolo Lugli, for his patience, encouragement, immense knowledge, and endless support. He has been and will always be my best source of inspiration and support. His guidance helped me in all the time of research and writing of this thesis. I could not have imagined having a better advisor for my Ph.D study than him.

I am also deeply indebted to Dr. Almudena Rivadeneyra-Torres and Dr. José Fernández Salmeron for their invaluable advices, their insightful comments, and their support they have provided to make this thesis possible.

I would like also to thank my former mentor Dr. Alaa Abdellah because of his guidance during my initial work toward this thesis. I cannot also forget the role of my previous colleague Dr. Francesco Arca, through his continuous discussion we had on the work and also on the personal level. I am also grateful to the following university staff: Prof. Dr. Markus Becherer and Prof. Dr. Christian Jirauschek.

It was fantastic to have the opportunity to work with amazing and helpful colleagues at Nanoelectronics institute, I am deeply thanks all of them especially: Marco Bobinger, Aniello Falco, Andreas Albrecht, Amir Hossein Fallahpour, Saumya Joshi, Marius Loch, Vijay Bhatt, Alina Lyuleeva, Florin Loghin, and Michael Haider. My big words goes to my colleague Peter Tzenov and his wife for their continuous support and advices, Petar was always a source of motivation for me during my PhD.

Acknowledgment

I am very grateful to my previous supervisor in Egypt Prof. Dr. Asmaa Fahiem Mansour, she has always been available to advise me. I cannot deny her role and support for providing me with the opportunity to complete my PhD abroad.

I would like to thank my dearest friend and my sister Dr. Elshimaa Bendary for all the hard time and for all the fun we have had in the last three years. Without her I cannot imagine my life especially I was living without my family and she was and still represents my family here.

A very special gratitude goes out to my Egyptian Government especially Cultural Affairs and Mission Sector for providing me with the fund necessary to complete my PhD. Partially fund from TUM-Graduate school is also acknowledged.

Finally, I would like to express my very profound gratitude to my family in Egypt, my husband Dr. Ahmed Hammad, and my lovely daughters Jana & Larin, who have provided me through moral and emotional support throughout my years of study, through the process of researching, writing this thesis, and in general through all my life. Without their encouragement, this dissertation would not be possible.